

Investigating multi-regional neural dynamics associated with cocaine-paired memory

Charlie Clarke-Williams

St Edmund Hall

University of Oxford

Supervised by Prof. David Dupret & Prof. David Bannerman

Submitted: March 2021

Thesis submitted for the degree of Doctor of Philosophy

Abstract

Investigating multi-regional neural dynamics associated with drug-paired memory

Rewarding experiences bias the formation of memories such that future re-exposure to corresponding stimuli biases behavioural selection such to increase the probability of re-encountering reward. This crucial feature of the nervous system is hijacked by drugs of abuse such as cocaine; whose neuropharmacological actions impose dramatic enhancement of neural reward signals, forging the formation of cocaine-paired memories. These memories constitute a diverse range of informational modalities spanning multiple brain areas. Due to the powerfully rewarding nature of cocaine, these brain-wide representations tend to outcompete other, more useful memories, precipitating stubborn patterns of cocaine-seeking behaviour. This thesis combined a novel model of dynamic cocaine-seeking behaviour with a parallel five brain site electrophysiological recording strategy. These experimental tools enabled me to explore the hypothesis that specific patterns of frequency-specific multiregional co-ordination support the recall of cocaine-paired experience and precipitate cocaine-seeking behaviour. My results suggest that cocaine-seeking behaviour, expressed initially after conditioning and renewed following an extinction period, was most linked to the enhancement of patterns of multiregional co-ordination ("barcodes") in the beta (15–25 Hz) range. VTA 4 Hz oscillations emerged as an important agent for the temporal orchestration of beta activities, showing cycle-specific correlates of beta-selective modulation. Using a preliminary cell-type prediction pipeline, the putative dopaminergic population in the VTA showed firing properties which were reminiscent of the control of beta activities across regions, The results in this thesis provide the scaffolding onto which a final experiment will be developed, which aims to provide a causal demonstration to the conclusions from this thesis; that VTA 4 Hz and dopamine-controlled multiregional beta co-ordination patterns are involved in the precipitation of cocaine-seeking behaviour.

Acknowledgements

I am blessed to be a part of the Dupret lab and (more broadly) the MRC Brain Network Dynamics Unit (BNDU), which is home to a diverse range of talented individuals. I owe much of my scientific development to so many of these inspirational and friendly people. Thanks in particular to Prof. Peter Brown and now Prof. Pete Magil for leading the great initiatives of the BNDU; building a well-connected scientific network, nurturing its individuals at every career stage, and having a great level of outreach to the wider public community. I also thanks to Savita Anderson and Dr Vivienne Collins for organising these ventures and their superb administrative support. Thanks to Ben Micklem and Dr Rosemary Painter for always being there for any of my technological needs, and to Jane Janson for the training and the exquisite running of the animal house.

I have been thoroughly supported by all members of the Dupret Lab. I thank them all for making me smile in the lab, pub, and in more recent times, during zoom calls. I thank Natalia Campo-Urriza for her expertise in making head stage drives. For his unparalleled technical professionalism and assistance, I thank Dr Pavel Perestenko. The development of the behavioural model was largely thanks to the inputs of Dr Stéphanie Trouche and Prof. David Bannerman, the latter of whom also has provided me with valuable ideas, feedback and support throughout this project. On this note, I also thank Prof. Mark Woolrich and Prof. Mark Walton for their thoughts and guidance at the critical stages of the PhD. Many thanks to Roman Rothaermel, who spent a lot of time recording and processing some of the data I was able to use for this thesis. A big thanks to Dr Vítor Lopes dos Santos, who has been instrumental to the development of my programming skills, and the way I think about neural data. Similarly, I thank Dr Mohamady El-Gaby, Dr Laura Lefevré, Dr Stephen McHugh, Dr Helen Barron and Dr Alex Morley for the valuable tuition and much-trusted (scientific and life) advice.

The time I have spent being a PhD student has been the most challenging, exciting, and significant part of my life so far. Things were very stressful at times, impacting on my mental health and in some of the darker moments made me question if I could complete this academic journey. I am delighted to say that I have been successful (academically and mentally) and am as excited as much as ever about life and science. Helping me with this more personal side, I am hugely grateful for the support and love I have received from many friends who I feel

honoured to be connected to. Particularly, I am hugely thankful to my ex-girlfriend, Sarah; who is truly one of the most resilient and caring people I know – and someone who was always there for me.

Finally, and most crucially, I thank my supervisor, Prof. David Dupret. Right when I joined the lab, he told me that his door was always open. True to his word, David has provided unparalleled support throughout my PhD (and beyond); over technical, scientific, and emotional dimensions. Being able to provide this bespoke service to me and all other lab members is a testament to his strengths as a scientist and human being. I hope I've done you proud.

Watermelon.

Contents

Abstract **1**

Acknowledgements **3**

Figures & Table **10**

Abbreviations **13**

1 | Introduction **16**

1.1 | Psychological framework for reward-orientated behaviour **18**

Pavlovian and instrumental conditioning 18

Context-dependent behaviour 20

Modelling cocaine-seeking behaviour in rodents 22

1.2 | Neural representation of reward and cocaine **24**

Reward prediction and the temporal difference algorithm 24

Dopamine as a reward prediction error signal 28

Neuropharmacology of cocaine 32

1.3 | Brain regions supporting cocaine-seeking behaviour **33**

The ventral tegmental area (VTA) 33

The nucleus accumbens (NAc) 34

Amygdala (Amy) 35

Hippocampus (HPC) 36

Prefrontal cortex (PFC) 37

1.4 | Neural oscillations and brain synchrony/co-ordination **38**

Oscillations report coordinated activity of neural populations 38

Interneurons gate excitability dynamics in oscillating neural networks 39

Functional relevance of neural oscillations in the rodent hippocampus 39

Dynamics of between-region oscillatory interactions 40

2 | Experimental Methodology 42

2.1 | Animals 42

2.2 | Microdrive implantation 42

2.3 | Behavioural protocol 43

2.4 | Multichannel data acquisition and position tracking 45

2.5 | Spike detection and unit isolation 46

2.6 | Statistical analysis 47

Mean difference estimation ("Gardner-Altman") plots 47

Reverse cumulative frequency distribution comparison plot 48

Rank over-representation plot 48

2.7 | Analytical details for Chapter 3 49

Behavioural Factor Analysis 49

2.8 | Analytical details for Chapter 4 50

Tetrode nomination 50

Barcode interaction profiles 50

2.8 | Analytical details for Chapter 5 50

Barcode CPMR scoring 50

2.9 | Analytical details for Chapter 6 51

Phase-amplitude coupling (PAC) scoring 51

Opto-tagging assay 51

ISI-based VTA cell-type classification 51

Rayleigh phase coherence 52

VTA cell-type triggered spectrograms- 52

3 | Modelling dynamic cocaine-seeking behaviour 54

3.1 | Outline 54

3.2 | A "pseudo-instrumental" cocaine conditioning protocol 54

3.3 | Simple behavioural analyses 57

3.4 | Multidimensional analysis of cocaine-seeking behaviour 61

3.5 | Discussion 61

4 | Analyses of LFP interaction dynamics 64

4.1 | Outline 64

4.2 | Simple LFP overview 65

4.3 | Empirical Mode Decomposition of the local field potentials 69

Non-stationarity 69

Sifting 70

Ensemble EMD 74

Masked EMD 75

Tailored-mEMD 77

Spike validation of region-tailored IMFs....82

4.4 | Detecting LFP interaction motifs using Independent Component Analysis....84

Premise....84

Barcode detection method....85

Barcode evaluation....89

4.5 | Discussion....93

5 | Multiregional beta co-ordination relates to dynamic cocaine-seeking behaviour ...96

5.1 | Beta amplitude modulations most strongly reflect a signature of cocaine-paired retrieval....96

Beta barcode strength modulation relates to dynamic cocaine-seeking behaviour 96

Beta amplitudes....99

5.2 | Discussion....102

6 | Orchestration of multiregional beta coordination....105

6.1 | Temporal orchestration of global beta co-ordination by theta and 4 Hz oscillations....106

A role of VTA 4 Hz oscillations in modulating individual beta activities 106

A subset of VTA 4 Hz cycles exert strong phase modulation of beta barcodes....109

6.2 | VTA cell-type contributions to multiregional beta orchestration 115

Optogenetic identification and characterisation of glutamatergic and dopaminergic VTA cells 115

ISI-based classification of VTA cell-types....117

The firing properties of VTA putative dopaminergic cells are more related to beta co-ordination 119

6.3 | Discussion 122

Beta-specific phase modulation by VTA 4 Hz 122

Cycle-specific modulation of multiregional beta co-ordination by VTA 4 Hz 123

Validity of VTA cell-type classification method 124

Multiregional beta co-ordination, dopamine and cocaine-seeking behaviour 125

7 | Summary 127

References 128

Figures & Table

Figure 1.1: *Learning curve.* 19

Figure 1.2: *Temporal difference (TD) learning.* 27

Figure 1.3: *Example putative dopaminergic neuron firing responses to CS and reward.* 28

Figure 1.4: *Diversity of STDP windows.*.....30

Figure 1.5: *Describing an oscillatory signal.* 39

Table 2.1: *Behavioural metrics used for factor analysis.* 49

Figure 3.1: *Protocol outline.*.....56

Figure 3.2: *Quantification of key behavioural measures of cocaine-seeking behaviour*.....58

Figure 3.3: *Speed observations across stages and zones.*.....60

Figure 3.4: *Behavioural factor analysis of cocaine-seeking behaviour metrics across post-conditioning stages.* 63

Figure 4.1: *Five-site tetrode recording.*.....66

Figure 4.2: *Spectral consistency between tetrode LFP recordings.* 67

Figure 4.3: *Coherence between region LFPs.* 68

Figure 4.4: *Example of non-stationary 5 Hz oscillations.* 69

Figure 4.5: *Dummy signal composed of two non-stationary signals.*.....70

Figure 4.6: *Sifting algorithm for IMF extraction.*.....71

Figure 4.7: *Fourier-based filtering vs. empirical mode decomposition.* 72

Figure 4.8: *Applying classical EMD to raw CA1 LFP.* 73

Figure 4.9: *Classic- verses ensemble- empirical mode decomposition.* 74

Figure 4.10: *Dummy signal.*.....75

Figure 4.11: *EMD and eEMD both produce inappropriate decompositions.* 76

Figure 4.12: *Example mask-sifting operation.*.....77

Figure 4.13: *Mask Frequency optimisation intuition.*.....79

Figure 4.14: *Mask frequency optimisation algorithm for example CA1 LFP data.* 80

Figure 4.15: *Example region-tailored mEMD extraction.*.....81

Figure 4.16: *Cell spiking validation of region-tailored IMFs.* 83

Figure 4.17: *Validation of beta, slow- and mid-gamma IMFs by Amy spike train analyses.*..84

Figure 4.18: *Detecting and tracking barcodes.* 87

Figure 4.19: *Barcode visualisation.*.....89

Figure 4.20: *Detected barcodes are robust between animals.*.....90

Figure 4.21: *Barcode 4 interaction profile.* 91

Figure 4.22: *Barcode 7 interaction profile.* 92

Figure 4.23: *Barcode 12 interaction profile.* 93

Figure 5.1: *Beta barcodes show the strongest neural correlate of cocaine-seeking behaviour.* 98

Figure 5.2: *Beta IMF amplitudes show a neural correlate of cocaine-seeking behaviour across regions.*.....100

Figure 5.3: *Beta IMF amplitude modulation by speed across test stages.* 102

Figure 6.1: *Example extracted candidate coupling oscillations by tailored mEMD.*.....106

Figure 6.2: *VTA 4 Hz oscillations exert strong phase modulation and co-ordination of beta amplitudes.*.....107

Figure 6.3: *VTA 4 Hz PAC of supra-theta IMFs is well-tuned to beta.*.....109

Figure 6.4: *Phase amplitude modulation of beta barcodes.* 110

Figure 6.5: *High-PAC VTA 4 Hz cycles more strongly modulate beta barcodes.* 111

Figure 6.6: *VTA 4 Hz phase-specific cycle asymmetry predicts PAC of global beta co-ordination.*.....113

Figure 6.7: *VTA 4 Hz oscillations impose strong modulation of region spiking activities...*114

Figure 6.8: *Opto-tagging assay for VTA glutamatergic and dopaminergic cells.*.....116

Figure 6.9: *Electrophysiological profiling of opto-tagged glutamatergic and dopaminergic VTA cells.* 117

Figure 6.10: *ISI-based VTA cell-type classification.* 118

Figure 6.11: *The putative Glutamatergic cell population are more locked to VTA fast-gamma oscillations.* 119

Figure 6.12: *Putative VTA dopaminergic cells are preferentially tuned to multiregional beta.* 121

Figure 7.1: *Graphical summary of key findings.* 127

Abbreviations

AC	autocorrelogram
amp.	Amplitude
AMPAR	α-amino-3-hydroxy-5-methyl-4-isoxazolepropionic acid receptor
Amy	Amygdala
ANCOVA	analysis of covariance
ANOVA	analysis of variance
BLA	basolateral amygdala
BOLD	blood-oxygen-level dependent
Ca^{2+}	calcium ion
CAMKII	Calcium-dependent protein kinase 2
cAMP	cyclic adenosine monophosphate
COC	cocaine-paired zone
coh.	coherence
COND	Conditioning behavioural stage
CPP	conditioned place preference
CPMR	cocaine-paired memory retrieval
CR	conditioned response
Cre	cre recombinase
CRH	corticotrophin releasing hormone
CS	conditioned stimulus
D_1R	type-1 dopamine receptor
D_2R	type-2 dopamine receptor
DA	dopamine
DAergic	dopaminergic
DAT	dopamine transporter protein
dStr	dorsal striatum
EEG	electroencephalogram
eEMD	ensemble empirical mode decomposition
EMD	empirical mode decomposition
EXT	Extinction behavioural stage (*last 20-minutes*)
fMRI	functional magnetic resonance imaging
freq.	frequency
FSCV	fast-scan cyclic voltammetry
GABA	gamma-Aminobutyric acid
GAD	glutamate carboxylase
Glu	Glutamate
Glu-ergic	glutamatergic

HPC	Hippocampus
ICA	independent component analysis
IMF	intrinsic mode function
ISI	inter-spike interval
LD1	first linear discriminant component
LDA	linear discriminant analysis
LED	light-emitting diode
LFP	local field potential
LTD	long-term depression
LTP	long-term potentiation
mEMD	masked empirical mode decomposition
mPFC	medial prefrontal cortex
NA	noradrenaline
NAc	nucleus accumbens
NMDAR	N-methyl-D-aspartate receptor
PAC	phase-amplitude coupling
PCA	principal component analysis
PD	Parkinson's disease
perc.	percentile
PFC	prefrontal cortex
PIT	Pavlovian-instrumental transfer
PRE	Pre-test behavioural stage
prop.	proportion
PSD	power spectral density
REC	Recall behavioural stage
REN	Renewal behavioural stage
RPE	reward prediction error
SAL	saline-paired zone
SD	standard deviation
SEM	standard error of the mean
SNc	substantia nigra *pars compacta*
spec.	(morlet wavelet) spectrogram
STDP	spike timing-dependent plasticity
Str	striatum
TD	temporal difference
TDE	temporal difference error
TH	tyrosine hydroxylase
tLTD	timing-dependent long-term depression
tLTP	timing-dependent long-term potentiation
TMS	transcranial magnetic stimulation
tSNE	t-distributed stochastic neighbour embedding

UK	United Kingdom
US	unconditioned stimulus
vGluT2	vesicular glutamate transporter
vStr	ventral striatum

1 | Introduction

Charles Darwin's theory of evolution, colloquially referred to as "survival of the fittest", provides an elegant basis to explain the entire spectrum of biological complexity we see today. On Earth, the hallmark of this complexity is of course the human brain. The nervous system acts as an executive agent by which an organism can perceive and proactively interact with its environment such to maximise its chances of reproduction. The fundamental operational principle by which a nervous system is capable of exerting survival-optimised control of the organism's behaviour is its ability to map salient sensory inputs to appropriate behavioural outputs. This neuronal operation is a learning phenomenon – in that the rewarding effects of a "correct" behaviour are used to teach this mapping, such that the behaviour becomes an anticipated, reward-orientated response. At the biophysical level, this mapping is realised by means of neuronal plasticity, which is observed at the cellular level by the addition or removal of neurons, and at the sub-cellular level whereby the weights of synaptic connections between neurons are altered, gained or lost. Conceptually, this neurobiological substrate for storing behaviourally-relevant information can be thought of as a memory. Based on these assertions, the storage of a "memory" can be explained by its long-term utility to the organism in guiding survival-optimising behaviour. The brains of more complex organisms have a larger capacity for memory storage and as such offer a richer diversity of behavioural and cognitive possibilities, which are further prospered through inter- and intra-species competition.

However, in the case of drug addiction, this incredible feat of nature becomes maladaptive. Drugs of abuse, such as cocaine, yield extremely potent effects on the brain's reward system. The resulting reward signals during a cocaine experience produce powerful, long-lasting memories of the contextual landscape and the behavioural patterns which preceded them. Akin to non-pathological mechanisms, cocaine-paired memory retrieval (**CPMR**) encourages the precipitation of behaviours that more likely lead to drug availability (**cocaine-seeking behaviour**). Through repeated reinforcement of cocaine-seeking behaviour by cocaine-taking, the influence that these memories impose on an individual's behaviour and cognition begin to out-compete ones that either support the health of the individual and/or are of more value to society. The eventual domination that cocaine-paired memories have over an individual's

behaviour manifests in clinical addiction, whose consequences can be fatal for an individual and a burden for society. Cocaine sourcing also brings with it some severe ethical issues. The prevalence of cocaine use and addiction has thus prompted an important scientific mission in understanding its neurological basis, with the aim of developing effective therapeutic interventions.

Behavioural studies in rodents have largely contributed to the psychological framework used to explain drug-seeking behaviour and the development of addiction. Combining these assays with brain lesion techniques has implicated specific brain regions to psychological components of drug learning. A handful of more sophisticated studies have looked to investigate the electrophysiological dynamics of brain regions in relation to drug-seeking behaviour. These studies mostly considered a single, or pair of regions in isolation. While indeed helping to elucidate the neural dynamics of drug-paired memory, this design inherently neglects the notion that the retrieval of such a multimodal memory is facilitated by a much more complex pattern of interactions across multiple brain regions.

This thesis is placed to contribute to this niche by extensively exploring global neuronal dynamics across multiple brain regions in relation to CPMR. While the most damaging cases in society are of course at the extreme end of uncontrolled drug search and use [addiction], it makes scientific sense to focus this investigation on the initial formation of cocaine-paired memories: to ask how initial experiences of drug use yield memories that ultimately may eventually lead to addiction. This first chapter introduces some key concepts and experiments that have contributed to our understanding of cocaine-seeking behaviour and its supporting neural circuitry – and finally the neural basis by which these circuits interact to support (cocaine-related or otherwise) memory retrieval and behaviour.

These psychological and neurophysiological frameworks were used to inform the design of an experiment exploring multiregional neural correlates of CPMR (the details of which are outlined in **Chapter 2**). **Chapter 3** describes the "pseudo-instrumental" paradigm I developed to model dynamic cocaine-seeking behaviour in mice and explores some behavioural analytics used to measure cocaine-seeking behaviour. During this protocol, electrophysiological recordings were performed from five brain regions central to memory-guided behaviour. **Chapter 4** presents an analytical pipeline used to represent the frequency content of the local field potential signals recorded from these regions, and then to detect fine-scale interaction

dynamics ("**barcodes**") between these regions and frequency components. In **Chapter 5**, I relate these statistical descriptions of multiregional neural dynamics to the cocaine-seeking behaviour model, revealing an apparent specific role of beta band (15–25 Hz) global co-ordination patterns. Finally, in **Chapter 6**, I explore how beta co-ordination may be orchestrated by both temporal and cell-type specific mechanisms.

1.1| Psychological framework for reward-orientated behaviour

I will first outline some key psychological theories surrounding behavioural learning, ending by exploring how this framework has guided the development of behavioural models of cocaine-seeking behaviour.

Pavlovian and instrumental conditioning

As outlined, to optimise survival and proliferation of the organism, behaviour must be centric on maximising reward.[1] For this to manifest, two distinct learning processes, both centric on reward association, must be engaged during rewarding experiences. Pavlovian conditioning (also known as classical conditioning) refers to the association made between an environmental stimulus, known as a conditioned stimulus (CS), and an innately rewarding stimulus, known as the unconditioned stimulus (US). The result of Pavlovian conditioning is seen when a conditioned response (CR), an automatic, innately US-associated reflex, is elicited by CS presentation alone. Such a reward-paired stimulus typically precedes the occurrence of the reward (temporal contiguity) and is temporally correlated with its delivery (predictive contingency) (Everitt and Robbins, 2005). This learning phenomenon was famously described by Ivan Pavlov, who would ring a bell [CS] before feeding his dog (Pavlov, 1927). Following repeated pairings of the bell with the food reward [US], Pavlov observed that his dog would salivate [CR] after hearing the bell ring. This anticipatory response signified the successful learning of the predictive association between the bell and food, referred to thereafter as a Pavlovian association. Conditioned stimuli, by definition, are initially present some time *before*

[1] Note that while the avoidance of stress constitutes reward in the same way as innately positive experiences, for the purposes of this thesis, this form of "reward" will be not be emphasised.

reward delivery. As such, their predictive value is only realised if the agent perpetuates its behavioural interaction with the CS. The attractive quality inherited by a CS, which guides this perpetuation, is referred to as incentive salience – and is crucial for adaptive reward-seeking behaviour. Applying this principle to cocaine-seeking behaviour, incentive salience provides an explanation as to why drug-correlated behaviour persists for sustained periods in the absence of drug availability.

The second learning substrate required for reward-orientated behaviour (not to be confused with *automatic* incentive salience-evoked Pavlovian behaviour) is the association between the reward and the conscious action which directly led to its administration. This process is known as instrumental conditioning (also known as operant conditioning) and was classically demonstrated by Burrhus Skinner, who invented a behavioural apparatus specifically designed to explore behavioural reinforcement in the rat (APA Dictionary of Psychology, n.d.). Owing to its success, this apparatus became known as the "Skinner box" – and is a popular experimental model to this day. Here, a rat is placed in the box containing a lever. When this lever is pressed, a food pellet reward is dispensed. While the animal receives no explicit training, the sequential coincidence between a lever-press and subsequent reward delivery is thought to reinforce lever-pressing. This principle of behavioural reinforcement is regarded as the process of instrumental conditioning (Skinner, 1930). A simple graph of the lever-pressing rate as a function of time illustrates the learning progression of this instrumental response **(Figure 1.1**). This curve is also predicted by theoretical frameworks (Rescorla and Wagner, 1972).

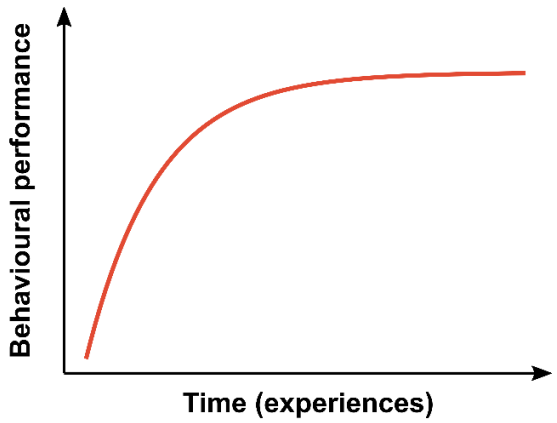


Figure 1.1: *Learning curve.*
Behavioural learning is initially rapid, but incrementally decreases as performance improves.

The utility of an instrumental response is vastly aided by (Pavlovian-mediated) incentive salience, which attracts the agent to a physical state where the reward-obtaining response is now viable. Taking the Skinner box experiment as an example, in a *non-perfect* sense, the perceptual representation of the lever itself acts as a CS, attracting the rat to a location where instrumental lever-pressing is physically possible. I use the term "non-perfect" as the lever only weakly qualifies as a CS (Rescorla, 1988; Everitt and Robbins, 2005): *within the box*, the lever offers no more predictive contingency than any other stimulus in the box (e.g. the wall). To model a true CS, reward availability should be transient, and cued by a preceding discrete stimulus, such as a light or tone. It logically follows that this reward-paired CS offers performance utility to the instrumental response. This has been empirically demonstrated in rats in a simple two-lever choice task (Cardinal et al., 2000). In this experiment, pressing one of these levers would immediately deliver a single food pellet reward, and pressing the other would deliver four pellets – but only after a specified delay period. Pairing this delay period with a light-CS enhanced the rats' ability to make the more economical delayed-response choice. This emergent interplay between Pavlovian and instrumental associations that are linked to the same reward is known as Pavlovian-instrumental transfer (PIT) (Everitt and Robbins, 2005).

Context-dependent behaviour

Pavlovian and instrumental learning mechanisms offer a parsimonious explanation for the emergence of sophisticated behavioural programmes which effectively result in reward delivery. However, such cue-evoked behaviour may not always be appropriate. appetitive behaviour as an example, there exist physical and cognitive factors which would suggest the discontinuation of food ingestion. Interoceptive signals, such as satiety (Kanoski et al., 2007) or stress (Hernández Ruiz de Eguilaz et al., 2018), will devalue the magnitude of the food reward representation. More abstractly, a complex logical signal may suggest greater value in discontinuing "myopic" appetitive behaviour for a more long-term reward, perhaps of a different nature (Coricelli et al., 2007). Or, under certain environmental settings, CS presentation may no longer lead to the food reward (Bouton, 1993). These forms of information mechanistically share the ability to disambiguate the salience of the CS. Psychologists use the umbrella-term "context" to refer to these informational modalities, which exist cognitively at a higher level than the CS representation (Bouton, 2004).

Experimentally, the last of these examples is most easily manipulated. Returning to the CS cued Skinner box example, after the acquisition of operant response behaviour in "box-A", the rat can then be placed in "box-B", which is geometrically-identical to box-A, but consists of a new environmental context – for example, a different floor texture. As well as this, lever-pressing in box-B will not result in reward delivery. Operant lever-pressing will initially persist in box-B, but eventually diminish as the instrumental response is no longer rewarded. This process is known as extinction. Early learning theories which adequately account for extinction predict the degradation of this learning (Rescorla and Wagner, 1972; McCloskey and Cohen, 1989), such that if the reward becomes again available (e.g. the rat is returned to box-A), operant responding must be re-learnt. However, it is empirically (and perhaps intuitively) obvious that this is not the case (Rescorla, 2001; Myers and Davis, 2002). In this thought-experiment, when the rat is re-exposed to box-A, operant lever-pressing will return showing minimal signs that this involves re-learning (Bouton and Peck, 1989). This particular example of the restoral of extinguished behaviour by contextual manipulation is known as "ABA" renewal (Bouton, 2004). Renewal is also clearly evidenced by ABC manipulations (Bouton, 1993; Khoo et al., 2020). Less-robustly, but nonetheless undeniably, it is also seen in ABB (Khoo et al., 2020) and AAA (Bouton, 2002) paradigms. These more counter-intuitive observations can be explained by other cognitive (e.g. timing-related, or for lack of a better term, "try just in-case"-type) signals, which exert more behavioural influence in renewal; despite the physical identicalness between the extinction and renewal contexts (Bouton, 2004). The re-emergence of extinguished behaviour is also evidenced in alternative circumstances, for example, with varying delay periods following extinction, or following an encounter with a relevant stimulus (Bouton, 2004). These variants each fall under different terminology, but for the purposes of this thesis, will not be dwelled upon. The renewal effect exemplifies an important aspect of cocaine-seeking behaviour: these potentially damaging behavioural programs are not ever erased following periods of abstinence (Childress et al., 1988; Girardeau et al., 2019), and will potently re-emerge following prolonged periods of dormancy. Indeed, cocaine addiction-relapse rates after drug rehabilitation are around 60% in the UK (UK drug situation report, 2019). While the more progressed stages of drug addiction are beyond the realms of this thesis, the dynamic expression of cocaine-seeking behaviour by extinction and renewal indeed applies to its early stages, and is thus a crucial element to consider.

Modelling cocaine-seeking behaviour in rodents

Discussed later in **1.2**, dopamine is the key neurochemical substrate by which reward is "represented" in the brain, and as such facilitates the Pavlovian and instrumental mechanisms of reward-orientated behaviour. Owing to its potent activation of the brain's dopaminergic system (Lacey et al., 1990), cocaine use forges powerful Pavlovian associations with drug-paired stimuli and contexts, and produces stubborn behavioural habits correlated with drug interaction. The two fundamental behavioural components of these habits are drug-seeking and drug-taking behaviour. These are respectively supported by Pavlovian and instrumental processes (Everitt and Robbins, 2005), and typically are modelled separately in rodents.

Cocaine-seeking behaviour is elicited by conditioned stimuli which acquire incentive salience after being paired with cocaine experience. The simplest and most popular method to provide this experience to a rodent is by an intraperitoneal injection of a saline solution containing the drug, and to pair this with specific environmental cues. This approach neglects the reward-*taking* aspect of cocaine use, as the animal has no behavioural control over the timing of drug delivery. Therefore, cocaine experience induction by the experimenter will only enforce cocaine-*seeking* behaviour. Cocaine has a biological half-life in mammals of roughly one hour (Zimmerman, 2012), meaning that compared to more transient rewards (e.g. sugar), a much longer time period defines the potential Pavlovian conditioning window.

Cocaine-seeking behaviour is commonly modelled in rodents by the conditioned place preference (CPP) assay (Rossi and Reid, 1976; Mueller and Stewart, 2000; Cunningham et al., 2006; Prus et al., 2009; Huston et al., 2013). Here, the rodent explores two environments, connected by either a small runway or a simple entry/exit hole. The two environments are perceptually distinct – this could be defined by their, for example, spatial geometry, colour, or odour. After habituation, the baseline preference the animal shows to explore one environment over the other is recorded in the "Pre-test". Next, in the conditioning stage, one of the environments is selected to be paired with a cocaine injection (typically between 5-20 mg kg^{-1}), and the other with saline solution at a separate timepoint. The chosen environment for each injection is determined by one of two ways. In the counterbalanced method, the cocaine environment is pre-designated for each animal in the cohort, such that half the cohort experience cocaine in one environment, and the other half in the second environment. More commonly used is the reverse conditioning method, where the environment which was less-

preferred in the Pre-test is paired with cocaine. In a single conditioning session, the animal is allowed explore one of the environments (with the exit closed-off), typically for 30-60 minutes after receiving an injection of the designated drug. Saline- and cocaine-conditioning sessions are interleaved, occurring either on the same day (saline being first to avoid conditioned aversion from the withdrawal effects of cocaine (Prus et al., 2009)), or instead separately over two days. After a designated number (typically 2-3) of conditioning "blocks" [one saline, one cocaine], the animal is re-subjected to the joined environments, and its place preference assessed just as it was in the Pre-test. Cocaine-seeking behaviour is observed as an increased preference of the animal to explore the cocaine-paired environment. Using the context-dependent principles described above, the extinction dynamics of cocaine-CPP behaviour and drug-primed reinstatement have also been investigated (Mueller and Stewart, 2000; Brenhouse and Andersen, 2008; McKendrick and Graziane, 2020).

Relating this behaviour to psychological principles, the expression of cocaine-CPP is typically explained by incentive salience-induced approach behaviour to the drug-paired environment (Bolles, 1972; Bindra, 1974). However, it is very likely that a more complex set of psychological and behavioural mechanisms are at play (discussed by Huston et al., 2013). While less empirically tractable, it is theoretically possible that instrumental processes also contribute to cocaine-CPP behaviour – i.e. specific behavioural sequences specific to the cocaine environment that were engaged during cocaine conditioning will be reinforced and subsequently encouraged in the subsequent preference test. Also, the *direct* actions of cocaine on behaviour (most notably, hyperlocomotion) will also precipitate by Pavlovian mechanisms in the cocaine paired environment post-conditioning (Carey and Damianopoulos, 1992; Carey et al., 2005). These additional and *valid* explanations prompt the notion that the modelling of cocaine-seeking behaviour[2] is inherently complex; perhaps warranting additional analytical approaches that are less categorically explicit. Another component of cocaine-seeking behaviour I will introduce here briefly is that of second-order reinforcement. This paradigm demonstrates that cocaine-seeking behaviour may be elicited by a stimulus which was never directly associated with drug experience, but was previously paired with a stimulus which then became conditioned to cocaine (Arroyo et al., 1998; Childress et al., 1999; Grant et al., 1996; Stewart et al., 1984). Such a paradigm has relevance for cocaine-seeking behaviour in humans.

[2] or any for that matter

For example, an individual is more likely to accept a party invitation [second-order CS] following an initial cocaine experience [US] at a previous party [CS].

1.2| Neural representation of reward and cocaine

The empirical and theoretical framework outlined in **1.1** provided the backbone by which these mechanisms of learning, which are "hijacked" by cocaine, could be mapped to neural substrates. Psychological and theoretical work posited that behavioural learning and performance is orientated by reward. This motivated the search for a neural mechanism which reflected this principle. The neurotransmitter, dopamine, robustly emerged as the central substrate that supports the learning of reward-guided behaviour. Owing to the scientific impact of these pioneering studies, (and probably, more sadly, to the societal impact of cocaine), this knowledge is widespread amongst the general population. This sub-chapter will discuss the famous experiments of Wolfram Schultz and others which provided key evidence that dopaminergic neurons showed properties emulating that of a reward prediction error signal. After discussing these observations and later work which built on these claims, we will then consider cocaine's biochemical interactions with dopaminergic and other pathways, combining this with the ideas outlined in **1.1** to explain why cocaine is such an addictive and dangerous drug of abuse.

Reward prediction and the temporal difference algorithm

Learning performance curves (**Figure 1.1**) and theoretical frameworks (McCloskey and Cohen, 1989; Rescorla and Wagner, 1972) reveal a hyperbolic relationship between time and performance – in that learning rate incrementally increases rapidly at first, but as optimal performance is approached, this gradient converges to zero. This makes logical and practical sense: an unexpected reward is as such because its statistical relationship with the environment and the actions of the agent has not been learned. Optimising reward-guided behaviour underpins evolutionarily driven survival, and as such, the learning of *more unexpected* rewards should impose priority on the neural system. This principle is neatly demonstrated empirically by the phenomenon of blocking (Williams, 1975). Consider again the light-cued Skinner box

experiment. Over time, the animal learns the relationship between the light cue and food pellet availability; which imposes increasingly more accurate control over lever-pressing. Now suppose that a second CS is introduced after this learning has become asymptotic: an auditory tone, which is temporally concurrent with the light cue [and reward]. Following a series of these so-called "compound pairings", responding is now tested[3] for each of these conditioned stimuli individually. The original light CS elicits operant responding reminiscent the CS-US relationship being successfully learned. However, this is not observed for the tone CS; which elicits minimal responding (if any). While the predictive capacity of each CS is equal, as the prior CS was already capable of precipitating accurate operant behaviour, there is no "surprise" about the reward outcome, thus no "survival benefit" in learning about the second CS-reward relationship: CS-1 "blocks" Pavlovian learning of CS-2.

To be put explicitly, the encountering of a reward dictates the degree of learning according to the magnitude of the reward and how poorly it was predicted. Inspired by these principles, the temporal difference (TD) algorithm comprises a simple set of equations developed to model the Pavlovian and instrumental processes of reward learning (Sutton, 1988). The details are unnecessary for the purposes of this thesis, so I will provide a brief outline, which is schematically illustrated in **Figure 1.2**. At a given time t, the neural representation of the environment (including anything that could be theoretically predictive of the reward) is given by the vector $\boldsymbol{x}(t)$. This sensory signal estimates the magnitude of reward $\hat{V}(t)$, defined as the discounted sum of future rewards. Computationally, this estimation yielded from $\boldsymbol{x}(t)$ is performed in the network by means of adaptable weights ($\boldsymbol{w}$) [synapses], which transform the sensory vector $\boldsymbol{x}(t)$ into the reward estimation $\hat{V}(t)$. The unexpectedness of the true, "experienced" reward signal, $V(t)$, is known as the temporal difference error, $\delta(t)$:

$$\delta(t) = V(t) - \hat{V}(t)$$

According to classical learning theory (Rescorla and Wagner, 1972) and as just logically outlined, learning should be emphasised when the TD error is high, such that upon future iterations, $\hat{V}(t)$ becomes increasingly closer to $V(t)$:

[3] here, the food pellet is unavailable.

$$\delta(t) \to 0$$

Here lies a puzzling paradox with reward prediction learning, known as the "distal reward problem" (Hull, 1943): how can the TDE signal drive learning about a CS which occurred in the past? The TD algorithm offers an elegant solution to this problem as follows. The reward representation magnitude $V(t)$ is defined as a discounted sum of future rewards:

$$V(t) = E[\gamma^0 r(t) + \gamma^1 r(t+1) + \gamma^2 r(t+2) + \cdots]$$

$$V(t) = E[\gamma^0 r(t) + V(t+1)]$$

where the value of γ^t exponentially decreases as $t \to \infty$, and E is the expected value function. Because the reward magnitude $V(t)$ is defined by (current and) past information, the TDE $\delta(t)$ represents a surrogate prediction of future reward – meaning that the updating of the weight vector $\boldsymbol{w}$ is influenced by future expectation. Thus, the same sensory representation evoked on a later, separate occasion $x(t')$ will elicit a stronger prediction of $V(t'+1)$. This mathematical assumption underlies the basis by which an encountered CS can be mapped to the expectation of a future US, and elicit appropriate Pavlovian and instrumental responding.

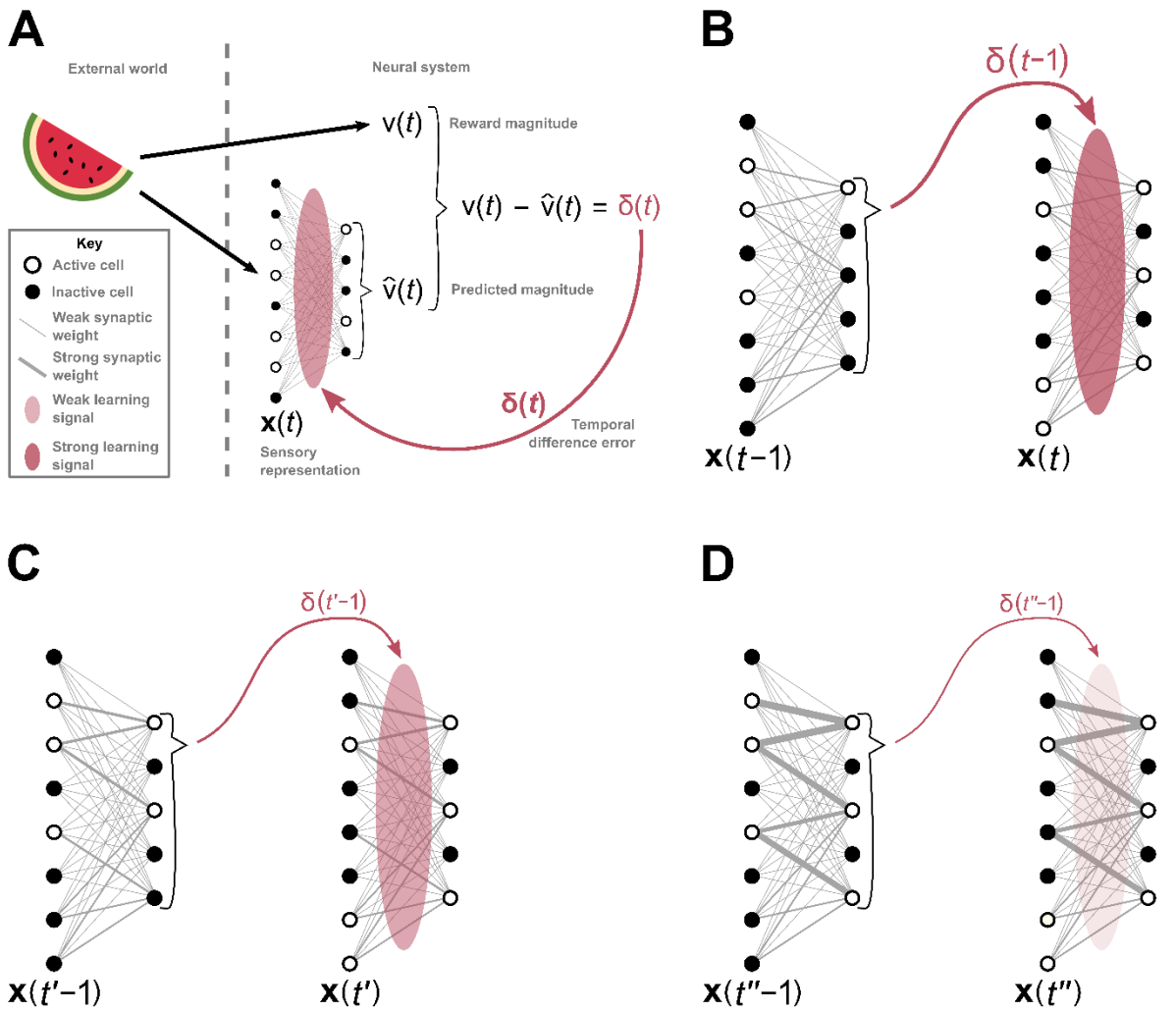


Figure 1.2: *Temporal difference (TD) learning.*

A: Key components of the TD algorithm. At a given instance (t), the temporal difference error (TDE) $\delta(t)$ is calculated as the difference between the predicted and actual magnitude of the reward experienced. The TDE is delivered (red oval) to synaptic targets of the sensory representation signal $\boldsymbol{x}$. Stronger TDE signals impose greater potentiation to the synaptic weights corresponding to current and past sensory representations. **B-D:** TD learning schematic. During early reward experiences (**B-C**), relevant synapses are strongly potentiated by the TDE signal, such that sensory representations that exist before the peak of the reward are able to elicit a stronger reward expectation and thus a lower TDE signal.

Dopamine as a reward prediction error signal

The elegance and theoretical validity of the TD algorithm makes it an attractive solution to the distal reward problem. Centric to this learning framework is the temporal difference error, more commonly known in the context of neuroscience as the reward prediction error (RPE) signal (Schultz et al., 1997). In a landmark experiment, Wolfram Shultz recorded from histologically- and pharmacologically validated dopaminergic (DAergic) neurons in the substantia nigra pars compacta (SNc) (and later also from the ventral tegmental area (VTA) (Schultz and Romo, 1990)) from the awake monkey in a stimulus-cued operant experiment (Schultz, 1986). Strikingly, the most typical firing response profiles of these DA-releasing neurons mimicked the properties of the RPE signal predicted by the TD algorithm. Firing would originally increase in response to the delivery of the unexpected reward (and *not* to the movement itself). Following learning, the firing-rate increase instead become locked to the onset of the CS. When the US was abruptly removed, the firing-rate of DAergic cells would decrease at the time where the reward was anticipated (**Figure 1.3**). This result has been reproduced across species and causally validated by optogenetic methods (Ljungberg et al., 1992; Chaudhury et al., 2013; Han et al., 2017; Fischbach-Weiss et al., 2018; Lak et al., 2020).

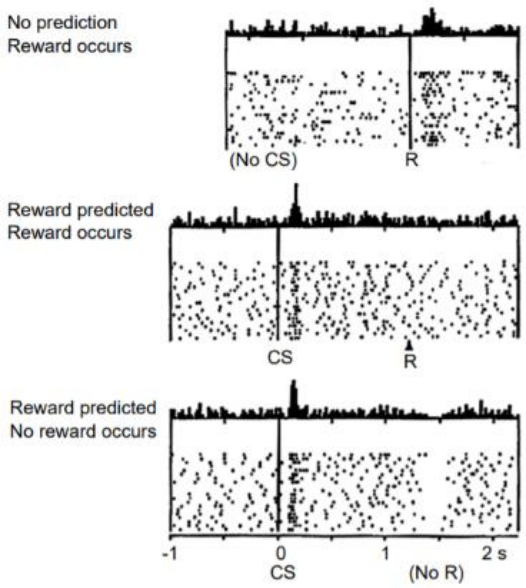


Figure 1.3: *Example putative dopaminergic neuron firing responses to CS and reward.* From Schultz et al., 1997.

The firing tendencies of DAergic neurons in response to conditioned- and unconditioned stimuli posit DA as a neural substrate which acts as an RPE signal. To fully accept this premise, DA should also satisfy the following:

(i) it should relate to the receipt of reward;
(ii) it should be delivered to necessary (reward-driven) learning sites;
(iii) it should be able to modify synaptic weights in a manner which is computationally in-line with the TD algorithm.

The first condition is well-evidenced by the experiments of Schultz and others as outlined above. Supplementing this, the ventro-medial counterpart of the SNc – the ventral tegmental area (VTA), is more strongly related to reward processing (Düzel et al., 2009; Krebs et al., 2011; Pignatelli and Bonci, 2015). In an extensive viral vector-assisted input–output mapping study of the mouse brain (Beier et al., 2015), the VTA was found to receive synaptic inputs from a range of sites that could provide relevant information about reward, including higher visual and valence-related cortical areas. Satisfying the second condition, and in-line with other studies, a considerable proportion of DAergic VTA cells which received these inputs project themselves to a wide range of computationally-relevant brain regions – including the amygdala (Amy) (Bissière et al., 2003), nucleus accumbens (NAc) (Yang et al., 2018; Heymann et al., 2020), medial prefrontal cortex (mPFC) (Pawlak and Kerr, 2008) and hippocampus (HPC) (Zhang et al., 2009; McNamara et al., 2014). The importance of these regions in mediating reward-orientated behaviour – with relevance to cocaine-seeking behaviour, is detailed in **1.3**.

Regarding the final condition, let's remind ourselves of the computation which the RPE signal must inform. According to the TD model (Sutton, 1988), the neural CS representation elicits a prediction of future reward availability via a modifiable weight transformation vector. Through the adjustment of these weights, this prediction is guided by iterative interactions with TDE signals to result in accurate anticipation of future reward. At the physical level, these adjustable weights are embodied by synapses in the brain. This knowledge first came to light from the discoveries that the synaptic weight between an afferent [sender] and efferent [receiver] neuron can both increase (long-term potentiation; LTP) (Bliss and Lomo, 1973) and decrease (long-term depression; LTD (Dudek and Bear, 1992). At the molecular level, these plasticity processes both typically depend on the calcium (Ca^{2+}) -permeable N-methyl-D-aspartate receptor (NMDAR) (Collingridge et al., 1988, 1983; Dudek and Bear, 1992). Ca^{2+} has been

well-attributed to the induction of LTP and LTD, which as a "rule-of-thumb" and amongst other mechanisms, are mediated via Ca^{2+}-dependent protein kinase 2 (CAMKII) (Baimbridge and Miller, 1981; Lynch et al., 1988; Lisman et al., 2002) or Ca^{2+}-dependent protein phosphatase (Huang et al., 2001; Kang-Park et al., 2003), respectively.

While the discoveries of LTP and LTD relied on rather "artificial" stimulation protocols, the most physiologically- and theoretically-motivated plasticity-inducing protocol is seen in spike timing-dependent plasticity (STDP) (Magee and Johnston, 1997; Markram et al., 1997; Bi and Poo, 1998). Elegantly emulating Donald Hebb's famous "fire together, wire together" postulate (Hebb, 1949), STDP refers to the associativity between two afferent neurons (neuron-A and neuron-B) whose spike trains have a consistent and delayed temporal relationship and both synaptically target the same efferent neuron. In the simplest case, where both afferent neurons are glutamatergic, the STDP phenomenon can be explained when the excitatory post-synaptic potential caused by neuron-A depolarises the efferent neuron such that the extracellular magnesium-block on its NMDARs is repelled, meaning that if neuron-B fires soon after, the glutamate molecules it releases are able to elicit a Ca^{2+} current via NMDAR activation, inducing calcium-dependent synaptic plasticity (Baimbridge and Miller, 1981; Bliss and Collingridge, 1993). Both the extent and direction of this plasticity is dependent on the time delay of glutamate release between the pair of neurons. Intuitively, these effects are sometimes referred to as timing-dependent potentiation (tLTP or tLTD). This phenomenon underpins the fact that there exist a variety of "critical windows" for STDP, depending on the pairs of neurons considered (Caporale and Dan, 2008) (**Figure 1.4**). Such a "palette" of STDP formulations makes for an elaborate synaptic basis by which time-delayed sensory and rewarding events can be neuronally connected.

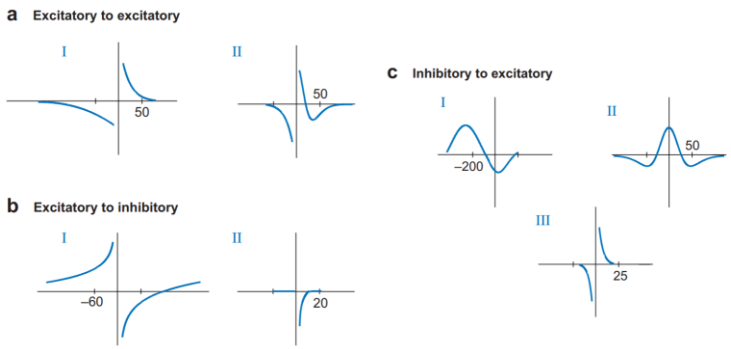


Figure 1.4: *Diversity of STDP windows.*

X-tick values are in milliseconds. The y-axis represents the magnitude of plasticity induced. (from Caporale and Dan, 2008).

In the context of distal reward prediction, when a reward is unexpected, the RPE is high, thus weights corresponding to recently-experienced (i.e., predictive) sensory information should be increased, such that next time this predictive sensory representation is able to elicit a greater reward prediction, thus a lower RPE. By this logic the reward expectation signal evolve to temporally lock to the onset of the true CS and match the true discounted reward value. We should thus ask the crucial question: does the delivery of dopamine [RPE] affect STDP in a way that enhances this process? The (*beautifully*) satisfying answer is yes.

DA exerts its action through G-protein-coupled receptors, the most common being D_1- (D_1R) and D_2 receptors (D_2R). The mechanisms of activation of these receptors by DA is antagonistic: D_1Rs are G_s–coupled, and D_2Rs are G_i–coupled, meaning they respectively activate and inhibit the generation of cyclic adenosine monophosphate (cAMP) (Neve et al., 2004). Intracellular cAMP increase activates a cascade of biochemical pathways linked to synaptic plasticity processes (Lisman et al., 2002; Nguyen and Woo, 2003; Waltereit and Weller, 2003; Kandel, 2012; Park et al., 2014). Inhibition of D_1Rs and/or D_2Rs reveal that DA is necessary for STDP in the Amy (Bissière et al., 2003), dStr (Shen et al., 2008), NAc (Ji et al., 2017), and PFC (Pawlak and Kerr, 2008). In these studies, the precise mechanisms by which DA mediated STDP was circuit-dependent, owing to the differences in the information processing of these regions and their computational requirements (discussed in **1.3**). A study by Zhang et al. (2009) revealed a slightly different story in the HPC. Unlike in the aforementioned regions, STDP *was* able to occur in hippocampal tissue in the absence of DA. However, DA was shown to dramatically extend the critical STDP window – and reverse the potentiation effect to a positive one for negative input-timing pairings. This study additionally showed that DA availability in the HPC decreased the number of pairings required to elicit Hebbian associativity by STDP. This result suggests a more computational role of the HPC in actively "unwriting" information which does not predict a reward. Upon delivery of DA, ongoing hippocampal representations become serialised, such to bias the *rapid* formation of mnemonic representations towards ones which are salience-predicting.

Other synaptically-acting substances, such as noradrenaline (NA) - which is more intimately connected to external behaviour , also enhances synaptic plasticity (Cahill and McGaugh, 1996; Robbins and Roberts, 2007). This "fight or flight" signal is also activated by cocaine; and indeed has been linked to the promotion of cocaine-seeking behaviour (Weinshenker and Schroeder, 2007; Otis and Mueller, 2011). In this next section, we will consider the

biochemical actions of cocaine, and how these dramatic effects to neurochemical states impact on long-term memory processing and behaviour.

Neuropharmacology of cocaine

The interaction cocaine has with the DAergic system has been known for some time – and indeed complemented the DA hypothesis of reward prediction error. Cocaine has a rapid onset of delivery to the brain, with peak dopamine-related effects being observed as quickly as four minutes post-intravenous administration (Fowler et al., 1989; Stathis et al., 1995). In line with the theoretical models discussed (Rescorla and Wagner, 1972; Sutton, 1988), the short delay between cocaine-taking behaviour and cocaine-induced reward more readily promotes the reinforcement of such behaviour. By the same token, conditioned stimuli which are paired with cocaine availability are more easily mapped to cocaine-induced reward by temporal difference learning. Re-exposure to cocaine-paired stimuli will hence more strongly elicit cocaine-seeking behaviour, and via PIT does this enhance the probability of cocaine-taking (Everitt and Robbins, 2005).

Cocaine's primary pharmacological actions are exerted on the dopamine transporter protein (DAT), which is found on the synaptic release terminals of DAergic neurons (Iversen, 2006). This was neatly demonstrated by Ritz et al. (1987), who used [^{3}H]mazindol, a radio-labelled competitive DAT inhibitor (Javitch et al., 1984), to estimate the extent of DAT inhibition by cocaine, and, incorporating data from other operant studies, found a linear relationship between DAT inhibition and operant cocaine self-administration. Supporting this, DA concentration measurement studies using microdialysis have revealed a linear relationship between cocaine bioavailability and synaptic DA concentration (Church et al., 1987; Nicolaysen et al., 1988). The direct relationship between cocaine's inhibitory action on DAT and its reinforcing operant properties was also demonstrated by Spealman et al. (1991), who compared cocaine to the analogue, 2 beta-carbomethoxy-3 beta-(4-fluorophenyl)tropane, which is roughly six-fold more pharmacologically potent. In an operant self-administration experiment, the level of instrumental responding for the analogue was also roughly six-times larger, mirroring its enhanced inhibitory action on DA reuptake. While the pharmacological actions of cocaine have since been found to also be exerted at other molecular sites (e.g. Wang et al., 2007), the addictive properties of cocaine are most strongly been attributed to DAT inhibition (Kuhar et

al., 1991). Increasing the availability of DA in this way enhances both the magnitude and prevalence of the RPE signal, meaning that neural representations of environmental stimuli which are temporally correlated with cocaine delivery develop stronger reward prediction abilities and in a more rapid fashion. The re-exposure to such stimuli invokes "cocaine-paired memory retrieval" (CPMR), activating reward expectation pathways and precipitating cocaine-seeking behaviour.

1.3| Brain regions supporting cocaine-seeking behaviour

In this penultimate introductory section, we consider some of the key brain regions which are implicated in memory-guided behaviour, exploring how their computational roles relate to CPMR and cocaine-seeking behaviour.

The ventral tegmental area (VTA)

As already alluded to, the ventral tegmental area (VTA) comprises a key locus of DAergic neurons, which innervate a diverse array of anatomically- and computationally distinct brain regions (Beier et al., 2015). VTA activity is enhanced during the processing of rewarding events (Düzel et al., 2009), and indeed during cocaine anticipation and -experience (Breiter et al., 1997). These observations are distinct from the inhibitory DAT model of cocaine action (Ritz et al., 1987; Kuhar et al., 1991), and are most parsimoniously explained by the inhibitory actions of dopamine and cocaine at GABAergic synapses onto VTA DAergic neurons (Cameron and Williams, 1994; Ye and Ren, 2006; Hoerbelt et al., 2015). More specific to cocaine, rodent studies point towards a rapid and persisting cocaine-induced sensitisation of VTA DAergic neural activity. Cocaine has been shown to block the potentiation of inhibitory GABAergic inputs to DAergic VTA cells (Nugent et al., 2007), thus increasing VTA DAergic excitability. Additionally, glutamatergic synaptic inputs to DAergic VTA neurons undergo LTP after just a single exposure to cocaine (Ungless et al., 2001). This rapid plasticity effect is dependent on reduced GABA activity (Liu et al., 2005) and is mediated by Ca^{2+}-permeable GluA2-AMPARs (Bellone and Lüscher, 2006). These results offer a plasticity-based explanation for the persistence of cocaine-seeking behaviour (Lüthi and Lüscher, 2014). Via

the powerful induction of VTA DAergic sensitisation, cocaine-paired sensory representations, which indeed target DAergic VTA cells (Beier et al., 2015), more strongly induce DAergic activation [incentive salience], and enforce greater dictatorship of cocaine-seeking behaviour. Supporting this claim, GluA2-lacking mice (whose VTA synapses are thus incapable of cocaine-induced plasticity (Bellone and Lüscher, 2006)) do not express cocaine-seeking behaviour in the CPP assay (Dong et al., 2004).

The nucleus accumbens (NAc)

DA is released in the NAc by the VTA via the mesostriatal pathway. Ninety-five percent of cells in the NAc are GABAergic medium spiny neurons (MSNs), which typically express either D_1- or D_2 receptors (Kupchik et al., 2015). So-called D_1-MSNs and D_2-MSNs both back-project to the VTA, primarily targeting GABAergic interneurons (Xia et al., 2011). Immunotoxic, immunohistochemical and optogenetic methods have linked both these cell types to reward-guided motivational behaviour (Kai et al., 2015; Durst et al., 2019; Tye et al., 2013; Soares-Cunha et al., 2020). Stereotactic lesions targeted to the NAc yield impairments in Pavlovian and instrumental responding [PIT] to an amphetamine[4]-conditioned stimulus (Parkinson et al., 1999). This effect is D_1R-dependent, and attributed to the core region of the NAc (NAc-c), whereas the shell region of the NAc (NAc-s), which receives much more cortical and limbic input (Li et al., 2018), is more involved in sustaining drug-seeking behaviour (Dalley et al., 2005). These studies posit an important role for the NAc in translating reward-predicting information into corresponding behaviours which increase the likelihood of drug re-encountering.

Mesostriatal DA release in the NAc by the VTA is indeed enhanced by drugs of abuse, such as cocaine (Di Chiara and Imperato, 1988). This drug-amplified RPE signal has been shown to evoke long-lasting synaptic changes which neatly explain the persistence and exaggeration of cocaine-related behaviour after long periods of drug unavailability – termed "Incubation of cocaine craving" (Terrier et al., 2016). A final consideration which posits the NAc as a crucial substrate for cocaine-related behavioural precipitation, is its anatomy. Receiving major inputs from (amongst others) the hippocampus (HPC), medial prefrontal cortex (mPFC) and basolateral amygdala (BLA) (Li et al., 2018), the NAc is well-placed to act as a "corticolimbic-

[4] Amphetamine is a pharmacologically-similar compound to cocaine (though less potent) (dela Peña et al., 2015).

motor hub", integrating multimodal, drug-related information represented by these regions in order to bias the selection of behavioural programmes in favour of ones which are more correlated with drug expectation (Groenewegen et al., 1996; Everitt et al., 2001).

Amygdala (Amy)

The amygdala (Amy) is a key brain region involved in the processing of emotional information. This function of the amygdala has been elucidated by human fMRI studies, which have further demonstrated that a variety of drugs used to treat mood disorders strongly interact with the Amy during emotional processing (Harmer et al., 2006; Roseman et al., 2018; Herwig et al., 2019). In-line with these observations, the Amy is activated by corticotrophin releasing hormone (CRH) (Gray and Bingaman, 1996). CRH induces synaptic plasticity in amygdala circuits which, in the pathological case, is thought to contribute to the development of mood disorders (Rainnie et al., 2004; Shekhar et al., 2005). In humans, there exists a high co-morbidity between addiction and mood disorders (Filip et al., 2013). Rodent studies have highlighted stress as an explanatory common denominator. CRH is enhanced during drug withdrawal (Merlo Pich et al., 1995; Pollandt et al., 2006), and is thought to contribute to the reinstatement of drug-seeking and long-term dependence by enhancement of Amy plasticity (Koob, 2009; Roberto et al., 2010). Rodent models of stress and mood disorders have revealed plasticity enhancements which have been mapped to an increased propensity to exhibit habit formation (Taylor et al., 2014) and drug-seeking behaviour (Whitaker et al., 2013).

The Amy has more classically been studied in the context conditioned fear behaviour. Electrophysiological recordings from individual Amy cells suggest an LTP-related mechanism of fear acquisition as seen by increased firing-rate responses to a CS paired with a foot-shock [US] after conditioning. This neural correlate of Pavlovian conditioning likely represents a CS-centric learning mechanism, as it precedes the behavioural expression of conditioned fear (Quirk et al., 1997; Rogan et al., 1997). This putative synaptic mechanism Pavlovian learning is DA-dependent (Rosenkranz and Grace, 2002), and is also evidenced in supporting the acquisition of positive (i.e. rewarding) CS-US associations (Bonnet et al., 2015; Douglass et al., 2017; Fadok et al., 2018). More relevant to this thesis, lesions to the BLA do not affect the acquisition of instrumental cocaine self-administration, but do disrupt maintained conditioned responding by PIT (Whitelaw et al., 1996; See et al., 2003). This result is also seen following

DAergic inhibition in the Amy (Miles et al., 2003). In a similar behavioural paradigm, optogenetic inhibition of glutamatergic BLA projections to either the NAc or mPFC is sufficient to block the reinstatement of cued cocaine self-administration in rats (Stefanik and Kalivas, 2013). These data posit the Amy as an important circuit for storing Pavlovian drug associations which are necessary to maintain cocaine-seeking behaviour via downstream interactions long enough to obtain the drug.

Hippocampus (HPC)

The role of the hippocampus (HPC) in memory was famously described by Scoville and Milner (1957), who reported stark memory deficits in patient H.M. following the surgery he received which removed his medial temporal lobe (primarily containing the HPC) to treat his epilepsy. While very distant memories were still perfectly intact, H.M. had very poor recall of more recent ones prior to his surgery, and was unable to form new memories of events thereafter (Scoville and Milner, 1957). This inferred role of the HPC to store and retrieve recent memories is reproduced in rodents in spatial memory tasks (Morris et al., 1982; Bird and Burgess, 2008; Bannerman et al., 2014). Computationally, the CA1 subfield of the HPC is thought to represent the most processed, accessible form of mnemonic information (Rolls, 1996) and as such is a key output field of the HPC. Most famously in rodent electrophysiology, neuroscientists John O'Keefe and his student, Jonathan Dostrovsky discovered so-called "place cells" in the CA1 hippocampal subfield of the rat HPC (O'Keefe and Dostrovsky, 1971). In this hugely influential study, they recorded from cells in the CA1 region and noted a strong proportion had spatially-tuned firing profiles – meaning that they would increase their firing-rate when the animal entered a certain spatial location in the environment. This discovery has inspired the work of countless behavioural experiments and theoretical models of the hippocampus.

To this day, theories of hippocampal function are disputed, but consistent is the idea that the HPC encodes mnemonic information relating to salient experiences, which is used to guide behaviour. Specially relating this notion to cocaine-paired memory, a study by Trouche et al. (2016) used the CPP model of cocaine-seeking behaviour in transgenic mice. This transgenic model allowed the experimenters to define a time-window whereby hippocampal CA1 principal cells which were active in this window would be "tagged" with the inhibitory opsin, ArchT. In the experiment, this time window corresponded to the cocaine conditioning session

– i.e. CA1 cells which were actively engaged in representing the cocaine-paired environment would express ArchT. In the subsequent test, upon photoinhibition of these "cocaine-engram cells", CPP behaviour was abolished. This manipulation demonstrated the necessity of CA1-driven retrieval of cocaine experience in eliciting incentive salience and cocaine-seeking behaviour.

Prefrontal cortex (PFC)

The prefrontal cortex (PFC) can be thought of as a "more conscious" part of the brain – and is associated with higher-order information processing. Human studies have highlighted correlates of PFC activity to complex decision-making and abstract rule-learning tasks (Kennerley and Walton, 2011; Domenech and Koechlin, 2015; Rouault et al., 2019). The medial PFC (mPFC) has been evidenced in rodents (Hardung et al., 2017) and humans (Bechara, 2004; Pompanin et al., 2014) to enforce behavioural inhibition. This operation entails the cessation of automatic, "myopic" reward-seeking behaviour, under the assumption that this will lead to the encountering of a more valuable, distal reward. Damage to the mPFC has been correlated with more impulsive behaviour, which predisposes individuals to a higher risk of developing addiction (Bechara, 2004; MacKillop et al., 2011). In a human fMRI study, transcranial magnetic stimulation (TMS) delivered to the PFC evoked a lower BOLD response in the NAc, but not the dorsal striatum, for cocaine users compared to controls (Hanlon et al., 2016). This result fits with the idea that as drug habits progress, the PFC is able to exert less "executive control" over motivational centres such as the NAc, manifesting in the stubborn formation of drug habits – which become progressively more dependent on the dStr (Everitt et al., 2001; Yin et al., 2004). This loss of executive control can be mechanistically understood from the observations in rodents which have linked repeated cocaine administration to neuroarchitectural changes in the PFC and NAc (Robinson and Kolb, 1999; Kim et al., 2011). By a similar token, contextual representations in the PFC are thought to impose a strong influence on the extinction and renewal of cocaine-seeking behaviour. A variety of inactivation strategies targeted to the mPFC have been demonstrated to yield CS-drug extinction deficits (Groblewski et al., 2012; Groblewski and Cunningham, 2012; Van den Oever et al., 2013). As well as exerting inhibition over NAc-related cocaine-seeking programmes during extinction, the PFC is also evidenced to support the processing of cocaine-related information by a different neuronal rate code during reinstatement (Rebec and Sun, 2005). Taken together, the

higher-order processing capabilities of the PFC place it as an important, dynamic regulator of cocaine-seeking behaviour.

1.4| Neural oscillations and brain synchrony/co-ordination

This introductory chapter has discussed the psychological and neurobiological substrates by which neural systems are able to process and translate multimodal representations of the world into behaviour. Underpinning this operation is the brain-wide integration of information sources. The binding of this information is thought to be physically realised via the co-activations of neurons which, via dopamine-facilitated STDP mechanisms, increase their associativity to bind salient information. In this final section, we will explore how neural oscillations may report these associative processes to mediate the coherent flow of computationally relevant information. In this thesis, I will explore how these macroscopic principles of brain function may bias global network activity during CPMR.

Oscillations report coordinated activity of neural populations

Neural oscillations were first described in the 1920's by Hans Berger, who developed electroencephalogram (EEG) technique to non-invasively record brain activity (Berger, 1929). Readouts of large-scale neural activity, such as EEG, report the summed activity of neural populations at a fine-scale temporal resolution. The existence of neural oscillations, which are robustly seen across species, report rhythmic temporal co-ordination of firing amongst the recorded neural population. As population activity is inherently monitored extracellularly, the *trough* of a recorded oscillatory cycle relates to a transient peak of excitability amongst the recorded neural population. As well as their characteristic **frequency**, oscillations are described by their angular **phase**; where troughs (by convention) correspond to middle of the cycle ($-\pi$ rad. or 180^{o}), and **amplitude**; which relates to the extent of synchronisation amongst the recorded neural population. Recent work also suggests cycle waveform as a fourth feature reporting the underlying neuronal dynamics (Dijk et al., 2010; Jones, 2016; Cole and Voytek, 2017; Schaworonkow and Nikulin, 2019), which can be described by considering the **instantaneous phase** of the oscillation (**Figure 1.5)**.

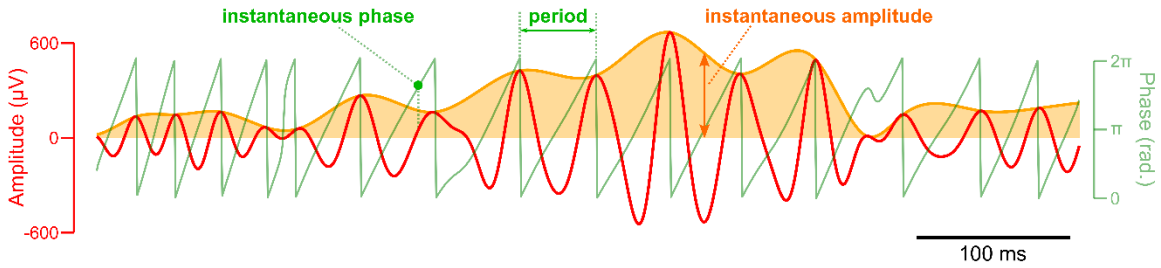


Figure 1.5: *Describing an oscillatory signal.*
The duration of a given oscillatory cycle in a signal (red) is known as the cycle period. The instantaneous phase (green) describes the angular position of the oscillation at a given moment. The instantaneous amplitude (orange) is calculated using the Hilbert envelope, and relates to the magnitude of the oscillation.

Interneurons gate excitability dynamics in oscillating neural networks

Computational and empirical evidence highlights the vital necessity of inhibitory GABAergic interneurons for the emergence of neural oscillations (Lytton and Sejnowski, 1991; Whittington et al., 2000; Buzsáki and Wang, 2012; Nicola and Clopath, 2019). As a crude "rule of thumb", interneurons have local and extensive synaptic connections to both glutamatergic principal cells as well as other interneurons, whereas the glutamatergic principal cell population have global projections to other brain regions, and locally target interneurons exclusively (Klausberger and Somogyi, 2008). Recent work has however also described the existence of cross-regional GABAergic projections between brain regions (Jinno et al., 2007; Sun et al., 2019). Principal cell activation typically leads to glutamate release which causes AMPAR-mediated activation of efferent GABAergic interneurons (Hestrin, 1993). In turn, activated interneurons evoke inhibitory postsynaptic potentials (IPSPs) in their post-synaptic targets, most importantly via $GABA_A$ receptor activation (Johnston and Wu, 1995). These key principles of neural circuit connectomics are computationally necessary for the network to exhibit oscillatory activity.

Functional relevance of neural oscillations in the rodent hippocampus

In rodents, intracranial local field potential (LFP) recordings provide the most common readout of neural population activity by which oscillations can be investigated (Buzsáki, 2004). A classic case-study is the hippocampus – in particular, its CA1 subfield. Extensive anatomical

and electrophysiological observations of the rodent hippocampal network have painted a detailed picture of its cell-type- and connectomic diversity (Klausberger and Somogyi, 2008), which, as emulated by computational hippocampal models (Kiss et al., 2006; Hummos and Nair, 2017; Aussel et al., 2018; Rennó-Costa et al., 2019), give rise to the observed oscillatory phenomena. During active behaviour, theta (4–12 Hz) oscillations dominate the oscillatory readout of the CA1 LFP signal (O'Keefe and Nadel, 1978; Buzsáki, 2002). Nested within individual theta cycles are faster processes spanning the beta (13–25 Hz) and gamma (25–125 Hz) ranges (Bragin et al., 1995; Colgin et al., 2009; Fernández-Ruiz et al., 2017; Lopes-dos-Santos et al., 2018). The amplitude of these faster oscillations is typically stronger at the descending phase of theta. This relationship between theta and gamma is an example of phase-amplitude coupling (PAC). Theta-gamma PAC in the hippocampus has been intensely studied and linked to a wide range of behavioural and computational processes. For example, the strength of theta–gamma coupling has been demonstrated to predict spatial memory performance (Shirvalkar et al., 2010). Mechanistically, CA1 theta–gamma coupling is thought to underpin theta-phase precession (Senior et al., 2008; Lisman and Jensen, 2013): a phenomenon whereby spatial information is encoded by the theta phase at which a CA1 principal cell fires (O'Keefe and Recce, 1993; Skaggs et al., 1996). The excitability windows offered by the CA1 theta rhythm can be thought to provide a temporal basis by which spatial information may be represented by smaller populations of gamma-oscillating principal cells.

Dynamics of between-region oscillatory interactions

Fuelling these oscillatory dynamics are external inputs. A given brain region receives synaptic innervation from many different regions. Thus, the oscillatory activity in one such input region should influence the same frequency oscillation in the other. The greater this influence, the more consistent the phase relationship between the two oscillations will be over time. This phenomenon is mathematically measured as coherence, and is thought to be a biomarker of intra-region communication (Fries, 2005). Communication between a given sender- and receiver network should be dynamic; and not persist such to block the transfer of other informational items represented by different sender networks, which will be more functionally relevant on other occasions (Salinas and Sejnowski, 2001; Fries, 2005). Oscillatory coherence between the receiver and appropriate sender network has been computationally demonstrated to solve this "convergent pathway" problem, acting as a temporal filter by which the coherently

oscillating network may exert a dominant influence over the receiving network (Akam and Kullmann, 2014).

Cross-regional neural networks are larger and more sparsely connected, and thus preferentially synchronise at slower frequencies, such as theta (4–12 Hz) and delta (0.5–4 Hz). (Whittington et al., 2000; Engel et al., 2001; Fries, 2005). Within this large cohort of neurons, smaller groups of cross regional pairs may oscillate at faster rhythms (Kopell et al., 2000; Engel et al., 2001; Buzsáki and Schomburg, 2015), which indeed have been linked to different cognitive and behavioural functions (Meador et al., 2002; Brunet et al., 2014; Harris and Gordon, 2015; Sokolenko et al., 2019). This sophisticated "oscillatory nesting system" manifests as PAC, where the slower "nesting" oscillation rhythmically gates excitability windows to support inter-regional coherence at faster (i.e. beta and gamma) frequencies. Theta-nested gamma oscillations in CA1, for example, have been demonstrated to support inter-regional communication with the entorhinal cortex/CA3 system (Mizuseki et al., 2009), Amy (Zheng et al., 2017), ventral striatum (van der Meer and Redish, 2011) and PFC (Sirota et al., 2008). On a larger scale, parallel recordings from VTA, CA1 and PFC have revealed the functional significance of a 4 Hz rhythm, which synchronises gamma oscillations across these three structures during working memory demand (Fujisawa and Buzsáki, 2011).

The timescale of synchronous neural firing events implied by gamma frequencies is short enough to facilitate spike timing-dependent plasticity (STDP) mechanisms (see **1.2**) (Magee and Johnston, 1997; Markram et al., 1997; Bi and Poo, 1998). Thus, between-region gamma coherence, which is nested by slower oscillation such as theta and 4 Hz, represents a process of cross-regional plasticity (Buzsáki and Schomburg, 2015; Zarnadze et al., 2016). Such cross-regional associativity supports the brain-wide integration of multimodal information sources, facilitating the elegant transformation of sensory and cognitive information into an appropriate behavioural response. **The aim of this thesis is to explore the fine-scale temporal dynamics of brain-wide motifs of multiregional co-ordination, to test the hypothesis that specific oscillatory co-ordinations between regions relate to cocaine-paired memory retrieval (CPMR).**

2 | Experimental Methodology

2.1 | Animals

Animals used were male adult (4–6 months old) C57BL/6J mice (Charles River, UK) or transgenic heterozygous Vglut2-ires-cre mice (Jackson Laboratories; obtained from C57BL/6J crossed with Vglut2-ires-cre B6J.129S6(FVB)-Slc17a6tm2(cre)Lowl/MwarJ, stock number 028863, RRID: IMSR_JAX:028863). All animals had free access to water and food in a dedicated housing facility with a 12h-12h light/dark cycle (lights on 7 a.m. to 7 p.m.). They shared a cage with their littermates until the surgery and were singly-housed from thereon. All experiments involving animals were conducted according to the UK Animals (Scientific Procedures) Act 1986 under personal and project licenses issued by the Home Office following ethical review.

2.2 | Microdrive implantation

Animals were implanted with a custom-made microdrive during a surgical procedure performed under deep anaesthesia using isoflurane (0.5–2 %) and oxygen (2 l/min), with analgesia (0.1 mg/kg vetergesic) provided before and after. The drive was designed with 12-14 independently movable tetrodes, with each tetrode constructed by twisting together four insulated tungsten wires (12 µm diameter, California Fine Wire) and shortly heating them to bind them together in a single bundle. Each tetrode was attached to a M1.0 screw to enable their independent movement. Tetrodes were inserted to the right brain hemisphere under stereotaxic control in reference to bregma with respect to the following coordinates: medial prefrontal cortex: +1.98mm AP, +0.2mm ML, 1.25-2.5mm DV; NAc: +1.28mm AP, 1.0mm ML, 4.0-4.5mm DV; amygdala: -1.30mm AP, 3.0mm ML, 4.125-5.1mm DV; hippocampal dCA1: -1.94mm anteroposterior (AP), 1.3 and 1.7mm lateral from bregma (ML) and 1.2-1.4mm ventral from the brain surface (DV); ventral tegmental area: -3.08mm AP, 0.35mm ML, 4.2-4.75mm DV. The exposed parts of the tetrodes were covered with paraffin wax and the

drive was then secured to the skull using dental cement. For extra stability, stainless-steel anchor screws had first been inserted into the skull. Two of the anchor screws, which were inserted above the cerebellum, were attached to 50 µm tungsten wires (California Fine Wire) and served as ground and reference electrodes during the recordings. The placement of the tetrodes was confirmed by the electrophysiological profile of the local field potentials and their anatomical electrode tracks.

2.3 | Behavioural protocol

Following full surgical recovery, each mouse was first handled in a dedicated handling cloth, connected to the recording system and exposed to a circular-walled enclosure (the "familiar enclosure"; 36 cm diameter, 30 cm height) to familiarize the animal with the recording procedure over a period of one week prior to the start of the experiment itself. During this period, tetrodes were gradually lowered to their corresponding target region using their estimated depth location, neuronal spike waveforms and LFP features. An electrical commutator (Imetronic, Bordeaux, France) was installed above the behavioural apparatus, dimly lit and surrounded by an opaque black curtain, to hold the recording cable and prevent its twisting while the animal explored the environment. All recording days began with a 20-minute exploration of the familiar enclosure. The other two enclosures used in the pseudo-instrumental cocaine-paired memory protocol (see below) were referred to as the test and the conditioning enclosures.

The first stage of this protocol (See **Figure 3.1**) occurred in the test enclosure ("Pre-test"; **PRE**). This enclosure had a **bow-tie shape** (outer dimension: 46 cm width; 38 cm height), a **designated floor-type** (dark-coloured and smooth or light-coloured and rough, counterbalanced between animals) and contained **two LED wall-displays** placed on two opposing walls (green L-shape and orange circle-shape. Along each wall holding an LED-display, an **LED zone** was defined (taking up > 1/3 of the total area) and **split into four equally-sized quadrants**. The boundaries of these zones were invisible to the animal. We used this test enclosure with an open loop system (Imetronic, Bordeaux, France) to track the animal's position in real time and generate TTL-pulses to activate in turn the corresponding LED-display for up to 1500 ms upon quadrant boundary crossings. To reactivate the LED, the

animal had to move into one of the neighbouring zone quadrants. For example, entering the main zone (i.e. starting from the centre of the arena) of an LED would activate it for up to 1500 ms. If the animal moved into a neighbouring quadrant before this time, the LED would transiently deactivate and reactivate upon this crossing, or simple be reactivated if the 1500 ms surpassed. Mice experienced these two sets of zone-LED associations while exploring the test enclosure for two days (60 minutes on day 1; 20 minutes on day 2), with the exposure on day 2 used to quantify the baseline LED activation preference (i.e. difference in number of LED trigger events) of each mouse.

The second stage of this protocol occurred in the conditioning enclosure ("Conditioning"; **COND**). The aim of this stage was to **pair the light stimulus from one of the LED displays with a cocaine experience**, and the other with saline as a control. The arena used for **COND** was the same physical enclosure (including the same floor-type) as before with the triangular blocks removed (i.e., a (square-walled, 46 cm width, 38 cm height open field). The Conditioning stage started 30 minutes after the Pre-test (d1) and was repeated on d2 and d3. On each conditioning day, the more preferred LED in **PRE** was conditioned to saline in the morning and in the afternoon, the less-preferred LED to cocaine. In the morning session, the LED-display that the mouse had *preferentially* activated during the pre-test was attached to one of the walls of the conditioning enclosure and the animal was allowed to explore that enclosure for 10 minutes with the LED inactive. Next, the animal was removed from the enclosure to receive one intraperitoneal injection of saline solution (200µl). The animal was then immediately re-introduced to the conditioning enclosure where we emulated its own pattern of LED self-activation observed during **PRE**, randomly sampling from the interquartile range of LED self-activation to directly activate that LED-display. This procedure was repeated 4 hours after the saline conditioning session (in the afternoon), this time attaching in the conditioning enclosure the *less-preferred* LED from **PRE** and injecting the animal with a 12 mg/kg cocaine solution (200µl).

The last three stages occurred in the test enclosure ("Recall"; **REC**, "Extinction" **EXT** and "Renewal"; **REN**), commencing 23 hours after the last conditioning session and being all separated by ~10-minutes. These stages were designed to **model the context-dependent processes of behaviour** (extinction and renewal; see **1.1**). In all three of these stages, the mouse was able to activate again the two LED-displays in the test enclosure, as in the pre-test. Both the recall and renewal stages lasted 20 minutes in the test enclosure equipped with the floor

used during pre-test. The extinction stage consisted of 10-minute blocks during each of which the animal's preference for the cocaine-paired versus the saline-paired LED was measured. To promote behavioural extinction of cocaine seeking, we replaced the floor used during **PRE**, **COND** and **REC** by another floor texture, thereby introducing a contextual change within the test enclosure while preserving its spatial layout. To further promote the extinction of the LED-cocaine association and subsequent cocaine seeking, a white noise was played during all task stages but not in the familiar enclosure nor during **EXT**. We identified the penultimate extinction block as a clear reduction in the animal's preference for activating the cocaine-paired LED. To binarize this decision, a threshold was defined as the mid-way value between the **PRE** and **REC** scores (number of extinction blocks required = 2–14; mean = 6.25, SD = 4.18, n = 8 mice). For all analyses (unless stated otherwise), the last 20 minutes of active exploration during the Extinction stage were used. Finally, in the Renewal stage (**REN**), the animal returned to the same test arena as in **PRE** and **REC**.

2.4 | Multichannel data acquisition and position tracking

The extracellular signals from each tetrode channel were amplified, multiplexed, and digitized using a single integrated circuit located on the head of the animal (RHD2164, Intan Technologies; pass band 0.09 Hz to 7.60 kHz). The amplified and filtered electrophysiological signals were digitized at 20 kHz and saved to disk along with the synchronization signals from the animal's position tracking and those of the LED-display activations. The location of the animal was tracked using three differently coloured LED clusters attached to the electrode casing and captured at 39 frames per second by an overhead color camera (https://github.com/kevin-allen/positrack/wiki). In addition, online location of the animal was used to trigger the corresponding LED-displays in an open-loop manner, using the real time movement of the animal into the trigger quadrants (Imetronic, Bordeaux, France). The LFPs were down-sampled to 1250 Hz for all subsequent analyses.

2.5 | Spike detection and unit isolation

For the offline detection of spikes, the recorded signals were first bandpass filtered (800 Hz to 5 kHz). Spikes were then detected based on the power (root-mean-square) of the filtered signal calculated in 0.2-ms sliding windows. Detected spikes of the individual electrodes were combined per tetrode. To isolate spikes belonging to the same neuron, spike waveforms were first up-sampled to 40 kHz and aligned to their maximal trough (Csicsvari et al., 1998). Principal component analysis was applied to these waveforms ± 0.5 ms from the trough to extract the first three or four principal components per channel, such that each individual spike was represented by 12 waveform parameters. An automatic clustering program (KlustaKwik, http://klusta-team.github.io) was run on this principal component space and the resulting clusters were manually recombined and further isolated based on cloud shape in the principal component space, cross-channels spike waveforms, auto-correlation histograms and cross-correlation histograms (Harris et al., 2000; Kadir et al., 2014). All sessions recorded on the same day were concatenated and clustered together. Each cluster used for further analysis showed throughout the entire recording day stable cross-channels spike waveforms, a clear refractory period in its auto-correlation histogram, well-defined cluster boundaries and an absence of refractory period in its cross-correlation histograms with the other clusters. We further used an automated clustering pipeline using Kilosort (https://github.com/cortex-lab/KiloSort) (Pachitariu et al., 2016) via the SpikeForest sorting framework (https://github.com/flatironinstitute/spikeforest) (Magland et al., 2020). To apply KiloSort to data acquired using tetrodes, the algorithm restricts templates to channels within a given tetrode bundle, while masking all other recording channels. The resulting clusters were manually curated to check all clusters and remove spurious cells using metrics derived from the waveforms and spike times, and then verified by the operator. This procedure was cross-validated using several data sets and verified against manual curation, by computing confusion matrices to validate that clusters obtained automatically were also obtained with the previous method.

2.6 | Statistical analysis

Data were analysed in Python 3.6 (https://www.python.org/downloads/release/python-3610/). All operations relating to EMD (**4.3**) were performed using the emd 0.2.0 package (Quinn et al., 2021). Null hypothesis significance tests were performed using scipy 0.18.1 (https://pypi.org/project/scipy/) or statsmodels 0.9.0 (https://pypi.org/project/statsmodels/) packages. Details of any of these statistical tests can be found in corresponding text or figure legends. While I do quote p-values for these analyses, most of the statistical data interpretations in this thesis are graphically represented; and do not yield p-values (see below for details). This is in-keeping with recent proposals that (often underpowered) biological data analysis should move away from significance measurements (which enforce statistical assumptions about the data) and towards effect size certainty estimates (Halsey et al., 2015; Claridge-Chang and Assam, 2016; Morey et al., 2016).

Mean difference estimation ("Gardner-Altman") plots

"Gardner-Altman" plots have been suggested as the most extensive way represent effect sizes between two groups (Ho et al., 2019). To estimate the effect sizes of unpaired observations from distributions A & B, the empirical mean difference is first calculated:

$$\Delta = \bar{A} - \bar{B}$$

The group mean difference Δ is then subtracted from a series of null mean difference estimates, obtained by shuffling the group labels and then bootstrapping (n=5000, unless states otherwise) from each of the shuffled distributions. This shuffling operation is repeated 1000 times, to obtain a probability distribution estimate of the true mean difference. The 2.5^{th}- and 97.5^{th} percentiles are taken as confidence intervals from this distribution. Paired mean difference estimation plots, are computed in a similar fashion whereby for each shuffle, paired labels are randomly swapped or preserved with equal chance.

Reverse cumulative frequency distribution comparison plot

"Reverse cumulative frequency distribution comparison plots" were designed to appreciate distribution differences specifically relating to the larger values of two distributions (A and B) without making any assumptions (e.g. gaussianity) about the distributions. To approximate these distributions, equally spaced bin edges were defined from the 99.5th to the 0.5th percentile of the combined distribution AB. The number of bin edges was chosen such that 1000 bins covered the range spanning $\mu - \sigma$ to $\mu + \sigma$.[5] These bins were used to approximate the probability distribution vectors, $\hat{A}$ & $\hat{B}$. As the bins ranged from highest-to-lowest, the cumulative sum of either of these vectors was referred as the *reverse* cumulative frequency distribution approximation. The difference of these two vectors $\hat{\Delta}$ was taken to represent the degree and threshold by which the larger values of A outranked those of B. To assess the significance of these reverse cumulative distribution differences, a null distribution for $\hat{\Delta}$ was derived. Here, dummy $\hat{A}$ & $\hat{B}$ vectors were sampled from the combined distribution estimate $\widehat{AB}$, to generate 100 null $\hat{\Delta}$ vectors whereby 99 % confidence intervals were calculated.

Rank over-representation plot

Rank over-representation analysis applies a similar logic as the reverse cumulative frequency comparison method but is better suited for smaller sample sizes. This visual analysis compares the rankings of a series of measured values from two or more groups. First, the group rank vector $\boldsymbol{r}$ is defined, where each element corresponds to the group identity belonging to that rank order (index). For a given group (A), a binary vector $\boldsymbol{r}^A$, which identifies the indices corresponding to group A, is derived. Taking the cumulative sum of $\boldsymbol{r}^A$ and dividing by the total number of group A observations gives the ranked cumulative proportion of group A observations. To represent the null hypothesis that an observation belonging to group A does not influence its rank relative to all groups, dummy vectors $\boldsymbol{r}^{A'}$ are generated by shuffling the indices within $\boldsymbol{r}^A$ vectors 100 times to define 95 % confidence intervals.

[5] Though this choice should also depend on the sample sizes of the distributions.

2.7 | Analytical details for Chapter 3

Behavioural Factor Analysis

To represent the multivariate nature of cocaine-seeking behaviour, a series of behavioural metrics (**Table 2.1**) were collected for each animal and test stage. Metrics with the suffix, "Score" refer to a zone preference score:

$$preference\ score = \frac{x^{COC} - x^{SAL}}{x^{COC} + x^{SAL}}$$

Each of these post-conditioning metrics was then normalised by the Pre-test observation to form a feature matrix. Each feature column was then z-scored, after which factor analysis was applied, using the scikit-learn 0.19.1 package (https://pypi.org/project/scikit-learn/).

Metric	Description
trigRateScore	Zone preference-scored number of LED trigger events in the session
trigRateDiff	COC–SAL difference in LED trigger events in the session
zoneTrigRateScore	Zone preference-scored within-zone trigger rate (i.e. number of trigger events in zone, divided by time spent in zone)
durScore	Zone preference-scored time spent in zones
outProp	Proportion of time spent in the central area between zones.
medianSpeedScore	Zone preference-scored median zone speed
speedSDScore	Zone preference-scored standard deviation zone speed
entryScore	Zone preference-scored number of zone entries
sideScore	Zone preference-scored number LED trigger events on either of the side quadrant boundaries
centreScore	Zone preference-scored number LED trigger events on the centre quadrant boundary
medianIPIScore	Zone preference-scored median of inter-pulse-interval (i.e., median time between LED trigger events)

Table 2.1: *Behavioural metrics used for factor analysis.*

2.8 | Analytical details for Chapter 4

Tetrode nomination

To proceed with downstream LFP analysis, a single tetrode channel per animal was to be nominated. Here, the tetrode whose PSD had the highest correlation to the median PSD computed over all tetrodes for that region was selected for each animal. This choice was further verified by checking the estimated depth and anatomical placement *post-mortem*.

Barcode interaction profiles

Cross-correlation plots were derived by measuring the Pearson correlation coefficient between the focus barcode and each other barcode for a given shift (relative to the focus barcode). Barcode strength peaks separated by at least 500 ms and with a strength above 1.5 standard deviations from the mean where used to trigger then average LFP and spiking responses. To generate null distributions, these peaks were shuffled 20 times, preserving the inter-peak intervals and the 0.5^{th} and 99.5^{th} percentiles of the null responses triggered from these 50 shuffles graphically shown as confidence intervals.

2.9 | Analytical details for Chapter 5

Barcode CPMR scoring

To identify the barcodes whose engagement dynamics most related to CPMR, Barcode strengths were windowed into 1 s bins to calculate COC–SAL effect sizes (Cohen, 1977) for each stage. The barcode CPMR score for each animal was then taken as the dot-product between this stage-wise vector and the CPMR vector (**Figure 5.1A**).

2.10 | Analytical details for Chapter 6

Phase-amplitude coupling (PAC) scoring

To measure the modulation strength by theta or 4 Hz oscillations on a given strength time series (x), the average amplitudes of x (z-scored) within 32 equally spaced phase bins was calculated. The modulation strength of x was then defined as the amplitude difference between the most- and least-preferred bin indices (these being specific to each animal). To measure cycle -specific PAC, the median amplitudes of x within the same most- and least-preferred phase bins was used to compute this difference.

Opto-tagging assay

To assess whether a cell was opto-tagged, the laser pulse times to be used (see later for details) were randomly split into two halves (half-1 and half-2). For each half-set of laser times, the spiking responses of all VTA cells were centred relative to the time of the laser pulse, averaged over pulses and then binned into 2 ms (for glutamatergic assay) or 10 ms bins (for dopaminergic assay).[6] For a given cell, the time bin corresponding to the peak firing response for half-1 was used to sample the binned firing response triggered by half-2. For the cell to be determined as "opto-tagged", this firing response had to be above the 99th percentile of binned firing response values observed between -1000 to -500 ms for both pulse splits – and time corresponding to the maximum response evoked by half-2 had to be within 6 ms (glutamatergic assay) of laser onset or in the first bin after laser onset (dopaminergic assay).

ISI-based VTA cell-type classification

To predict the molecular identity (Glu/DA) of each recorded VTA cell, inter-spike-interval (ISI) histograms were computed using bins (the first two being pre-defined as 0- and 1.21 ms) which exponentially scaled in size according to the following formula:

[6] The bin size was widened for the dopaminergic assay as in this experiment (McNamara et al., 2014), cells were stimulated using a theta burst stimulation protocol, and not with a primary intention for opto-tagging.

$$b_i = b_{i-1} + (b_{i-1} - b_{i-2}) * 1.05$$

Where b_i is the new bin entry to add and until the most $b_{i-1} < 10000$. Each histogram was normalised by its sum, and incorporated into a [nBins x nCells] feature matrix (shown transposed in **Figure 6.10**). To reduce the dimensionality of this matrix, principal component analysis (PCA) was used to represent the ISI distributions of each cell by its first 3 principal component (PC) weights. These PCs were then used to train a linear discriminant analysis (LDA) for the opto-tagged (i.e. labelled) cells. This yielded the optimal projection axis by which the opto-tagged cells could be PCs could be linearly separated according to their label. The PCs of all the non-identifiable VTA cells were then projected onto the LD axis to preduct their molecular identity. Of the opto-tagged animals, any VTA cells were not opto-tagged were not considered here or in subsequent analysis.

Rayleigh phase coherence

To measure the spike-phase coherence for a given cell, its coherence was given by the Rayleigh test:

$$abs\left(mean\left(e^{\boldsymbol{p}\cdot j}\right)\right)$$

Where $\boldsymbol{p}$ is the vector of spike-sampled phases (in radians) and $j = \sqrt{-1}$. When less than 200 phases were sampled, the coherence value was ignored.

VTA cell-type triggered spectrograms

Spectrograms were computed to the z-scored LFP of each region using a set of complex Morlet wavelets (using scipy.signal.morlet function) with main frequencies from 2–200 Hz, with 1-Hz steps up to 100 Hz and 5-Hz steps up to 200 Hz. For each cell, spike trains were filtered such that only the first spike in a burst was used – i.e., a spike would be neglected if a preceding spike occurred within 250 ms. If at least 20 spikes remained, these spikes were used to trigger the average spectrogram responses in each of the recorded regions. As a control, the instantaneous speed of the animal was binned into 100 percentile bins. Each of the selected

spikes were then randomly assigned a new speed bin -matched time, ensuring this did not correspond to a real spiking event. For each cell-type, the corresponding triggered spectrograms of the real and speed-controlled spikes were averaged to compute the mean spectral response, and then z-scored for each frequency wavelet to assess the frequency-specific changes relating to the time of the spikes. The speed-controlled spectrogram response was then subtracted from the original to produce the spike-triggered spectrogram responses. While not shown, both using the unfiltered spike times and resampling the spike times (filtered or otherwise) by bootstrapping gave very similar results to those in **Figure 6.12**, suggesting that the beta-specific effects of the dopaminergic population were not related to firing rate differences between the two putative cell-type groups.

3 | Modelling dynamic cocaine-seeking behaviour

3.1 | Outline

I designed and trialled a novel behavioural paradigm whereby dynamic cocaine-seeking behaviour could be assessed while *in-vivo* tetrode recordings could be performed in-parallel. A self-administration assay would not have been practical due to the technical issues when combining this with in vivo large-scale network electrophysiological recordings. A conditioned place preference (CPP; see **1.2**) assay would be suitable, however I wanted to capture a more *instrumental-like* behaviour, which could be assayed under different, tractable contexts. Based on these requirements, I designed a "**pseudo-instrumental**" **second-order cocaine conditioning assay to model cocaine-seeking behaviour**. As well as testing for cocaine-seeking behaviour after the acquisition of cocaine-paired memory, this assay then included two additional stages (Extinction (**EXT**) and Renewal (**REN**)), whereby contextual changes to the testing apparatus were used to encourage the reduction and re-emergence, respectively, of drug-seeking behaviour. This chapter will describe this behavioural model (**3.2)** and then explore analytical interpretations relating to cocaine-seeking behaviour (**3.3-4)**.

3.2 | A "pseudo-instrumental" cocaine conditioning protocol

I designed a "pseudo-instrumental" second-order cocaine conditioning task to assay cocaine seeking behaviour. Full details of this protocol can be found in **2.3**. Briefly, mice first learnt two distinct place-stimulus associations in the "test arena". Here, the crossing of an unmarked zone boundary would trigger the activation of an LED-display corresponding to the zone quadrant the animal had entered (**Figure 3.1A-B**). The LED-display would be lit for up to 1.5 seconds – and re-triggered upon entering a neighbouring zone quadrant. After an initial incidental learning session, where the mice learnt to relate two sets of spatial behaviours to

discrete LED-display activations, the baseline preference to trigger each LED-display was assayed the following day in the Pre-test (**PRE**). Akin to the reverse-conditioning method often adopted in the Conditioned Place Preference (CPP) assay (see **1.1**), the LED which was least-preferred was conditioned to a cocaine experience, and the more preferred to a saline control. In this next stage (Conditioning, **COND**), mice would explore an arena which shared non-spatial ("contextual") features with the test arena (floor texture, white noise), but was spatially distinct and contained just a one of the two LED-displays, which was paired with either saline or cocaine. In a single conditioning session, mice would explore this arena for 10 minutes with the LED-display off, before receiving an intraperitoneal injection of saline or 12 mg kg^{-1} cocaine solution, and were then immediately returned to the arena – where the LED-display would flash in a pattern emulating the on-off train generated in the Pre-test. On each conditioning day, the saline session happened in the morning and the cocaine 4 h later in the afternoon, so as to not pair any aversive effects of cocaine withdrawal with the saline-paired LED.

Cocaine-seeking behaviour was then assayed on the following day in the Recall, Extinction and Renewal stages. The Recall stage was identical to the Pre-test, only now the animal had learned the pairing of one of the LEDs with 2 or 3[7] cocaine experiences. Accordingly, mice would revert their LED trigger preference in **PRE** to the LED which was paired with cocaine. We hypothesised that this trigger preference (discussed in **2.2-3**) is related to a cocaine expectation inference made by the animal, which encourages the LED-display to be more persistently activated. This increased preference to trigger the cocaine-paired LED-display is thus an example of cocaine-seeking behaviour.

Alterations to drug-paired contexts promote the extinction of drug seeking (Bouton, 2004) (see **1.1**). This was modelled in the Extinction stage, which differed from the Recall stage in that the "contextual" features (floor texture and sound; see **2.3**) of the test arena were changed. Here, the preference for the cocaine-paired LED-display reduced. For analytical purposes, the extinction period (**EXT**) was defined as the last 20-minutes of this stage. Finally, in the Renewal assay, the animal returned to the original test arena (matching Pre-test and Recall), where the trigger preference for the cocaine-paired LED returned, demonstrating renewal. This

[7] to promote the reliability of conditioning, the number of conditioning sessions was increased after the first two animals

experimental design offered the dynamic expression of active cocaine-seeking behaviour to be assayed while multiregional dynamics of the brain could be simultaneously recorded.

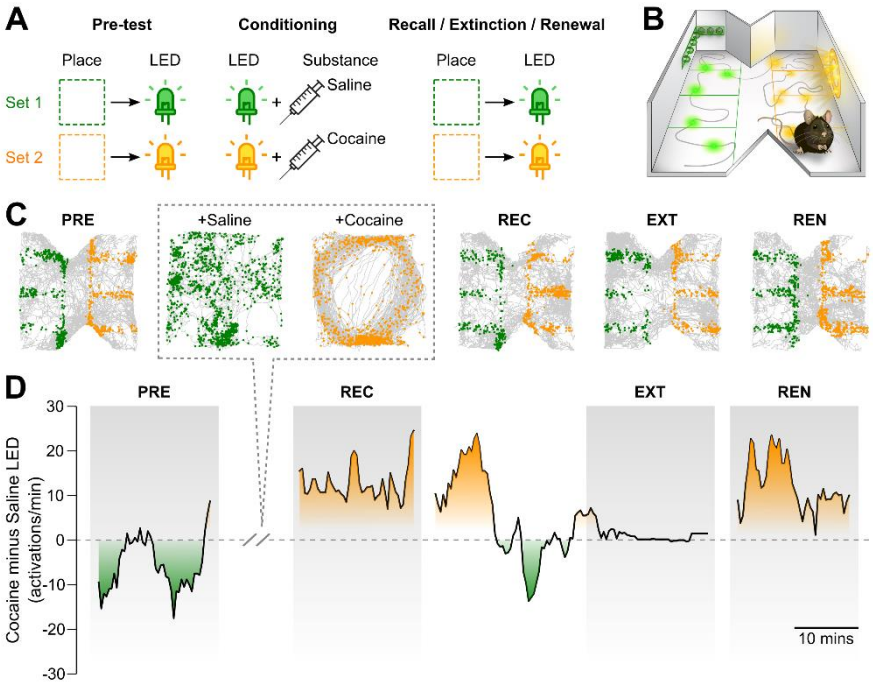


Figure 3.1: *Protocol outline.*

A: Layout of the 5-stage task structure including two sets of memory items. **B:** Schematic of the test enclosure used for pre-test, recall, extinction, and renewal. **C:** Example animal paths (grey) during each task stage. For each stage, the green and orange dots overlaid on the animal's path represent the animal's position when the green and the orange LED were activated, respectively. **D:** COC–SAL LED 3-minute sliding binned trigger rate difference timecourse for example animal.

The psychological processes of reward-guided behaviour (discussed in **1.1**) can be mapped to the material elements of this protocol as follows. During a cocaine conditioning session [**COND**], neural responses to drug delivery [US] become associated with the flashing LED-display [CS] experienced in the cocaine-paired context (floor texture). When the animal returns to the test arena [**REC**], neural representations of the drug-paired LED-display and context elicit an incentive salience signal – this comprising the process of cocaine-paired memory retrieval. This attracts LED-triggering; a learnt behaviour which now is indirectly reinforced by cocaine. In a novel context (which is not associated with cocaine) [**EXT**], cocaine-seeking

behaviour is extinguished, as COC-LED-triggering is not succeeded by cocaine experience. Upon returning to the original drug-paired context [**REN**], cocaine anticipation is re-inferred [CPMR], renewing the expression of cocaine-seeking behaviour. In this next section, we explore and discuss some of the key observable behavioural metrics from this paradigm that could be described as "cocaine-seeking behaviour".

3.3 | Simple behavioural analyses

To quantify cocaine-seeking behaviour across the test stages of the protocol, three key behavioural metrics hypothesised to be driven by CPMR were compared between the saline- and cocaine-paired zones. These three behaviours were: the rate at which the LED-display was triggered; proportion of time spent in the zone; and speed of locomotion in the zone. The preference of these behavioural measures observed in each zone can be quantified either as the raw difference in observed values (**Figure 3.2**, top row) or as a preference score[8] (**Figure 3.2**, bottom row):

$$raw\ difference = x^{COC} - x^{SAL}$$

$$preference\ score = \frac{x^{COC} - x^{SAL}}{x^{COC} + x^{SAL}}$$

The "more instrumental" of these is the LED trigger preference, which as outlined in **3.2** is likely driven by a more cognitive CPMR component. The second of these metrics is akin to a conditioned place preference (CPP; see **1.1**) score. Two key features distinguish "CPP" in this protocol from a typical CPP assay. First, the spatial environment where the place preference is observed is less explicit: in this assay, they are part of the same enclosure, but in CPP they are more distinctly enclosed (and sometimes more spatially separate). Second, and more crucially, the spatial environment is never directly experienced with cocaine. Thus, a zone preference in my task would be linked to an incentive salience response associated with the LED-display (CS), rather than the spatial environment. As discussed in **1.1**, it has been argued that an

[8] Note that this is will not affect the place preference metric.

incentive salience explanation for CPP is an oversimplification of what is a more complex repertoire of conditioned behaviours (Huston et al., 2013). This principle indeed applies here – and is considered in **3.4**. One such conditioned behaviour is locomotion speed: the third behavioural metric quantified in **Figure 3.2**. Cocaine delivery in rodents produces very strong locomotive effects (Benuck et al., 1987) – which was indeed reproduced in my conditioning dataset (data not shown). Therefore, re-encountering of the cocaine-paired LED-display may induce a conditioned-hyperlocomotion response (Carey and Damianopoulos, 1992; Carey et al., 2005).

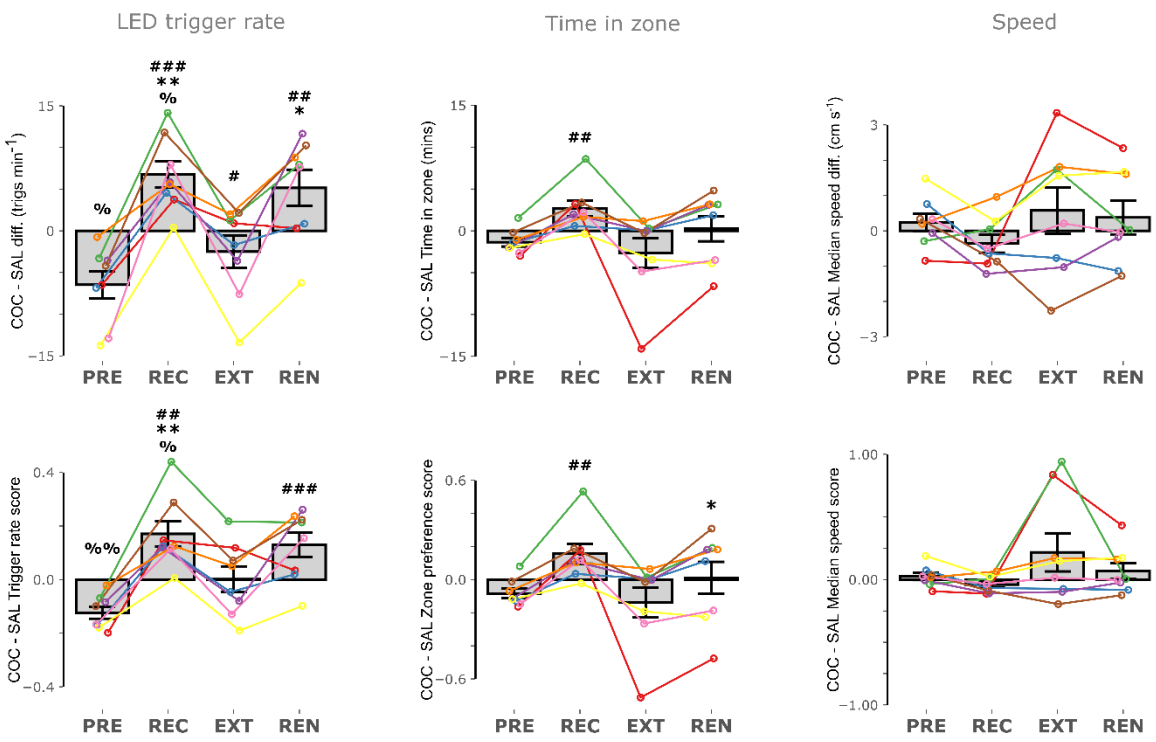


Figure 3.2: *Quantification of key behavioural measures of cocaine-seeking behaviour.*

Top row: COC-SAL raw difference comparison. **Bottom row:** COC-SAL preference score observations. #: vs **PRE**; *: vs **EXT**, 1-way repeated measures ANOVA for pairwise assay-assay interactions; % vs chance-level zone bias, 1-sample t-test, all with Bonferoni correction for multiple comparisons. For any significance symbol, ***p < 0.001, **p < 0.01; *p < 0.05.

The behavioural measure which showed the most obvious correlate of CPMR was the raw trigger rate difference (**Figure 3.2**, left column), which was significantly greater in the recall stage compared to Pre-test ($p=1.019 \times 10^{-4}$) and Extinction ($p=4.361 \times 10^{-3}$) and was also significantly greater in the Renewal stage compared to the Pre-test ($p=2.387 \times 10^{-4}$). There was

a significant increase in place preference seen between the Pre-test and Recall stages ($p=6.200 \times 10^{-4}$) (**Figure 3.2**, middle column), and no bias in zone speed difference between stages (**Figure 3.2**, right column).

Speed was also compared between zones for each stage (**Figure 3.3**). While again no significant differences were found at the group level, two individuals seemed to show increased speeds in the cocaine-paired zone; one in both Extinction and Renewal and the other just in Extinction (**Figure 3.3A**). Closer inspection comparing these to zone speeds in the other stages revealed that this speed difference was attributed to slower saline zone speeds. Though group-level analysis suggested that speed was less related to CPMR, these observations were still taken into consideration for later analyses.

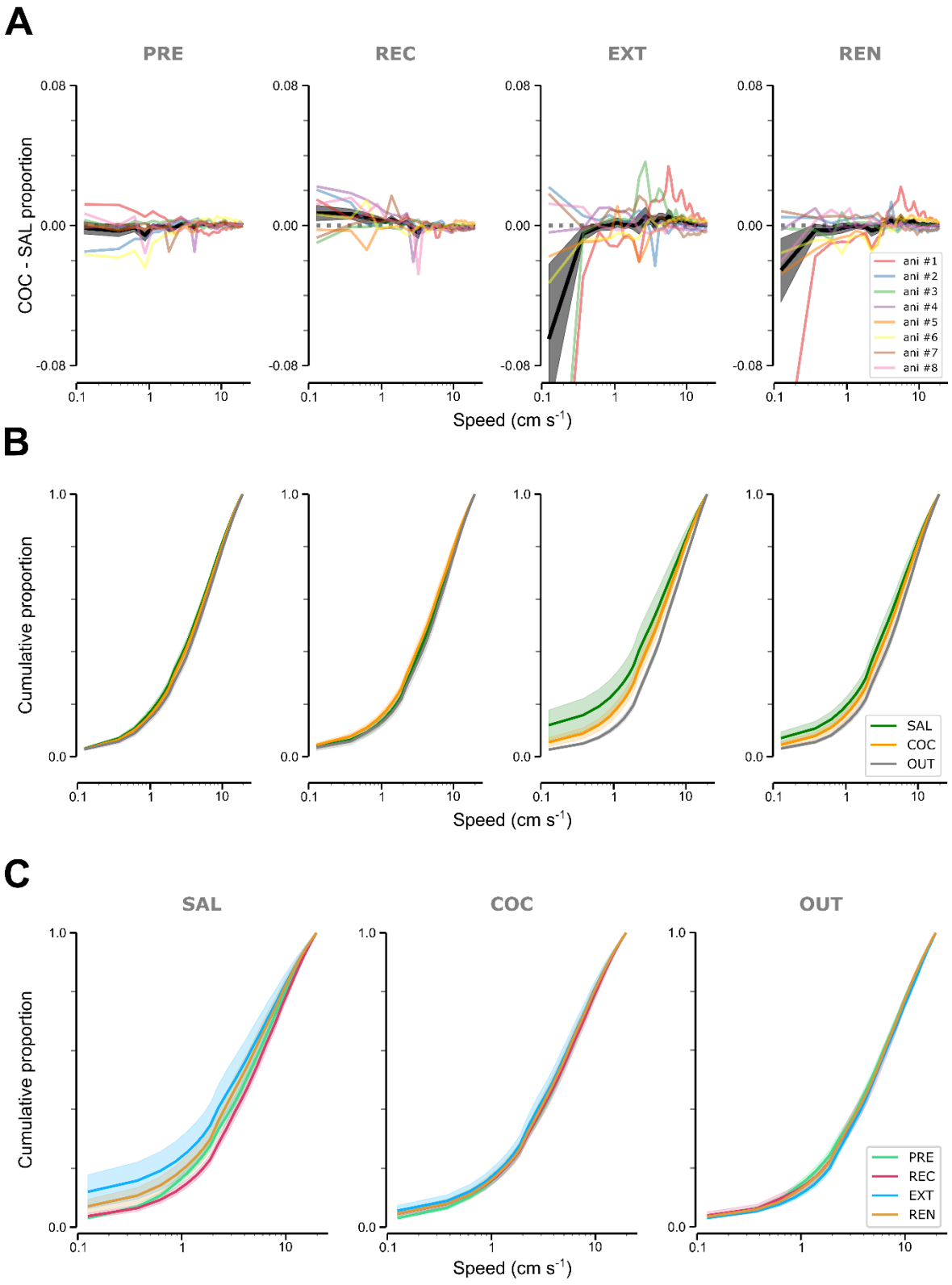


Figure 3.3: *Speed observations across stages and zones.*

A: COC – SAL speed distribution difference. Black: mean ± SEM; Coloured lines: individual observations. **B:** Cumulative distribution for each zone (mean ± SEM). **C:** Cumulative distribution for each test stage (mean ± SEM).

3.4 | Multidimensional analysis of cocaine-seeking behaviour

The analyses in **3.3** revealed that cocaine-seeking behaviour is reflected in several behavioural metrics. To appreciate the relationships between these behaviours, and how they may change over the test stages, I performed a factor analysis (see **2.7** for details) on an extended set of (mainly) zone difference-based behavioural metrics observed for each post-conditioning test stage. Factor analysis explores co-variance relationships between a set of observable measurements, aiming to reflect these relationships as a series of fewer underlying "factors", which are real phenomena that have varying influences on the observable measurements. This statistical approach has previously been used in a similar fashion (Spiteri et al., 2000) to reveal behavioural factors which distinguish food- from morphine-CPP. Here, I adopted factor analysis to visualise how "cocaine-seeking behaviour" may underlie the variety of observable behavioural items in my experiment. In support of this, the Recall and Renewal stages (where CPMR is hypothesised to occur) were well-separated in factor space (**Figure 3.4A**). The "optimal origin-passing axis of CPMR separation" (**Figure 3.4A**, dashed line) highlighted that "cocaine-seeking behaviour" composited a complex composition of different measurable behavioural metrics. Factor 1 and Factor 2 looked to respectively underpin covariation of zone spatial preference and LED trigger-related metrics, respectively. These types of insights should be eventually be considered by mature behavioural-neural analyses.

3.5 | Discussion

Cocaine-seeking behaviour was assessed using three key behavioural metrics. It was deemed that dynamic cocaine-seeking behaviour was successfully modelled across the post-conditioning test stages; where it was initially present in Recall, diminished in Extinction and re-emerged in the Renewal stage. Reassuringly, LED trigger preference, which was the "more instrumental" of the behaviour measures, most strongly validated this model of cocaine-seeking behaviour. This gave me confidence to proceed in using these same behavioural windows (zone visits) to explore neural correlates of CPMR. The results also highlighted that speed was less related to cocaine-seeking behaviour than the more task-specific behaviours. Applying factor analysis to the extended set of observable measures collected across the post-conditioning test stages enabled me to appreciate these elements as multidimensional

behavioural features and intuit how strongly they may relate to CPMR. Before these multidimensional descriptions of cocaine-seeking behaviour are married with neuronal variables, analytical attention must also be paid to the neural dynamics simultaneously recorded from dCA1, Amy, NAc, mPFC and VTA. This next chapter describes the steps chosen to perform such analysis.

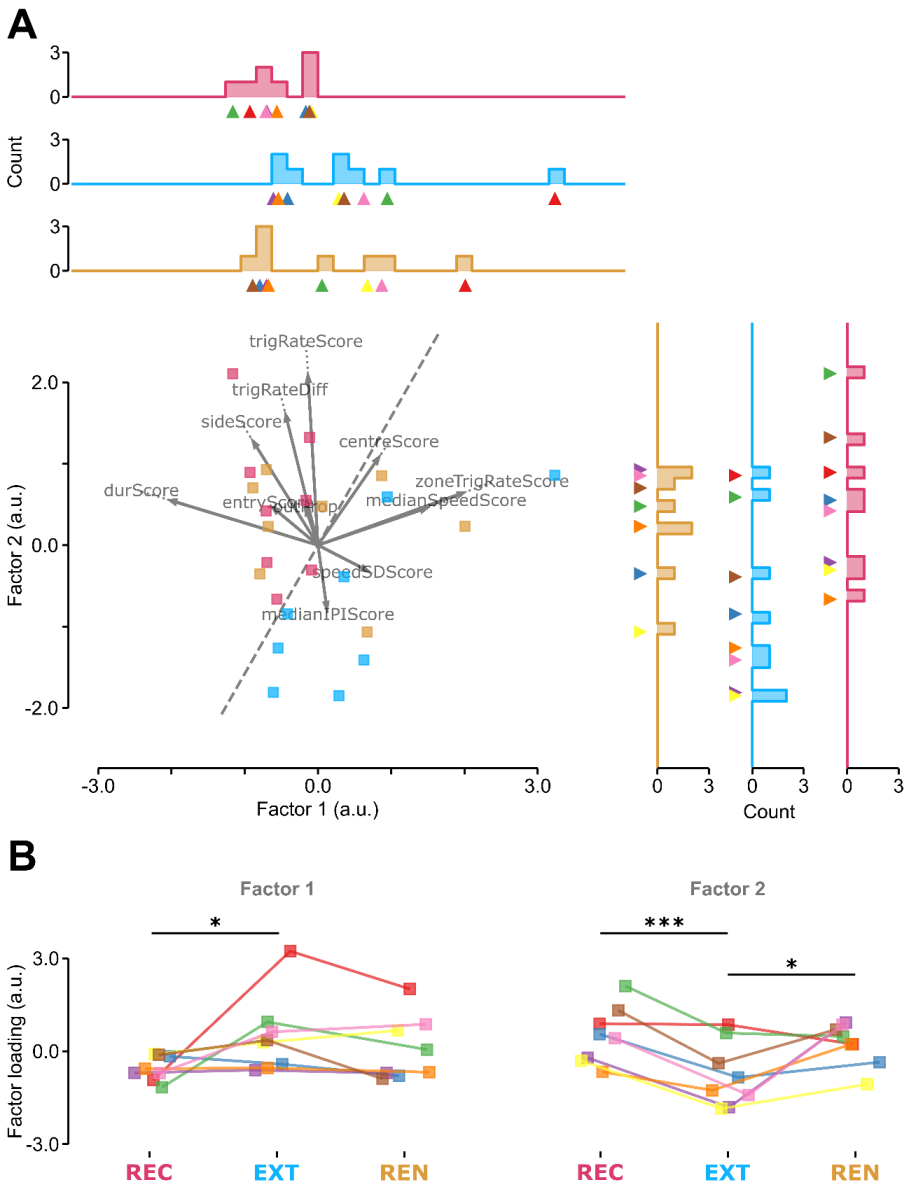


Figure 3.4: *Behavioural factor analysis of cocaine-seeking behaviour metrics across post-conditioning stages.*

A: Behavioural stages for each animal in factor space. Note that Recall and Renewal are well-separated by both factors, this separation owing most crucially to CPP (durScore) behaviour. **B:** Animal factor loadings across test stages. ***p < 0.001, **p < 0.01, *p < 0.05; 1-way repeated measures ANOVA for pairwise stage-stage interaction, with Bonferoni correction for multiple comparisons. Coloured arrows represent each animal – these colours correspond to the datapoints in **B**. n = 8 animals.

4 | Analyses of LFP interaction dynamics

4.1 | Outline

To investigate multiregional neuronal dynamics associated with the cocaine-seeking behaviour described in **Chapter 3**, tetrode recordings were performed simultaneously from five brain regions central to memory-guided behaviour: the dorsal CA1 subfield of the hippocampus (CA1); amygdala (Amy); nucleus accumbens (NAc); medial prefrontal cortex (PFC); and ventral tegmental area (VTA) (for methodological details, see **2.3**). The cognitive functions of these regions have classically been studied in isolation, or as pairs (see **1.3**). While it is a useful first step in developing our understanding of the brain, the discretisation of neural operations by spatially-distinct brain regions is clearly a vast oversimplification (Steinmetz et al., 2019; Stringer et al., 2019). The level of sophistication by which the brain can dynamically control behaviour inherently requires access to a comprehensive, multimodal representation of the world and self. Indeed, many studies have demonstrated that a variety of cognitive operations relate to frequency-specific communication between two regions (e.g. Meador et al., 2002; Jones and Wilson, 2005; Brunet et al., 2014; Harris and Gordon, 2015; Sokolenko et al., 2019). Information transfer between two regions by oscillatory phase-coherence is a well-supported idea (Fries, 2005; Akam and Kullmann, 2014) (see **1.4**). These frequency-bound communication channels should be thought of not in isolation, but as a single "dimension" of a much more complex network of communication streams spanning the entire brain. This notion in mind, the aim of this chapter is to utilise the multidimensionality offered by our five-site recording strategy (see **2.2**) to describe frequency-resolved multidimensional interaction patterns within the CA1–Amy–NAc–PFC–VTA network. This chapter details the analysis and thought processes I used to detect such interaction patterns, termed "**barcodes**". These barcodes were then used to test my hypothesis that CPMR would relate to the biasing of specific motifs of multiregional co-ordination (**5.2**).

After considering some more basic features of the recorded raw data in **4.2**, I introduce **empirical mode decomposition** (**EMD**) (**4.3**); a data-driven approach that extracts a series of oscillatory components of a time-series (Huang et al., 1998). I provide an intuition-based

overview of EMD and its variants (ensemble-EMD (eEMD) and masked-EMD (mEMD)), as well as the advantages and disadvantages of using this method to extract (neural) oscillations from the data. I propose a way of addressing one of these disadvantages, which enabled a non-arbitrary, **mEMD-based, region-tailored frequency extraction**. Finally, in **4.4**, I describe the aforementioned "**barcode method**" used to uncover higher-order interactions between the extracted frequency components of each region.

4.2| Simple LFP overview

After some standard pre-processing of the tetrode recordings (see **2.4**), the available neural data takes two key forms: the local field potentials (LFPs) and also the spike times of individual cells (**Figure 4.1**). To explore frequency-resolved multiregional communication between these regions, the LFP signals are the obvious choice here, as they offer a population-based readout of neural activity; and also a more accessible and translatable one. To elaborate, the longer-term implications of this study would be to flag electrophysiological biomarkers relating to drug-paired memories which could be used in closed-loop systems in humans with drug use disorders. Such a system would be better suited to an LFP-like signal, which can be processed fast enough to deliver a neural intervention at the time scale required. The most popular non-invasive recording equivalent in humans is electroencephalogram (EEG) recordings. EEG signals are also the product of summed neural activity, making them more analogous to the LFP recordings here. The accessibility of LFP recordings over spikes also makes the results of this study more broadly applicable to other labs.

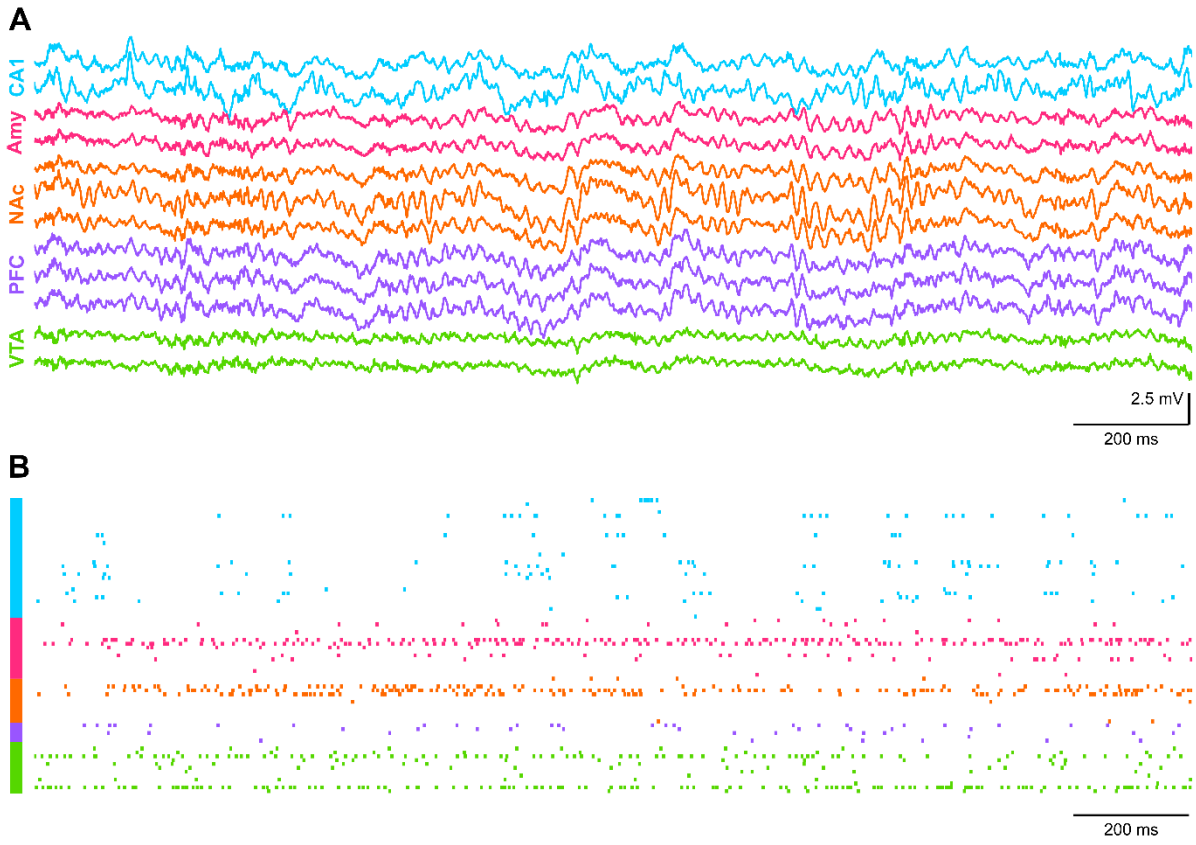


Figure 4.1: *Five-site tetrode recording.*

Example simultaneous LFP (**A**) and spike (**B**) recordings from CA1, Amy, NAc, PFC and VTA.

As outlined in **2.3**, several tetrodes were used to record from a given region. To proceed with more complex analysis relating to LFP interaction dynamics, for each group of tetrodes targeted to a region, one of these should be nominated to provide the LFP signal for downstream analysis. This decision was primarily based on the principle that for each region, the spectral consistency between animals should be maximised. To aid this decision (for details, see **2.8**), I computed the power spectral density (PSD) spectra of each corresponding tetrode (**Figure 4.2A**) to generate PSD correlation matrices for each region (**Figure 4.2B**).

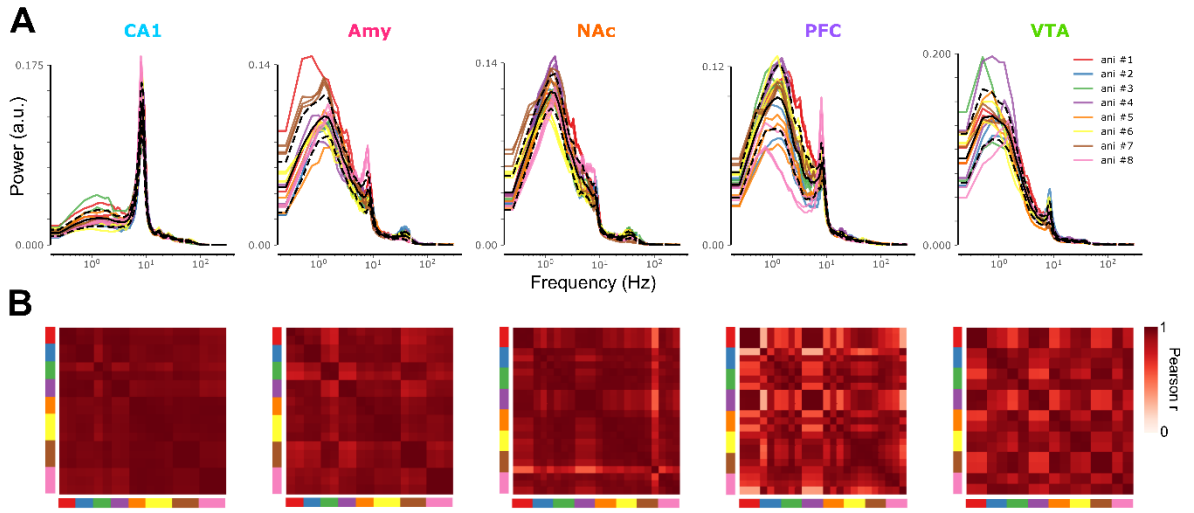


Figure 4.2: *Spectral consistency between tetrode LFP recordings.*

A: Power spectral density (PSD) spectra for the z-scored LFP of each region from every tetrode. Black lines: mean (bold) ± SD (dashed). **B:** correlation matrices comparing PSD spectra between tetrodes.

Having now nominated the tetrodes to provide the LFP signals for each animal and region, I next compared the coherence between pairs of regions, and compared the coherence spectra between animals (**Figure 4.3**). In line with the principles of neural synchronisation (see **1.4**), coherence between regions was indeed strongest at low (< 5 Hz) frequencies. CA1 consistently showed the strong coherence between all regions in the theta (4-12Hz) range, consistent with the strong theta power seen in CA1 LFP (O'Keefe and Nadel, 1978; Buzsáki, 2002) (**Figure 4.2A**). Coherence between non-CA1 pairs showed coherence peaks spanning the gamma (25-100Hz) range, consistent with previous reports (Fujisawa and Buzsáki, 2011; Donnelly et al., 2014; Stujenske et al., 2014; Catanese et al., 2016; Reakkamnuan et al., 2017).

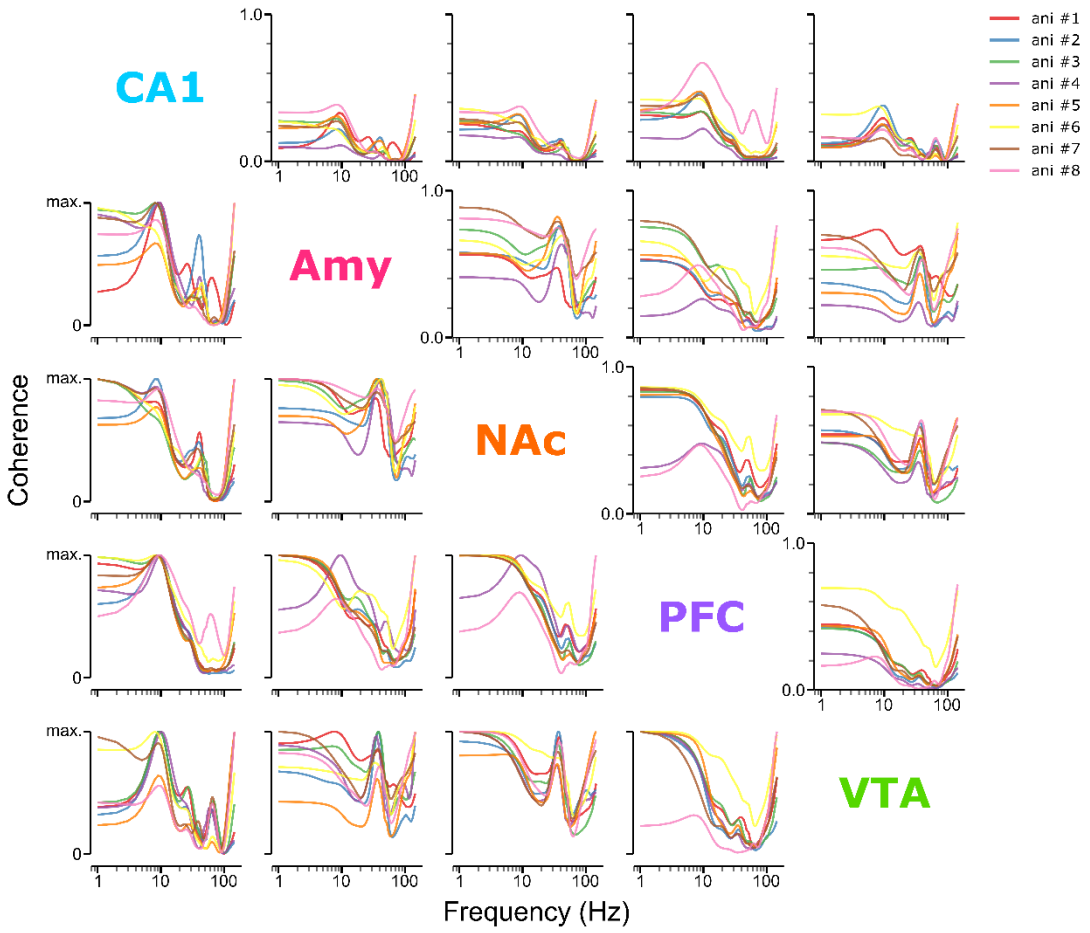


Figure 4.3: *Coherence between region LFPs.*

Coherence for each pairwise combination of regions. The raw coherence is plotted in the above diagonal plots, and the maximum-normalised in the lower diagonal, for each animal (colour).

Overall, region-pair coherences were convincingly consistent between animals. These Fourier-based methods provided simple spectral descriptions of the recorded LFP signals from each tetrode, and for allowed between-animal differences to be appreciated. To appreciate the fine-scale temporal dynamics of the spectral interactions between the five regions, the LFP data must represented both in the frequency and time domains.

4.3| Empirical Mode Decomposition of the local field potentials

Non-stationarity

Oscillatory activity is a physical phenomenon seen throughout nature, spanning through nanoscopic and macroscopic scales. In **1.4**, I discussed how the architecture and cell-type diversity of a neural circuit are thought to give rise to neural oscillations. As complex as these components are, so too are the inputs the circuit receives. These inputs come from a variety of different brain regions with varying cell-type-specific innervation configurations. The information stream made physically viable by a given region input is a dynamic and ever-changing one, owing to fluctuations in both internal brain dynamics [interoception] as well as the external environment [exteroception], which impose varying computational requirements. As such, the oscillatory activity generated by a neural circuit will vary considerably between cycles. Such variation to the rate at which the phase of an oscillation changes over the course of a cycle is an inherent property of many dynamic complex systems – and is referred to as non-stationarity (**Figure 4.4**).

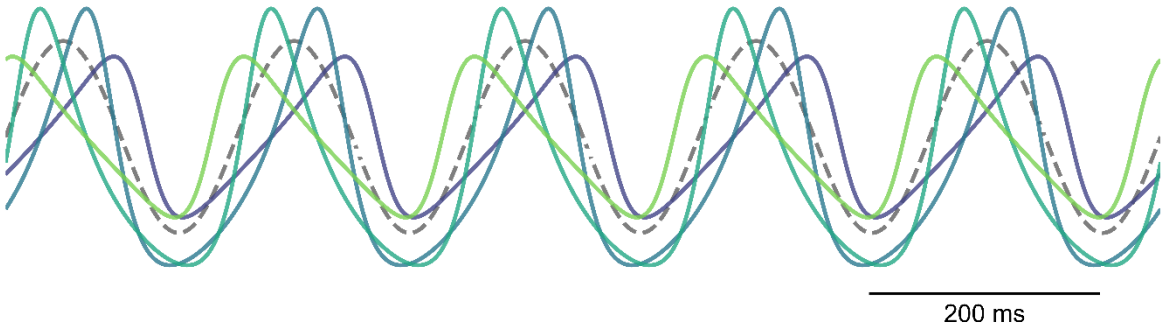


Figure 4.4: *Example of non-stationary 5 Hz oscillations.*

The dashed line shows a sinusoidal (i.e., stationary) 5 Hz signal, and the coloured lines show non-stationary examples. Note that while the period (cycle duration) is the same between these oscillations, the rate at which the phase progresses within a cycle varies.

Non-stationarity is indeed reported to be a functionally-relevant feature of brain oscillations (Dijk et al., 2010; Jones, 2016; Cole and Voytek, 2017; Schaworonkow and Nikulin, 2019). The theta oscillation in the rodent CA1 hippocampal subfield, for example, has a faster peak and a slower trough – and the degree of this asymmetry has been linked to behaviour and the

phase-modulation of gamma (Buzsáki et al., 1985; Belluscio et al., 2012). Given the prevalence and functional significance of non-stationary oscillations in the brain, it follows that when neural oscillations are analysed, this non-stationarity should be preserved in the analysis used to interpret the data. This principle is now being increasingly considered by the neuroscientific community, who are moving away from traditional Fourier-based approaches, which are based on the assumption that a signal can be defined as weighted sum of stationary sinusoids. While Fourier analysis is a useful tool in being able to describe a range of physical phenomena, this approach does injustice to biological data, whose non-stationary oscillatory dynamics result from complex, non-linear interactions. A solution is offered by empirical mode decomposition (EMD), which we I will now introduce.

Sifting

Let's consider a dummy signal comprised of two non-stationary 10 Hz and 50 Hz oscillations (**Figure 4.5**). Note that in this example, particularly the 10 Hz oscillation has a more asymmetric waveform, which has a faster descending phase.

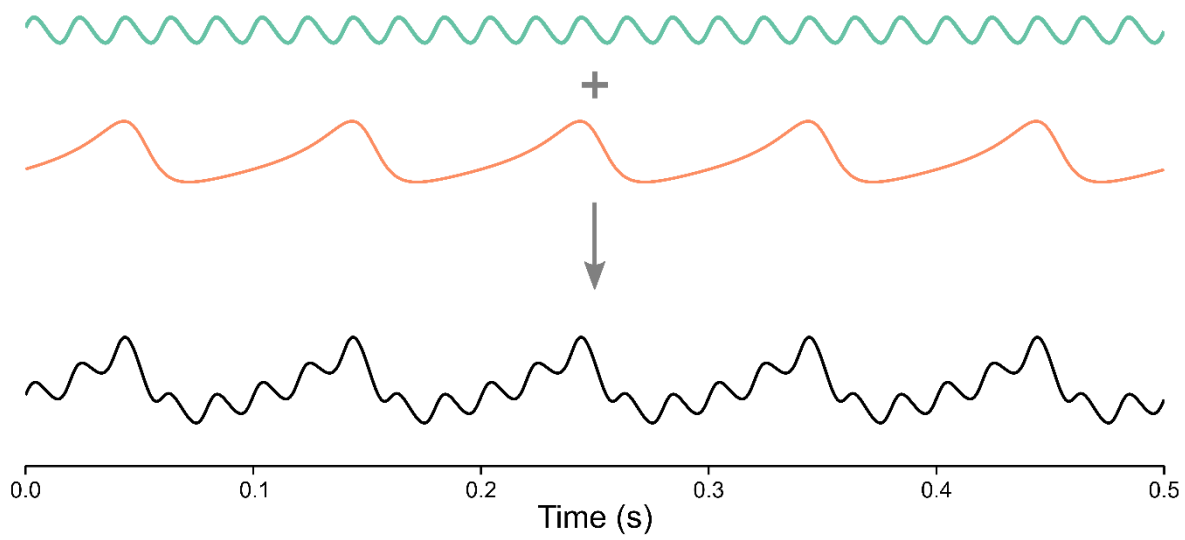


Figure 4.5: *Dummy signal composed of two non-stationary signals.*

Empirical mode decomposition (EMD) takes such a signal and splits it into a series of frequency components, termed intrinsic mode functions (IMFs). Each IMF is iteratively extracted (starting with the fastest IMF) by a process known as sifting. **Figure 4.6** illustrates a single sifting operation applied to the dummy signal in **Figure 4.5**. As each sift splits the signal into the next IMF and residual trace, the number of IMFs extracted by EMD is one-more than the number of sifts. In this "ground-truth" example, the number of components which made up the signal [IMFs] is explicitly obvious. Thus, we know that only a single sift is necessary to decompose the data.

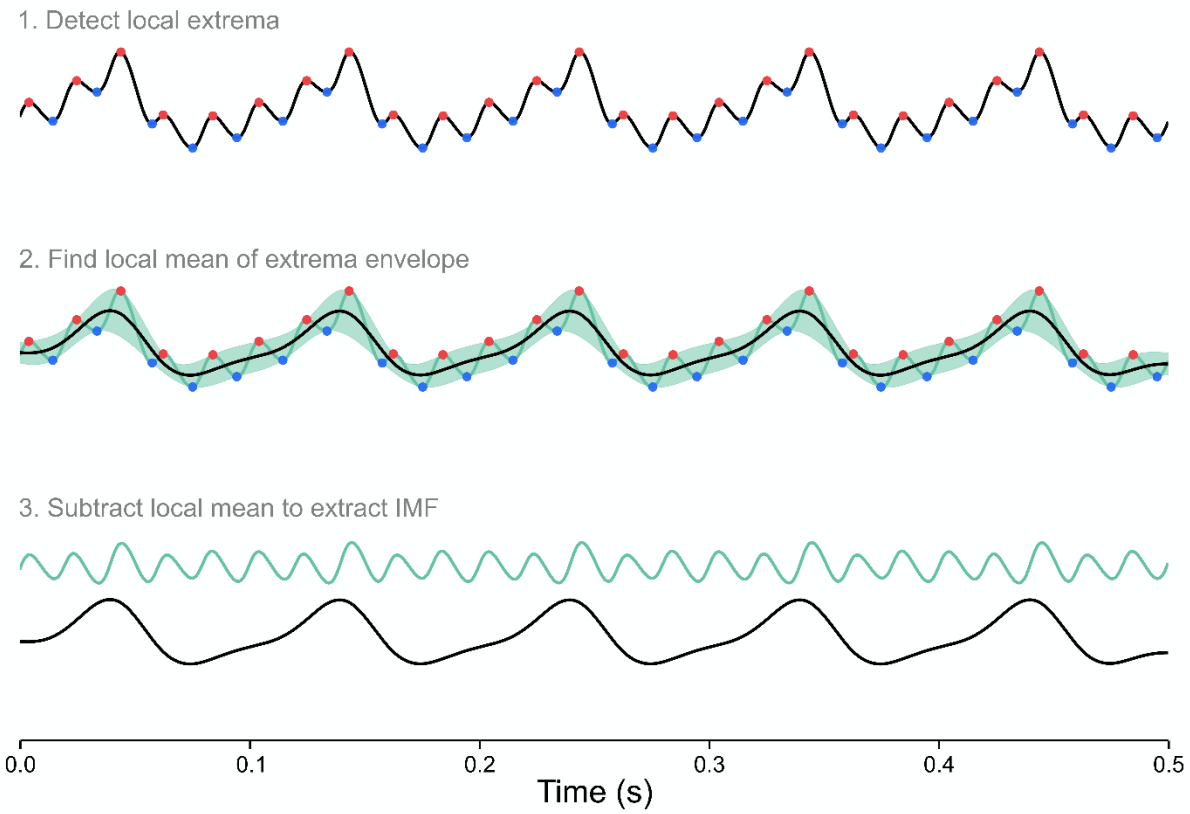


Figure 4.6: *Sifting algorithm for IMF extraction.*

As alluded to, the key advantage of using EMD over Fourier-based filtering methods to decompose a time-series is that the non-stationary properties of the extracted oscillations are more preserved. This is because the sifting process of EMD is directly informed by the local frequency dynamics of the signal. By contrast, an equivalent Fourier-based bandpass-filtering approach would not consider the local features in the data and instead rely on external sinusoidal assumptions. Knowing the ground truth, we can bandpass-filter the dummy signal for its the known frequencies (50 Hz and 10 Hz) which defined the dummy signal. **Figure 4.7**

compares the result of this Fourier-based extraction to an EMD sift. Note that the less-stationary 10 Hz oscillation is much better recapitulated by EMD.

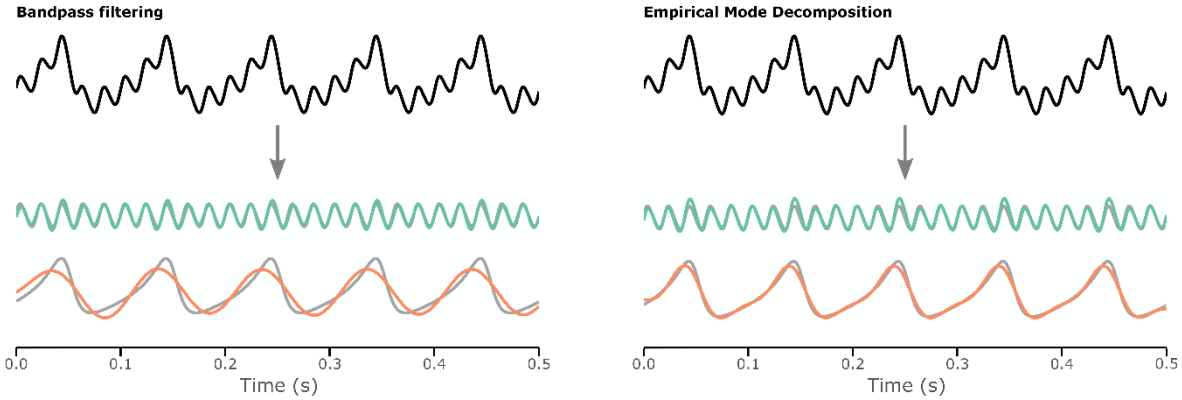


Figure 4.7: *Fourier-based filtering vs. empirical mode decomposition.*

Black traces: raw dummy trace as in **Figure 4.6**. **Coloured traces:** signal components extracted using Fourier-based Butterworth bandpass filtering (left) and IMFs extracted using EMD (right). **Gray traces:** original dummy components. Note how the slower signal extracted using EMD much better captures the non-stationary properties of the original dummy component.

Of course, neural LFP signals comprise a much more extensive frequency make-up. An example CA1 LFP recording is shown in **Figure 4.8A**. Note how the clearly observable theta cycles vary in amplitude, duration, and shape from cycle to cycle (this also being true of faster oscillations). To decompose such a signal, the sifting process is applied multiple times until a pre-defined intensity threshold is crossed (Huang et al., 1998). These sifting iterations comprise the full EMD operation. We can visualise the frequency range covered by each extracted IMF by computing its PSD (**Figure 4.8B**).

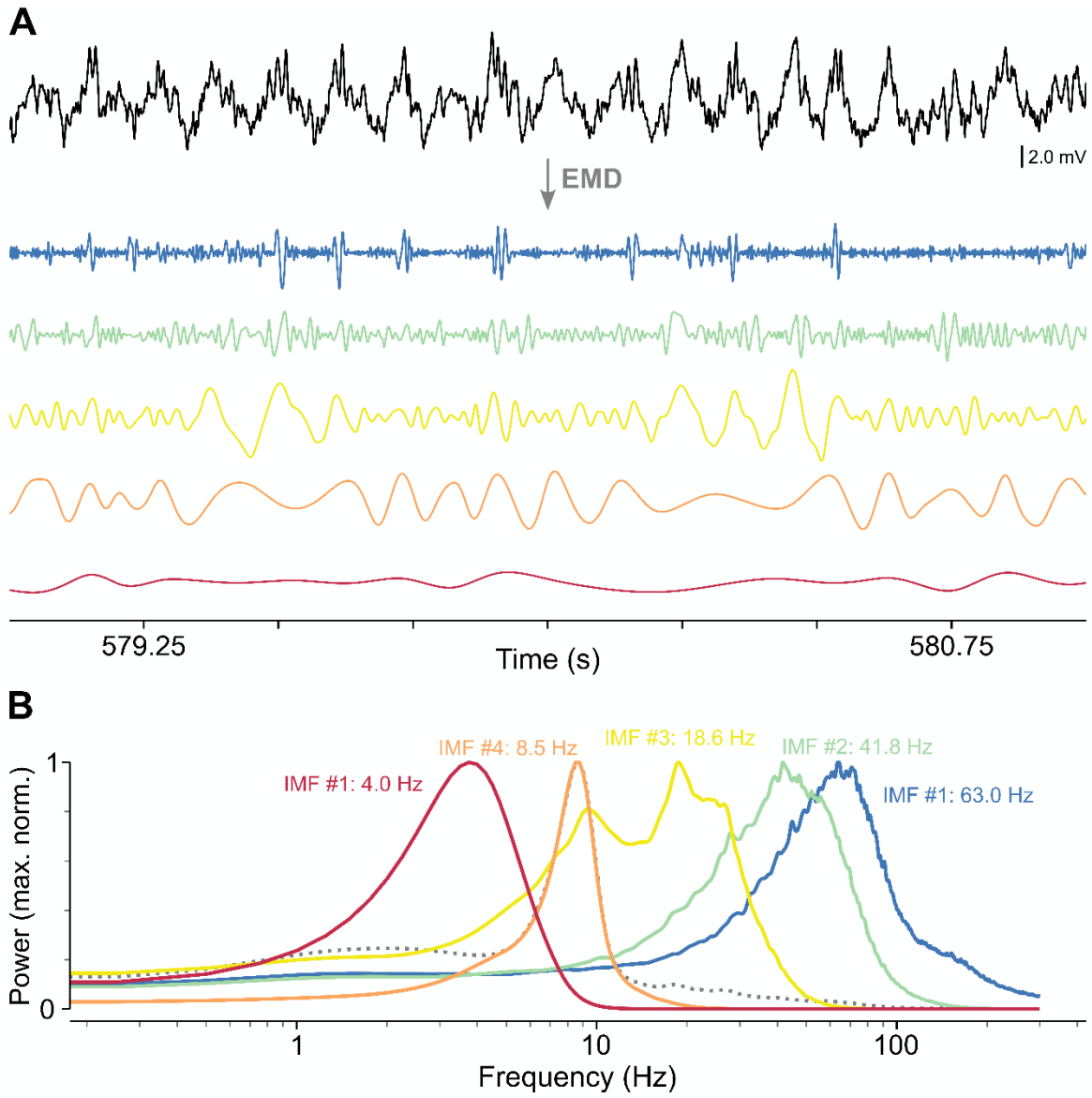


Figure 4.8: *Applying classical EMD to raw CA1 LFP.*

A: Example decomposition. **B:** Power spectral density spectra for each resulting IMF.

Inspection of both the IMFs and their power spectra show that there is an overlap in the frequency ranges covered between the IMFs. For example, the theta (4-12Hz) rhythm is best captured by the penultimate IMF (orange), however, we observe for example at 580.25–580.50 seconds that the theta "jumps" to the preceding IMF (yellow) (**Figure 4.8A**). This is confirmed by the presence of theta peaks seen in the PSDs of both these IMFs (**Figure 4.8B**). This effect is known as "mode mixing". We will now consider some variants of classical EMD which have been designed to deal with this issue.

Ensemble EMD

The first proposed solution to consider is known as ensemble EMD (eEMD) (Wu and Huang, 2009; Colominas et al., 2012). eEMD comprises of the averaging of an "ensemble" of IMFs extracted by EMD. For each ensemble entry, white noise is added to the raw signal prior to the sifting process. The logic behind this approach is that mixing between "true" IMFs is discouraged by the added noise, meaning that when averaging over the ensembles, the "frequency purity" of the resulting IMFs is enhanced. **Figure 4.9** shows that after applying eEMD, the power spectra of the IMFs are indeed more defined. Note that due to this random noise approach, the first IMF (grey) represents the residual of this averaged noise and should be discarded. While the gamma IMFs are more distinct, theta now appears to be captured by two IMFs, the faster of which also spanning the beta (13–25Hz) range. These CA1 IMFs produced by eEMD also could do better in reflecting the more diverse range of well-described, functionally-distinct, hippocampal frequency bands (Colgin et al., 2009; Scheffer-Teixeira et al., 2013; Schomburg et al., 2014; Middleton and McHugh, 2016; Lasztóczi and Klausberger, 2017; Lopes-dos-Santos et al., 2018). Let's now consider masked EMD, which addresses this, as well as the mode mixing problem.

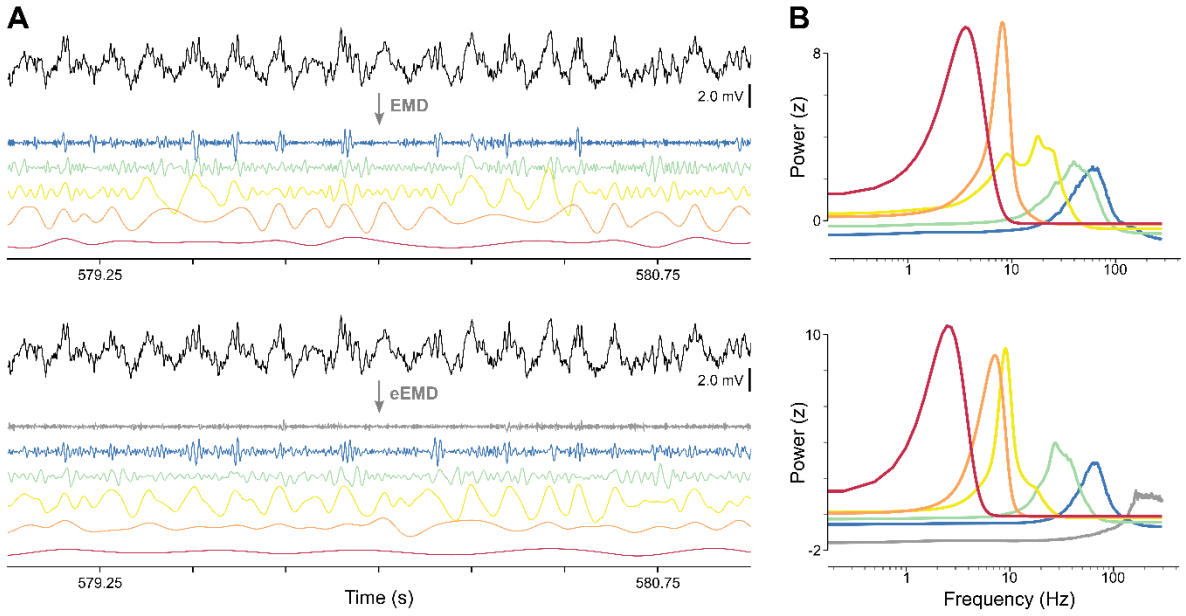


Figure 4.9: *Classic- versus ensemble- empirical mode decomposition.*

Comparison of IMF traces (**A**) and their PSD spectra (**B**) extracted by canonical EMD (top) and ensemble-EMD.

Masked EMD

Consider the dummy signal in **Figure 4.10** – comprised of: a "bursty" 25Hz, which varies in amplitude; and a "steady" 6Hz oscillation (with a fixed amplitude).

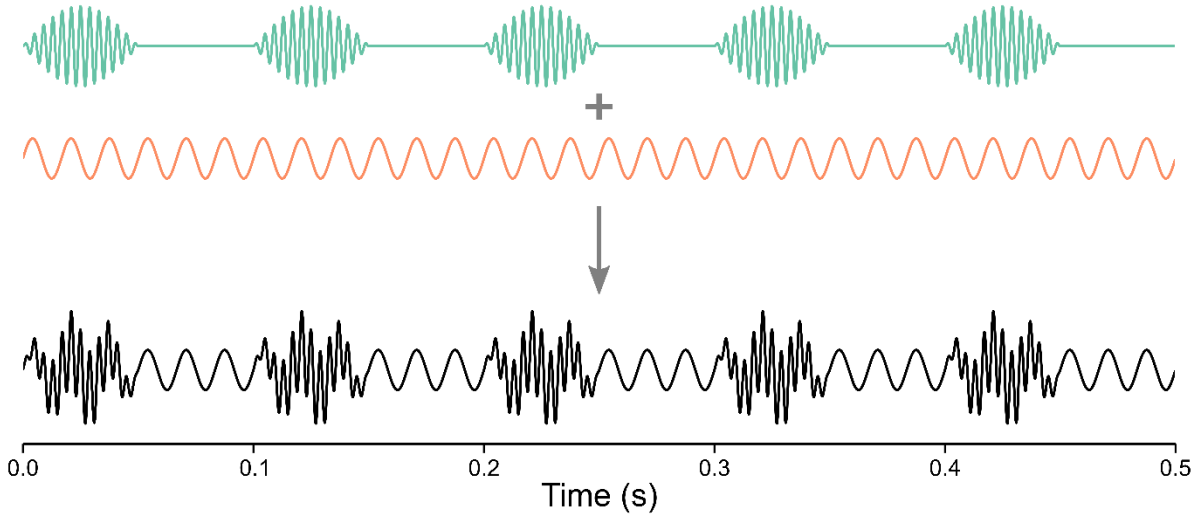


Figure 4.10: *Dummy signal.*

When EMD is applied to this signal (**Figure 4.11A**, top), mode mixing is seen during the periods where the 25 Hz oscillation diminishes in amplitude. Applying eEMD will isolate the 25 Hz oscillation as an individual IMF – but split the 6 Hz oscillation into two IMFs with a high correlation. While it is inappropriate to judge the quality of the IMFs based on ground-truth when it is known, IMFs, by definition, should be orthogonal (Huang et al., 1998). Given this, we should not be satisfied by the IMFs produced here by eEMD.

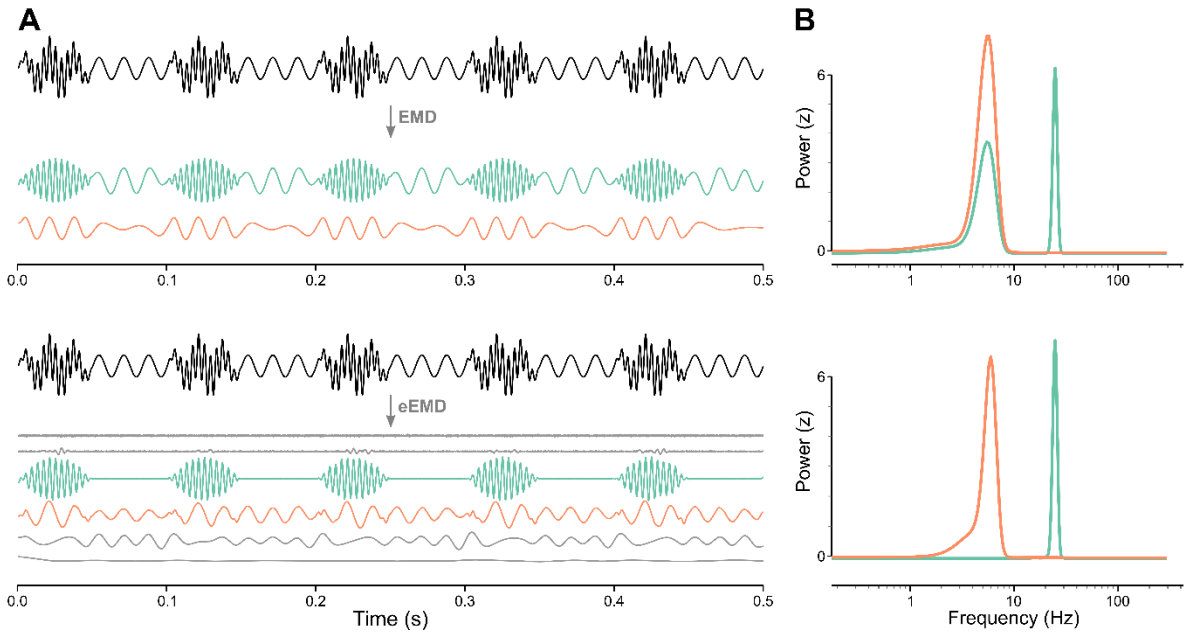


Figure 4.11: *EMD and eEMD both produce inappropriate decompositions.*

Comparison of IMF traces (**A**) and the PSD spectra of the coloured IMFs (**B**) extracted by canonical EMD (top) and ensemble-EMD (bottom).

Masked-EMD (mEMD) was proposed by Deering and Kaiser (2005) as a way to impose a lower bound on the frequency composition of an IMF in a given sift. This lower-bound is imposed by means of adding a sinusoidal masking signal of a specified frequency before the sift.[9] This operation is known as a 'mask sift' – and is depicted in **Figure 4.12**. When a sift is applied to the signal combined with 30 Hz masking signal, the time periods where the 25 Hz oscillation has zero-amplitude now contain extrema from the 30 Hz mask, and not the 6 Hz oscillation. In other words, the sift is now "blind" to the 6 Hz oscillation that it would otherwise "see" in the absence of the mask. The true IMF can then be obtained by simply subtracting the masking signal.

[9] To be exact, this operation is typically run for several masking signals, each commencing at a different, evenly-spaced start phase, and the average resulting IMF taken after mask signal subtraction.

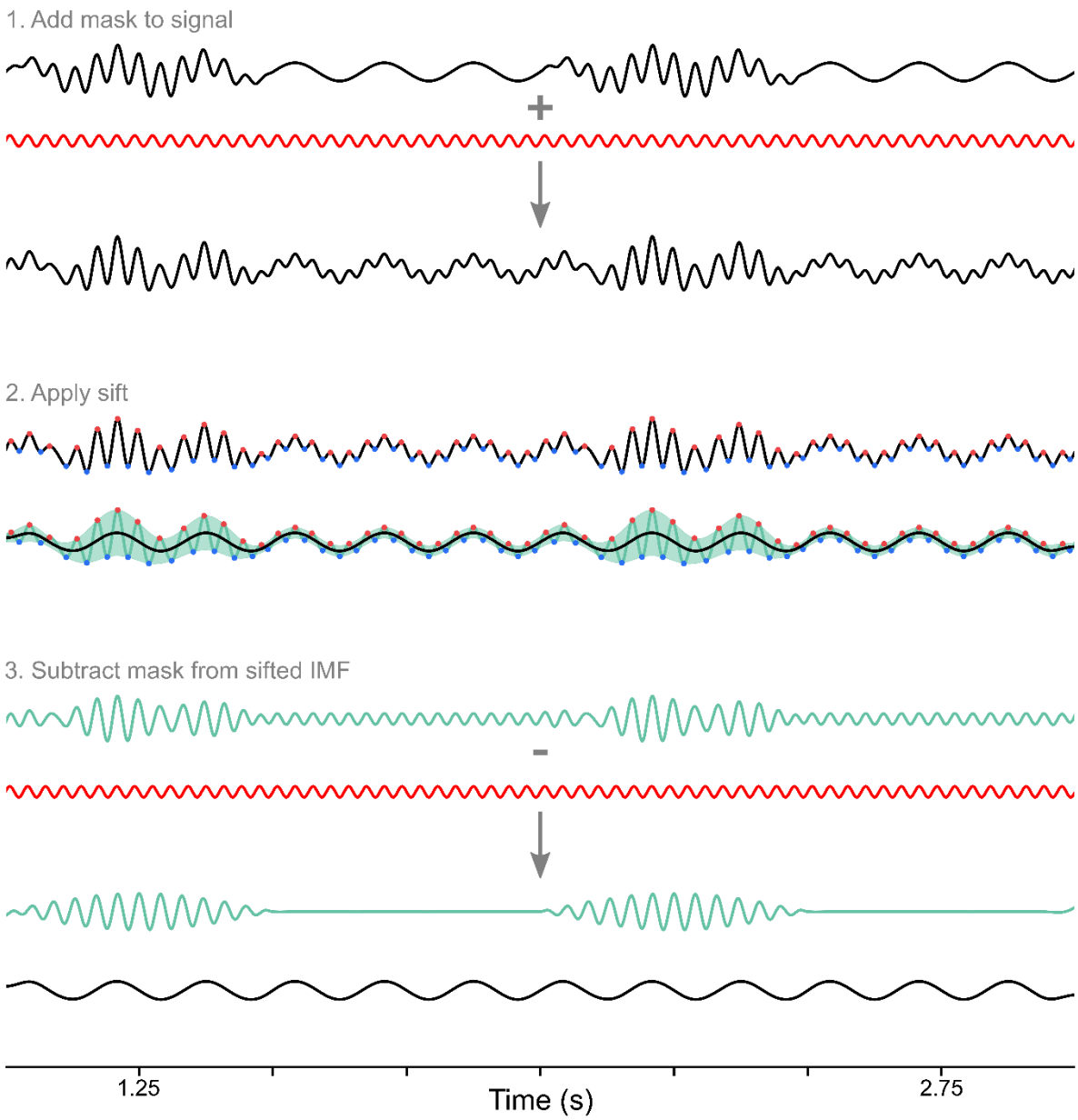


Figure 4.12: *Example mask-sifting operation.*

Tailored-mEMD

Of course, the performance of a mask sift will be dependent on the frequency chosen for the masking signal. Too high, and the faster [true] oscillation will not, or only partly, contribute to the extracted IMF. Too low, and the IMF will be a mixture of the true oscillations. Guidelines about choosing an appropriate masking signal have been suggested (Fosso and Molinas, 2017): If f_1, f_2 and f_m are the respective frequencies of the faster IMF, the slower IMF and the

masking signal, and if $\frac{f_1}{f_m} > 0.7$ and $\frac{f_2}{f_m} < 0.6$ can be and are met, the mask sift should separate f_1 and f_2 into successive IMFs (providing the mask amplitude is high enough). This mask frequency-designing strategy becomes harder to implement when f_1 and f_2 are unknown, and as the number of IMFs to be extracted increases. To the first point, this is indeed a problem I faced for all the five brain regions I recorded. While there is a general consensus on spectral definitions of CA1 LFP (Colgin et al., 2009; Scheffer-Teixeira et al., 2013; Schomburg et al., 2014; Middleton and McHugh, 2016; Lasztóczi and Klausberger, 2017; Lopes-dos-Santos et al., 2018), from which mask frequencies could be defined, less attention has been paid to the other regions. Also, defining masking signals based on external literature is still a somewhat arbitrary approach and takes away from the data-driven "unique selling point" of EMD.

To address this and the latter issue simultaneously, I developed a simple algorithm which optimises the set of mask frequencies to be used in mEMD and eliminates the otherwise arbitrary decisions required to arrive at mask frequency choices. To explain the principle behind this optimisation, let's consider the dummy signal from **Figure 4.10**. Here, a single mask frequency is to be found which will split the signal into its known composites. To converge on this frequency, a "mode mixing score" is defined to measure the mode mixing between the IMFs extracted by an EMD operation (in this case we are considering a single sift, so two IMFs will be used to compute the score). In accordance with the notion that IMFs should be orthogonal from one another (Huang et al., 1998), this score was defined as the average of all absolute pairwise Pearson correlations between IMFs. We can run multiple mEMD operations on the dummy signal, each time *randomly* choosing a frequency for the masking signal and measuring the resulting mode mixing between IMFs. If we did this for all possible mask frequencies within a suitable range, the frequency with the lowest mixing score can be deemed the optimised mask frequency to use for the mEMD extraction. This process is visualised in **Figure 4.13**.

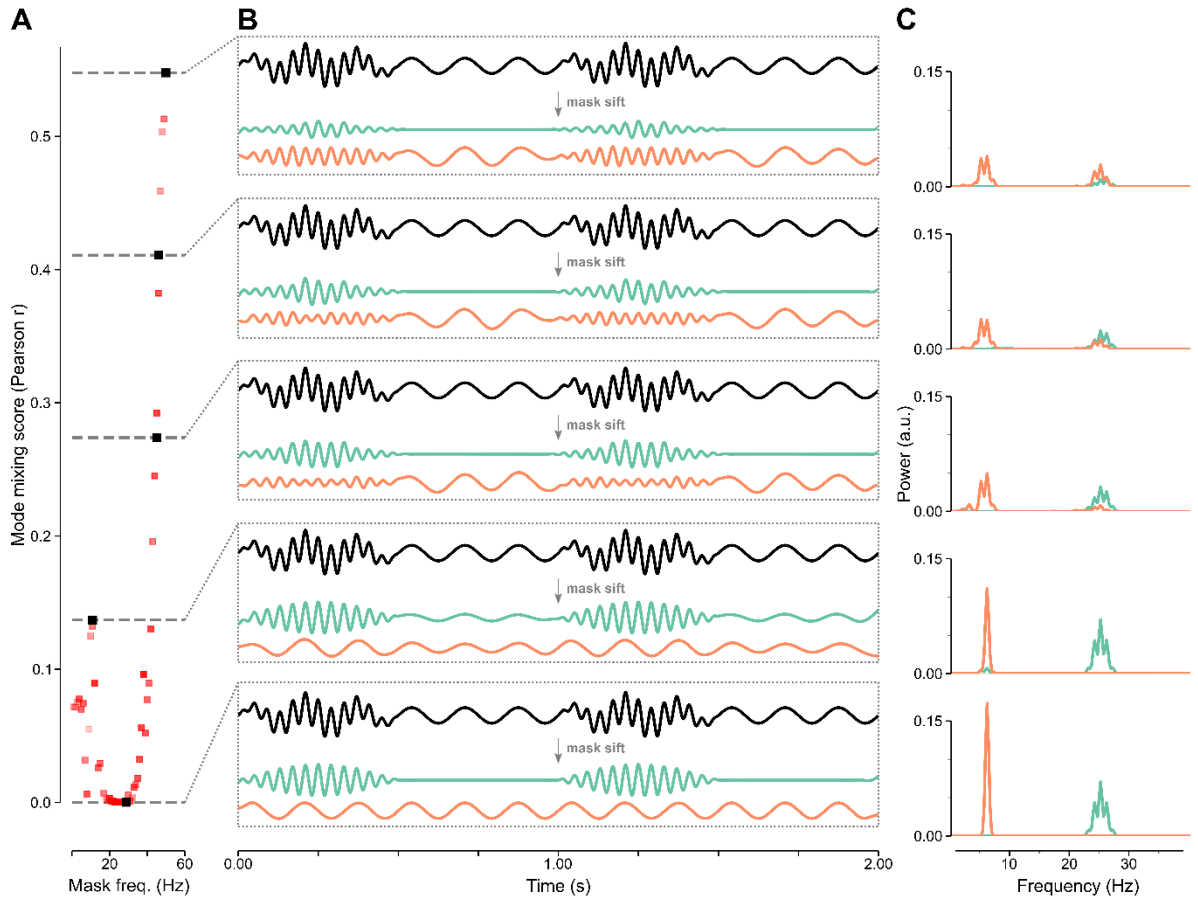


Figure 4.13: *Mask Frequency optimisation intuition.*

A: Mode mixing scores yielded for randomly selected mask frequencies (red squares). **B-C:** example IMFs (**B**) and PSDs (**C**) resulting from a mask sift corresponding to the mask frequencies indicated by the black dots in **A**.

The full algorithm is an extension of this principle and applies when there are several mask frequencies to be optimised – as is the case for my LFP data. Some key externally defined parameters are:

- a list of signals which are to be used to tune the optimisation
- the number of mask frequencies to be optimised
- the minimum and maximum values for these frequencies
- the mask frequency values which are to be fixed

Next, a series of iterations are implemented, each comprising a set number (200) of mEMD sub-iterations on the signals. In the first iteration, the mask frequency values to be used for each mEMD sub-iteration are randomly generated between the specified range. These masking

frequencies are saved, along with the mixing scores yielded for each of these sub-iterations. For subsequent iterations, random mask frequency generation is restricted to the frequency ranges observed in the top N of current mixing scores (in this case, $N = 5$). This iteration repeats until the ranges for each mask frequency converge to a single value; these values thus yielding the lowest mixing score. The implementation of this full algorithm to the example raw CA1 LFP trace is shown in **Figure 4.14**.[10]

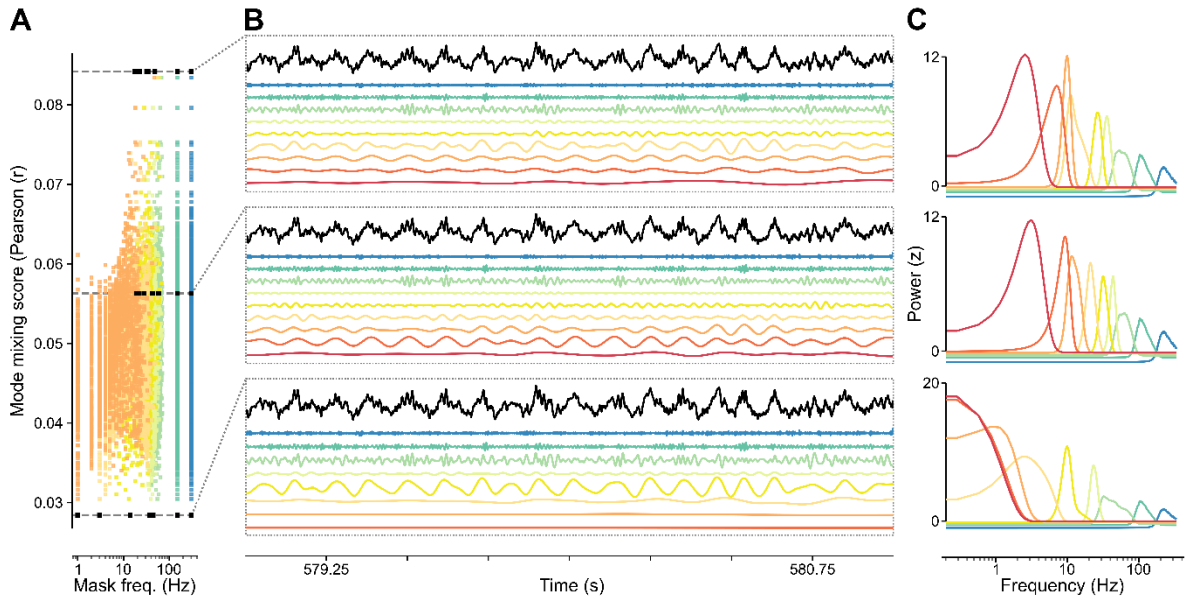


Figure 4.14: *Mask frequency optimisation algorithm for example CA1 LFP data.*

A: Mode mixing scores yielded for randomly-generated mask frequency sets (coloured squares). **B-C:** example IMFs (**B**) and PSDs (**C**) resulting from an mEMD operation corresponding to the mask frequency sets indicated by the black dots in **A**.

This algorithm was applied to each region and optimised over all recorded animals, such that the set of mask frequencies arrived at for each region yielded the lowest mean mixing score across animals.[11] The resulting IMFs from this tailored mEMD extraction are shown for the example animal in **Figure 4.15**.

[10] Currently available at: https://github.com/cjcw/optimise_emd. Following some additional work, this will be incorporated into the python module (https://pypi.org/project/emd/).

[11] Appling this procedure so as to tailor IMF extraction for individual animals would result in poorer spectral consistency between animals, coming at a bigger cost in terms of the complexity of the algorithm and later analysis.

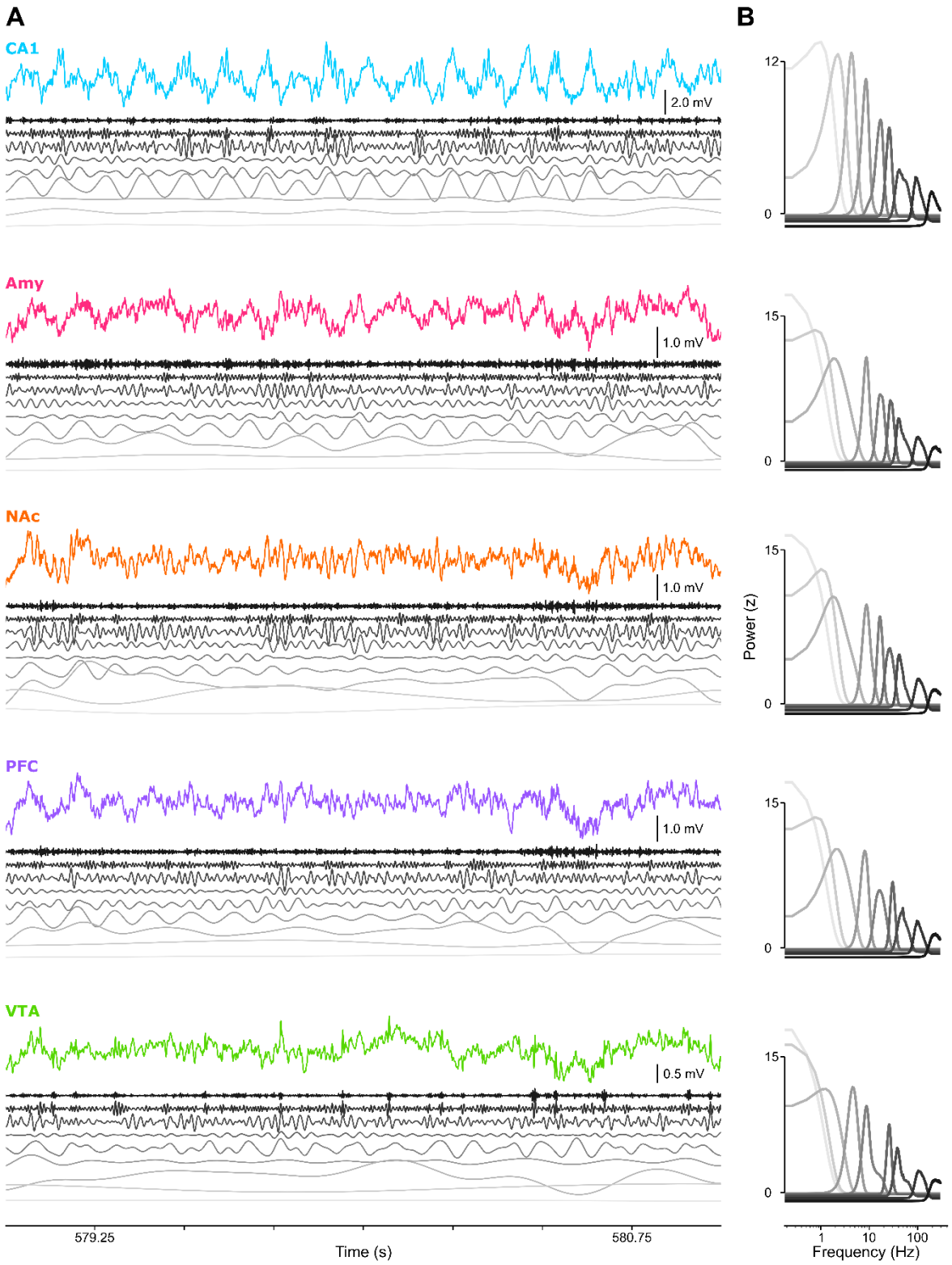


Figure 4.15: *Example region-tailored mEMD extraction.*

A: example LFP (coloured line) and IMFs (grey-scale lines) extracted by mEMD using the region-optimised set of mask frequencies. **B:** IMF power spectra.

Spike validation of region-tailored IMFs

In the next section (**4.4**), I describe the "barcode method", which uses the region-tailored IMFs to detect higher-order patterns of cross-regional network activity over fast-timescale processes. To proceed, it was important to increase confidence that these extracted oscillations were "real", and not a consequence of volume conduction. Cell spiking modulation by local IMFs in CA1, PFC and VTA strongly supported this notion (**Figure 4.16A,D-E**). The same was true of all NAc IMFs bar theta (**Figure 4.16C**), which in any case was not required for barcode detection. In the Amy, slow- and mid-gamma spike modulation was subtle, and has also been reported elsewhere (Stujenske et al., 2014). Amy spike modulation in these frequency ranges were also confirmed by the mode inter-spike intervals (ISIs) of a fair proportion of recorded cells (**Figure 4.17A**). A smaller proportion of cells had mode ISIs in the beta range (**Figure 4.17A**). In addition, the autocorrelograms of multiple cells were reminiscent of strong beta (and gamma) modulation (**Figure 4.17B**). I took these results to mean that it was appropriate to include all the supra-theta IMFs from all five regions for barcode detection and other downstream analyses.

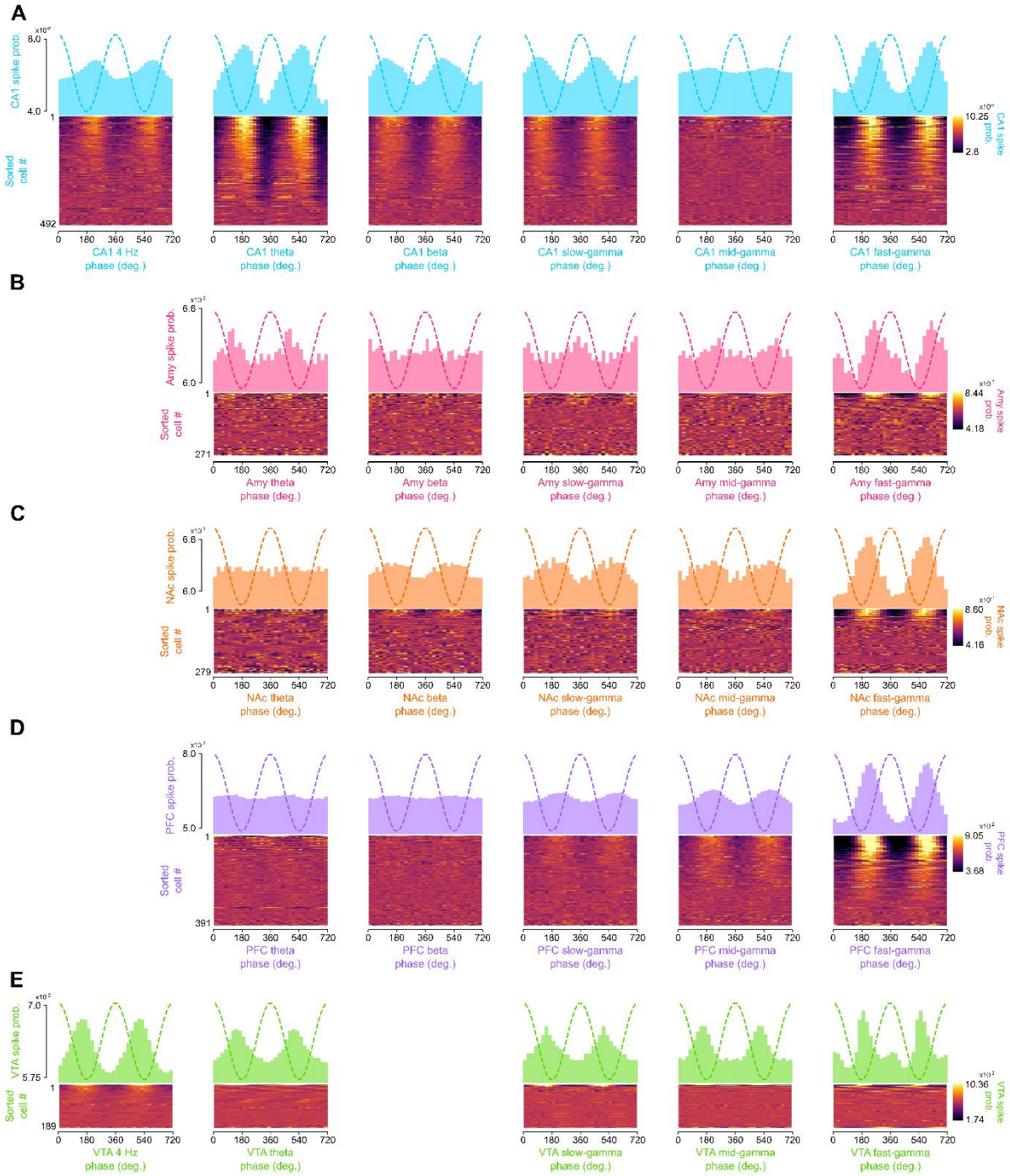


Figure 4.16: *Cell spiking validation of region-tailored IMFs.*

A-E: Mean spike probability as a function of local IMF phase (top), and tuning-sorted cell spike probability raster (bottom) for each recorded region. Cells firing less than 100 spikes were excluded. N = 492, 271, 279, 391 and 189 cells recorded from CA1, Amy, NAc, PFC and VTA, respectively.

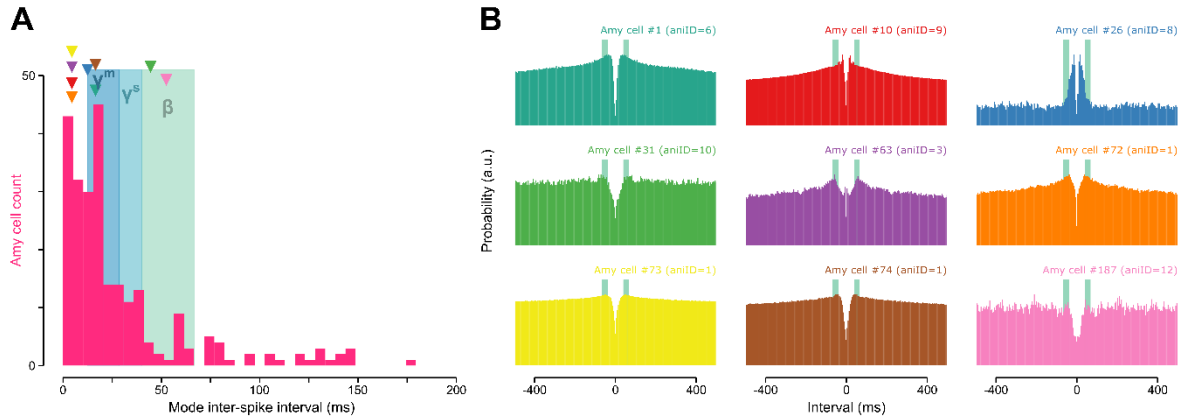


Figure 4.17: *Validation of beta, slow- and mid-gamma IMFs by Amy spike train analyses.*

A: Distribution of mode inter-spike intervals (ISIs) of all recorded Amy cells (n=271). Mode ISI ranges indicated by rectangle fills corresponding to ISIs in the mid-gamma (35–85Hz), slow-gamma (25–35Hz) and beta (15–25Hz) ranges. B: Example cell autocorrelograms coloured according to their mode ISI indicated by the arrows in (**A**). Rectangle fill corresponds to beta (15–25Hz) spike train modulation.

4.4| Detecting LFP interaction motifs using Independent Component Analysis

Premise

As visited in **1.3**, CA1, Amy, NAc, PFC and VTA have respectively been implemented (and by no means exclusively) in memory, conditioned reactions, motivation, decision making and reward representation. Clearly, these functions are individually crucial for the emergence of cocaine-seeking behaviour described in **Chapter 3**. These neural operations also heavily rely on one another. As a crude example, mnemonic representations [CA1] are a relevant informational item for conditioned behaviour [Amy], motivation [NAc], decision making [PFC] and reward processing [VTA]. Indeed, for most pairs of these regions, anatomical and optogenetic studies have indicated direct synaptic connectivity (e.g. Beier et al., 2015; McGarry and Carter, 2017; Trouche et al., 2019). Electrophysiological studies in rodents highlight the necessity of frequency-specific spectral interactions between regions for various cognitive operations (Meador et al., 2002; Jones and Wilson, 2005; Lesting et al., 2013; Brunet et al., 2014; Karalis et al., 2016; Zheng et al., 2019). There is an increasingly accepted premise in Neuroscience to move away from studying brain regions in isolation, and towards a more

interconnected system (Steinmetz et al., 2019; Stringer et al., 2019). Being in strong agreement with this premise myself – and leveraging the multidimensionality of this parallel CA1–Amy–NAc–PFC–VTA dataset, I decided to focus my analysis on the co-ordination patterns between these regions. I hypothesised that certain frequency-defined coordination patterns between regions would be more related to CPMR. I will now outline the method I developed to describe these higher-order patterns of CA1–Amy–NAc–PFC–VTA co-ordination, termed "barcodes".

Barcode detection method

Theoretical and empirical data reveal that coherence between anatomically-distinct brain regions will be stronger at slower frequencies (Whittington et al., 2000; Engel et al., 2001; Fries, 2005). These slower rhythms act as temporal gating mechanisms for more influential interactions to occur at faster timescales (Fries, 2005; Fujisawa and Buzsáki, 2011; Lisman and Jensen, 2013) (see **1.4**). Also, recent analysis focussing on CA1 LFP has revealed clear distinctions between theta cycles in their supra-theta frequency composition (Lopes-dos-Santos et al., 2018). Based on these notions, I set out to design a method which captured oscillatory nuances of fast-timescale interactivity in the CA1–Amy–NAc–PFC–VTA network, which was robust between animals. These nuances will be referred to hereon as "barcodes".

The time-series nature of the region-tailored IMFs (**Figure 4.15**), along with their data-driven and frequency-resolved properties, made them very suitable candidates to use for barcode detection. To focus on fast-timescale processes (i.e. relevant to synaptic potentiation (Markram et al., 1997)) IMFs with main frequencies within the 12–125 Hz range (i.e., beta and wide-gamma) were selected for this analysis (**Figure 4.18B**). Owing to the region-tailored nature of my mEMD algorithm (**Figure 4.14-4.15**), this selection yielded four IMFs each from CA1, Amy, NAc and PFC and three IMFs VTA (n = 19 total IMFs) (**Figure 4.18B**). The three IMFs which were common to all five regions corresponded to fast-, mid- and slow-gamma components. The fourth selected IMF seen not in the VTA but for all other regions was in the beta (13–25 Hz) range. Interestingly, and to note for later in this thesis, While the VTA lacked this beta IMF, the tailored-mEMD algorithm *did* uncover a 4 Hz IMF – which was also observed in CA1 but *not* in Amy, NAc or PFC (**Figure 4.15**). While this 4 Hz absence seems to contradict other reports in rodents (rats) which have revealed both the existence and functional significance of 4 Hz oscillations in these regions (e.g. Fujisawa and Buzsáki, 2011;

Karalis et al., 2016), the nature by which 4 Hz oscillations were isolated in these studies is very different to my mEMD-based, "mode mixing minimisation" approach (see **4.3**). 4 Hz IMF extraction by mEMD was indeed possible in all five regions if appropriate mask frequencies were used (data not shown). The fact that these mask frequencies were not arrived at for Amy, NAc and PFC (i.e., they yielded higher mode mixing) means that the algorithm was discouraged to separate these frequency bands. This suggests that 4 Hz is a less persistent phenomenon and one more correlated to theta in these regions.

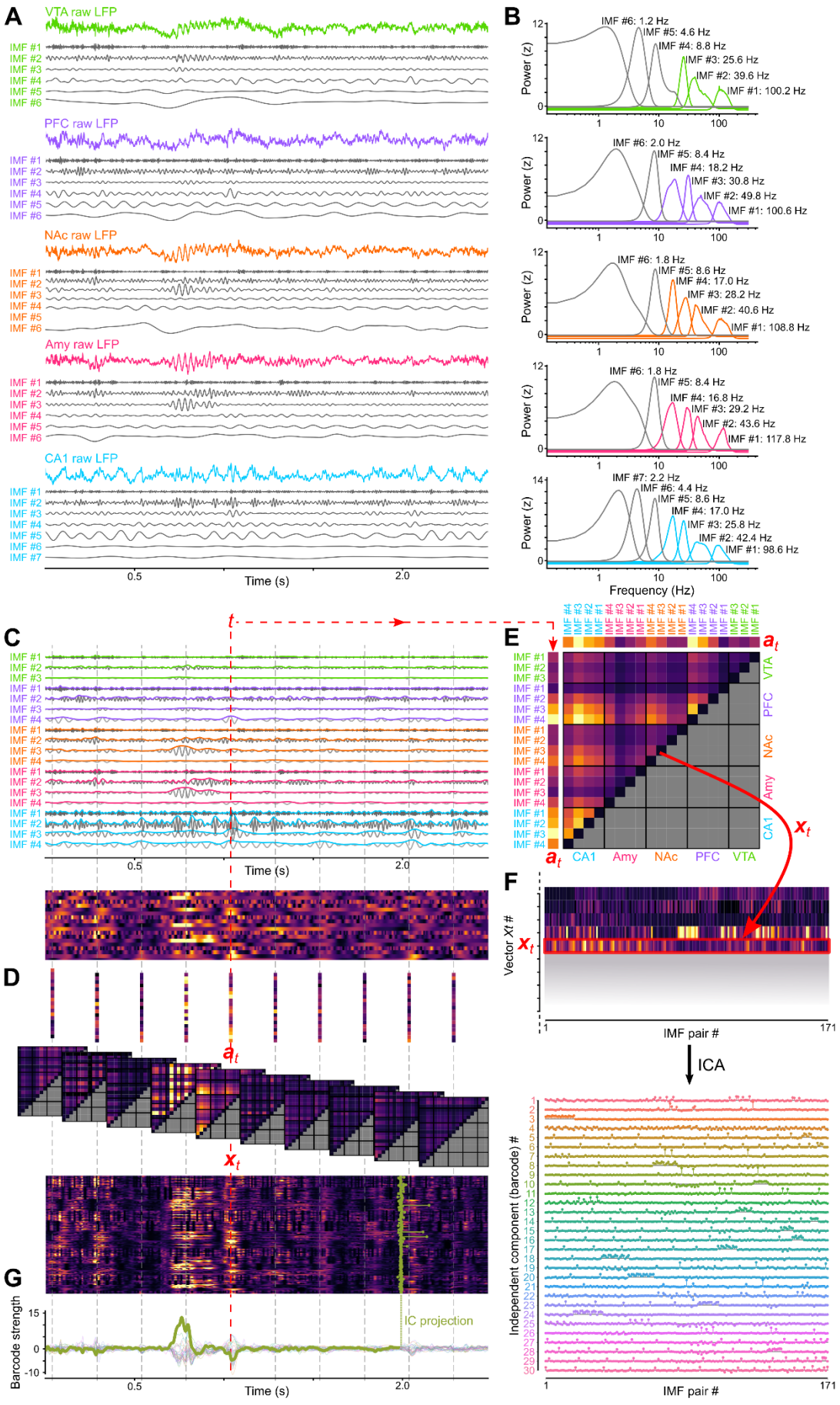
The selected IMFs in the 12–125 Hz range were used for the barcode detection method, which I will now describe. To each IMF signal, the Hilbert envelope was computed measure its instantaneous amplitude (**Figure 4.18C**, upper panel). These instantaneous amplitude signals were then normalised by their standard deviation, producing a time-series matrix where the amplitude of each IMF had unitary variance (**Figure 4.18C**, lower panel). At a given timepoint t, I defined a vector $\boldsymbol{a}_t$, which contained the normalised instantaneous amplitudes of these IMFs spanning the five brain regions (**Figure 4.18D**). For a given pair of IMFs, I took the product of their normalised instantaneous amplitudes at time t to represent their instantaneous co-engagement strength. Based on this principle, the set of all pairwise instantaneous IMF co-engagements were obtained by taking the outer product of the vector $\boldsymbol{a}_t$, only considering entries above and off the main diagonal such that all IMF pairs subsequently used were unique (i.e., each cross-IMF pair was only used once) and bipartite (i.e., no pairs were formed by a single IMF with itself) and (**Figure 4.18D-E**). This defined the vector $\boldsymbol{x}_t$, which therefore contained the set of instantaneous IMF co-engagement values (n = 171 cross-IMF pairs) at time t (**Figure 4.18D,F**).

To detect network motifs of coordinated oscillatory activities that consistently occur over time (i.e., the "barcodes" of co-engaged oscillatory activities), independent component analysis (ICA) was applied to a feature matrix X consisting of $\boldsymbol{x}_t$ vectors sampled every 250 ms (**Figure 4.18D,F**). Each extracted independent component is a weight vector with individual elements corresponding to the co-engagement of a given pair of IMFs (**Figure 4.18F**). The strength of a given barcode at time t was then defined as the dot-product between the weight vector of its independent component and the *non-normalised* instantaneous IMF co-engagement vector $\boldsymbol{x}_t$. This computation was performed on the co-engagement time-series matrix (derived from the non-normalised amplitude matrix) at original time resolution (1.25 kHz) to track the

instantaneous barcode strength (**Figure 4.18G**). For visualisation purposes, each barcode weight vector was converted to a square "interaction matrix" to depict the corresponding motif of IMF co-engagement it captured (**Figure 4.19**).

Figure 4.18: *Detecting and tracking barcodes* (**next page**).

A: Raw LFP traces (coloured) with decomposed oscillatory components (IMFs) extracted using region-tailored masked Empirical Mode Decomposition shown underneath. **B:** Power Spectral Density for each extracted IMF. IMFs with a main frequency within the 12–125 Hz range (coloured) were selected for barcode detection. **C:** Instantaneous amplitude time-courses for each of the selected IMFs from each region (top). These amplitudes were normalized by their standard deviation to produce the amplitude time-series matrix (bottom). **D-F:** Amplitude vectors $\boldsymbol{a}_t$ were sampled every 250 ms and converted to a co-engagement matrix by means of their outer product (**E**). Elements within the off-diagonal of this matrix were used to define the vector $\boldsymbol{x}_t$ which represented all unique pairwise co-engagements of IMFs. These $\boldsymbol{x}_t$ vectors were used to construct a feature matrix X (**F**, top), to which independent component analysis (ICA) was applied, resulting in 25 independent components ("barcodes") (**F**, bottom). **G:** The instantaneous strength of a given barcode vector was calculated by projecting its weight onto the non-normalised co-engagement time-series.


A
VTA raw LFP
PFC raw LFP
NAc raw LFP
Amy raw LFP
CA1 raw LFP
IMF #1
IMF #2
IMF #3
IMF #4
IMF #5
IMF #6
IMF #7
0.5
2.0
Time (s)
B
Power (z)
IMF #6: 1.2 Hz
IMF #5: 4.6 Hz
IMF #4: 8.8 Hz
IMF #3: 25.6 Hz
IMF #2: 39.6 Hz
IMF #1: 100.2 Hz
IMF #6: 2.0 Hz
IMF #5: 8.4 Hz
IMF #4: 18.2 Hz
IMF #3: 30.8 Hz
IMF #2: 49.8 Hz
IMF #1: 100.6 Hz
IMF #6: 1.8 Hz
IMF #5: 8.6 Hz
IMF #4: 17.0 Hz
IMF #3: 28.2 Hz
IMF #2: 40.6 Hz
IMF #1: 108.8 Hz
IMF #6: 1.8 Hz
IMF #5: 8.4 Hz
IMF #4: 16.8 Hz
IMF #3: 29.2 Hz
IMF #2: 43.6 Hz
IMF #1: 117.8 Hz
IMF #7: 2.2 Hz
IMF #6: 4.4 Hz
IMF #5: 8.6 Hz
IMF #4: 17.0 Hz
IMF #3: 25.8 Hz
IMF #2: 42.4 Hz
IMF #1: 98.6 Hz
Frequency (Hz)
C
t
Time (s)
D
a_t
x_t
E
a_t
VTA
PFC
NAc
Amy
CA1
x_t
F
Vector Xt #
IMF pair #
ICA
Independent component (barcode) #
G
Barcode strength
IC projection

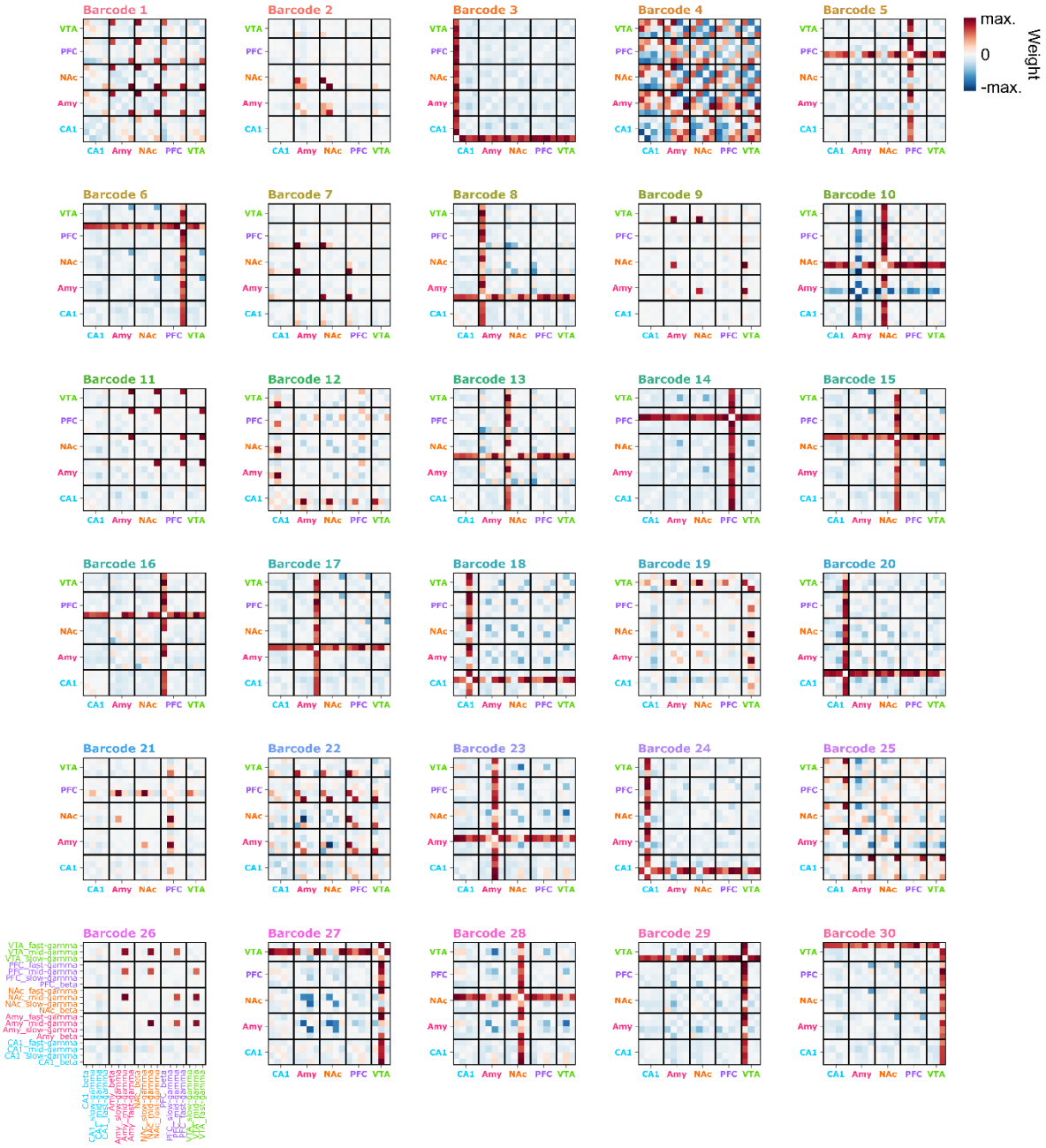


Figure 4.19: *Barcode visualisation.*

Each barcode independent component (**Figure 4.18F**) can be converted into a square matrix to visualize the co-engagement pattern it represents.

Barcode evaluation

Barcodes were detected for individual animals, as well as over the group data. To visualise the similarities between barcodes, I used the unsupervised clustering visualisation algorithm, *t-distributed stochastic neighbour embedding* (tSNE) (van der Maaten and Hinton, 2008)

(**Figure 4.20**). While there were some outliers, barcode consistency between animals was judged to be reasonable. This in mind, the barcodes detected at the group level (**Figure 4.18F, 4.19**) were used to calculate barcode strengths for subsequent analyses.

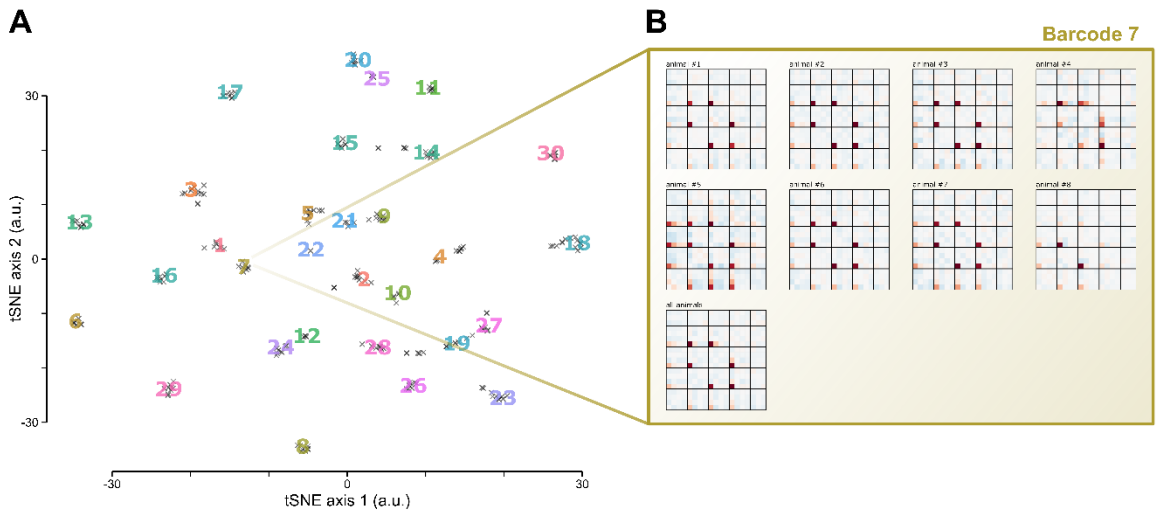


Figure 4.20: *Detected barcodes are robust between animals.*

A: Barcode independent component vector projections onto 2-D tSNE space. Crosses: barcodes detected from individual animals; coloured numbers: barcodes detected over all animals. **B:** Example barcode 7 cluster content.

To evaluate the physiological validity of a given barcode, the interaction between its strength time-course and other recorded variables (most importantly, spikes) was assessed. Shown in **Figures 4.21–4.23** are the "interaction profiles" of three example barcodes (see **2.8** for details). Barcode-barcode cross-correlations (**Panel B in Figures 4.21-4.23**) revealed a diversity of temporal relationships; many of these showing correlation peaks corresponding to time delays across multiple frequency bands. LFP and spike activity across the five regions triggered by barcode strength peaks (**Panel C and D, respectively Figures 4.21-4.23**) showed responses in-line with the region- and frequency-wise pattern of IMF co-modulation captured by the barcode. These results gave me the confidence that the barcodes indeed captured a physiologically relevant fine-scale motif of cross-regional and cross-frequency co-ordination – and could be pursued as candidate biomarkers of CPMR.

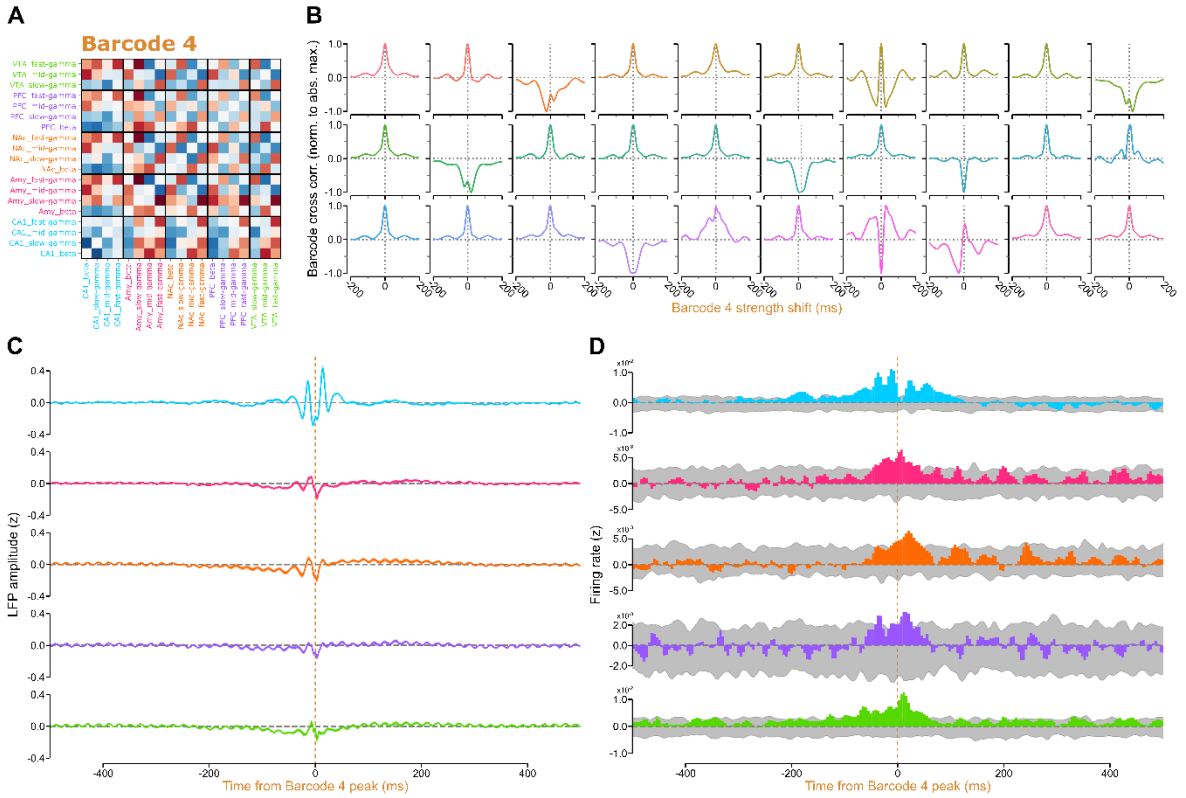


Figure 4.21: *Barcode 4 interaction profile.*

A: Barcode IMF co-modulation visualisation. **B:** Cross correlation of barcode strength against all other barcodes. **C-D:** barcode peak-triggered LFP (**C**) and spiking (**D**) responses. **C:** fill: mean ± SEM, n = 23 recording days from 15 animals. **D:** coloured plot: mean z-scored (5 ms) firing rates over cells. Grey fill: fill: 99% CI obtained from shuffled peaks. (See **2.8** for details). N = 493, 272, 281, 393 and 189 cells recorded from CA1, Amy, NAc, PFC and VTA, respectively.

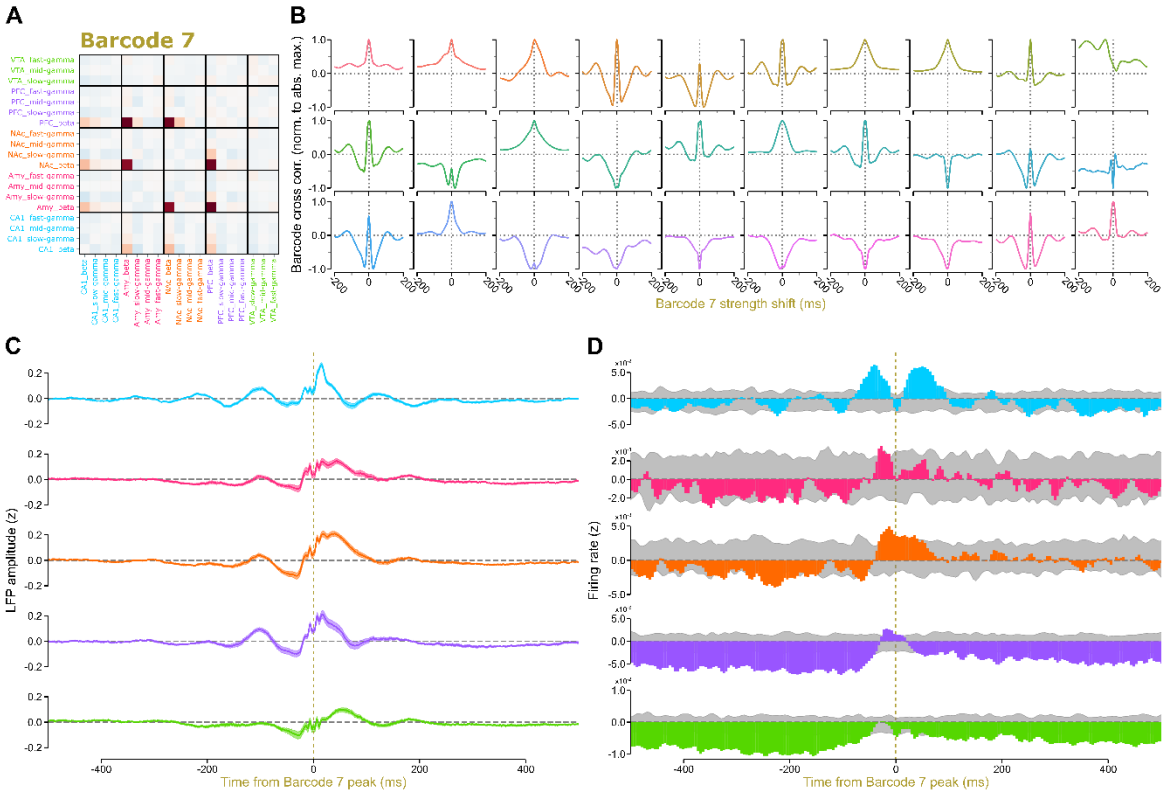


Figure 4.22: *Barcode 7 interaction profile.*

A: Barcode IMF co-modulation visualisation. **B:** Cross correlation of barcode strength against all other barcodes. **C-D:** barcode peak-triggered LFP (**C**) and spiking (**D**) responses. **C:** fill: mean ± SEM, n = 23 recording days from 15 animals. **D:** coloured plot: mean z-scored (5 ms) firing rates over cells. Grey fill: 99% CI obtained from shuffled peaks. (See **2.8** for details). N = 493, 272, 281, 393 and 189 cells recorded from CA1, Amy, NAc, PFC and VTA, respectively.

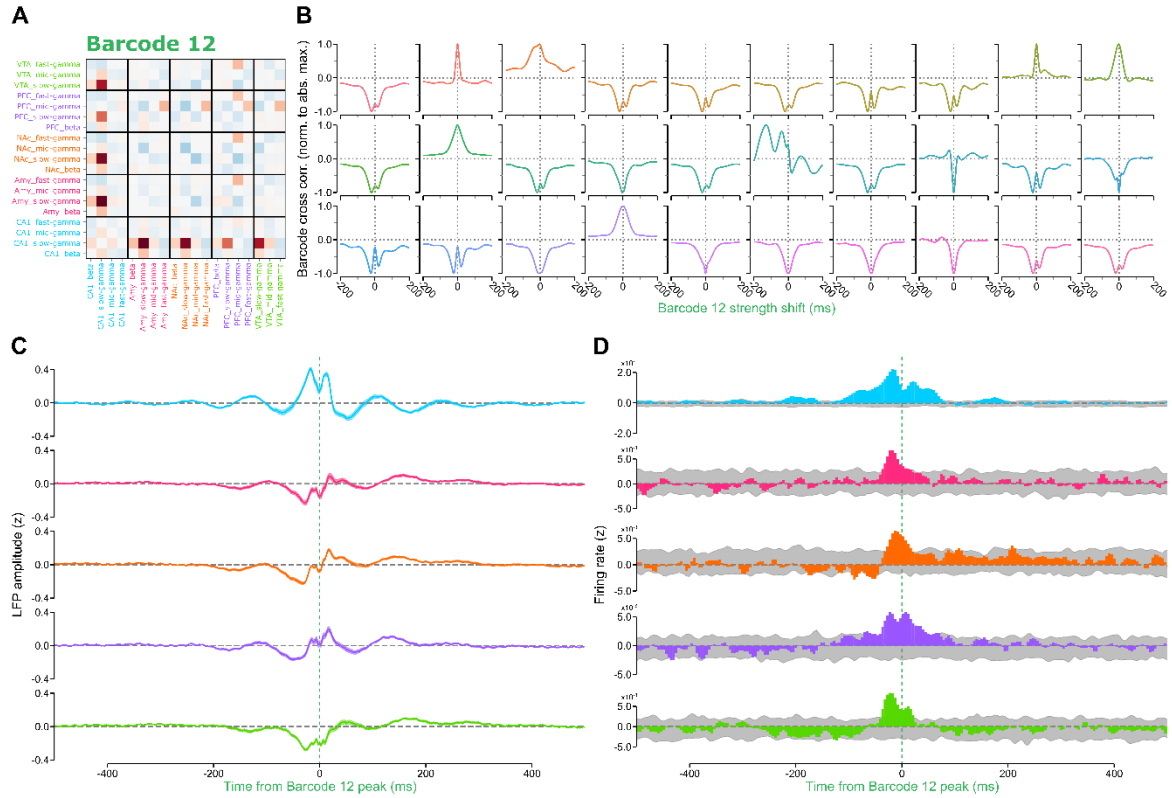


Figure 4.23: *Barcode 12 interaction profile.*

A: Barcode IMF co-modulation visualisation. **B:** Cross correlation of barcode strength against all other barcodes. **C-D:** barcode peak-triggered LFP (**C**) and spiking (**D**) responses. **C:** fill: mean ± SEM, n = 23 recording days from 15 animals. **D:** coloured plot: mean z-scored (5 ms) firing rates over cells. Grey fill: 99% CI obtained from shuffled peaks. (See **2.8** for details). N = 493, 272, 281, 393 and 189 cells recorded from CA1, Amy, NAc, PFC and VTA, respectively.

4.5| Discussion

Empirical mode decomposition offers a data-driven solution for the isolation of non-stationary frequency signals. While its elegance rivals more artificial Fourier-based methods, the unsupervised nature of EMD causes it "misbehave" under certain conditions, manifesting as mode mixing. This issue has spurred the development of the "*bycycle*" toolkit; which offers an alternative, non-stationarity-preserving, solution to EMD (Cole and Voytek, 2019). This approach extracts a non-stationary oscillation of a specified frequency range using a *broad* bandpass filter. A disadvantage of this method comes in the arbitrariness of this frequency band specification. This contrasts with the data-driven elegance of EMD, whose non-stationary

oscillatory components are directly informed by the signal, and further represent a complete decomposition, rather than just a single manufactured extraction. The authors of *bycycle* criticised EMD due to the mode mixing issue, and rather weakly passed off the eEMD and mEMD solutions as being "complicated" and "rarely applied in neuroscience". I believe my region-tailored mEMD algorithm addresses these criticisms by avoiding "parameter-fiddling" and offering a pragmatic, non-arbitrary route to the minimisation of mode mixing. Promisingly, the resulting IMFs of each region from this extraction were in-line with existing literature and physiologically validated by local spiking activities.

These IMFs comprised the base elements for the barcode method, which detects frequency-specific, cross-regional patterns of higher-order co-ordination within the CA1–Amy–NAc–PFC–VTA network at fine-scale time resolution. The resulting barcodes are yielded by independent component analysis (ICA). The goal of ICA is to converge to a set number of independent components (ICs) [barcodes] whose projections onto a multivariate signal [the feature matrix X] produce independent and non-gaussian signals (Jutten and Herault, 1991). Frequency- and region-specific interactions have been linked to a variety of flexible cognitive operations (e.g. Meador et al., 2002; Jones and Wilson, 2005; Brunet et al., 2014; Harris and Gordon, 2015; Sokolenko et al., 2019), making ICA an attractive option to model multiregional patterns of neural co-ordination. Indeed, ICA has been used for fMRI (Jarrahi et al., 2015; Nikolaou et al., 2018), EEG (Yuan et al., 2015), MEG (Brookes et al., 2011) and LFP (Korovaichuk et al., 2010; Lopes-dos-Santos et al., 2018) data analyses. Most relevantly, Lopes dos Santos et al. (2018) proposed a method which the supra-theta content of individual CA1 theta cycles could be described by ICA – and additionally demonstrated input- and behavioural specificity of these so-called theta-nested spectral components.

In developing the barcode method, I indeed considered the input options used by Lopes dos Santos and colleagues. Detecting supra-theta patterns of *multiregional* co-ordination nested in CA1 theta cycles would have been a biased and inappropriate choice, as my goal was to detect patterns of activity that were independent over fine timescales, rather than independent between [theta] cycles. It thus made sense to sample $\boldsymbol{x}_t$ vectors at coarse, down-sampled intervals. Using wavelet spectrograms as a time-frequency signal, rather than the instantaneous amplitudes of IMFs, led to greater barcode inconsistencies between animals. While it can be useful to consider between-subject spectral variation in analyses (Quinn et al., 2020), I believe the "mopping up" of this variation (**Figure 4.2**) represented a more practical analytical choice for

the purposes of this thesis. Additionally, the reduction of frequency dimensionality by IMF extraction made calculating barcode strengths a much less computationally-intensive operation.

Finally, ICA requires the number of ICs to be externally specified. Applying principal component analysis (PCA) to the feature matrix X of each animal revealed that 19–22 "PC-barcodes" were needed to explain 90 % of the variation in X, and 36–56 PCs were needed for 95% explained variance.[12] Using 20 ICs meant that almost all (18) barcodes showed "statistically inevitable" patterns (akin to e.g. barcodes 3, 6, 17 in **Figure 4.19**). This was due to the outer product derivation of the $\boldsymbol{x}_t$ vector (**Figure 4.18E**), which produced groups of inherently correlated dimensions in the feature matrix X. In other words, twenty was not a large enough number of ICs to "force" ICA to identify the *truly* higher-order patterns of multiregional co-ordination (e.g. barcodes 1, 2, 4, 7, etc. in **Figure 4.19**). Using 30 ICs meant that roughly one-third of the detected barcodes fell under this category. More pragmatically, the key conclusions in the next chapter, which assesses the relevance of the barcodes to cocaine-seeking behaviour, are insensitive to varying the number of detected barcodes.

[12] The orthogonality restriction imposed by PCA, along with the fact that the resulting components are designed to capture variance and not independence, made barcode detection using PCA an unsuitable choice.

5 | Multiregional beta co-ordination relates to dynamic cocaine-seeking behaviour

The psychological mechanisms of reward-seeking behaviour outlined in **1.1** informed the design of the behavioural paradigm which successfully modelled the expression, extinction, and renewal of cocaine-seeking behaviour (**Chapter 3**). Lacking from current literature is an understanding of how the oscillatory dynamics of the brain support "cocaine-paired memory retrieval" (CPMR) mechanisms; whereby anatomically-distinct, multimodal sources of information – relevant to cocaine experience – are retrieved and integrated across the brain via fine-timescale interactions. The barcode method (**4.4)** was inspired by this niche. This chapter addresses my hypothesis that the dynamic cocaine-seeking behaviour, precipitated by CPMR, relates to the engagement of specific co-ordinations of frequency-resolved multiregional neural activity. In this chapter, I reveal that barcodes consisting of beta-centric interactions show the strongest behavioural correlate of CPMR.

5.1 | Beta amplitude modulations most strongly reflect a signature of cocaine-paired retrieval

Beta barcode strength modulation relates to dynamic cocaine-seeking behaviour

The barcodes detected in **4.4** represent oscillatory motifs of network co-ordination spanning the beta–to–fast-gamma (15–125 Hz) range. I hypothesised that specific barcodes would relate more to the expression of cocaine-seeking behaviour observed in the Recall (**REC**) and Renewal (**REN**) stages of my behavioural assay (**Chapter 3**). Due to variability between animals in the length of the total extinction session, it was most analytically suitable to compare barcode strengths between the saline- and cocaine-paired zones for each test stage. To hone-in on the barcodes whose engagement dynamics across the protocol were most related to CPMR, a stage-wise "CPMR vector" was defined (**Figure 5.1A**), based on the psychological principles

of incentive salience outlined in **1.1**. This was used to calculate "CPMR scores" for each barcode (for details, see **2.9**) (**Figure 5.1B**). Importantly, beta-barcodes (**Figure 5.1C**) consistently yielded the highest CPMR scores – and were thus considered the strongest neural candidates for CPMR and the subsequent precipitation of cocaine-seeking behaviour. The stage-specific zone strength differences for the top three "CPMR-barcodes" are shown in **Figure 5.1D-E**. Note these barcodes all consist a high contribution from beta-interactions.

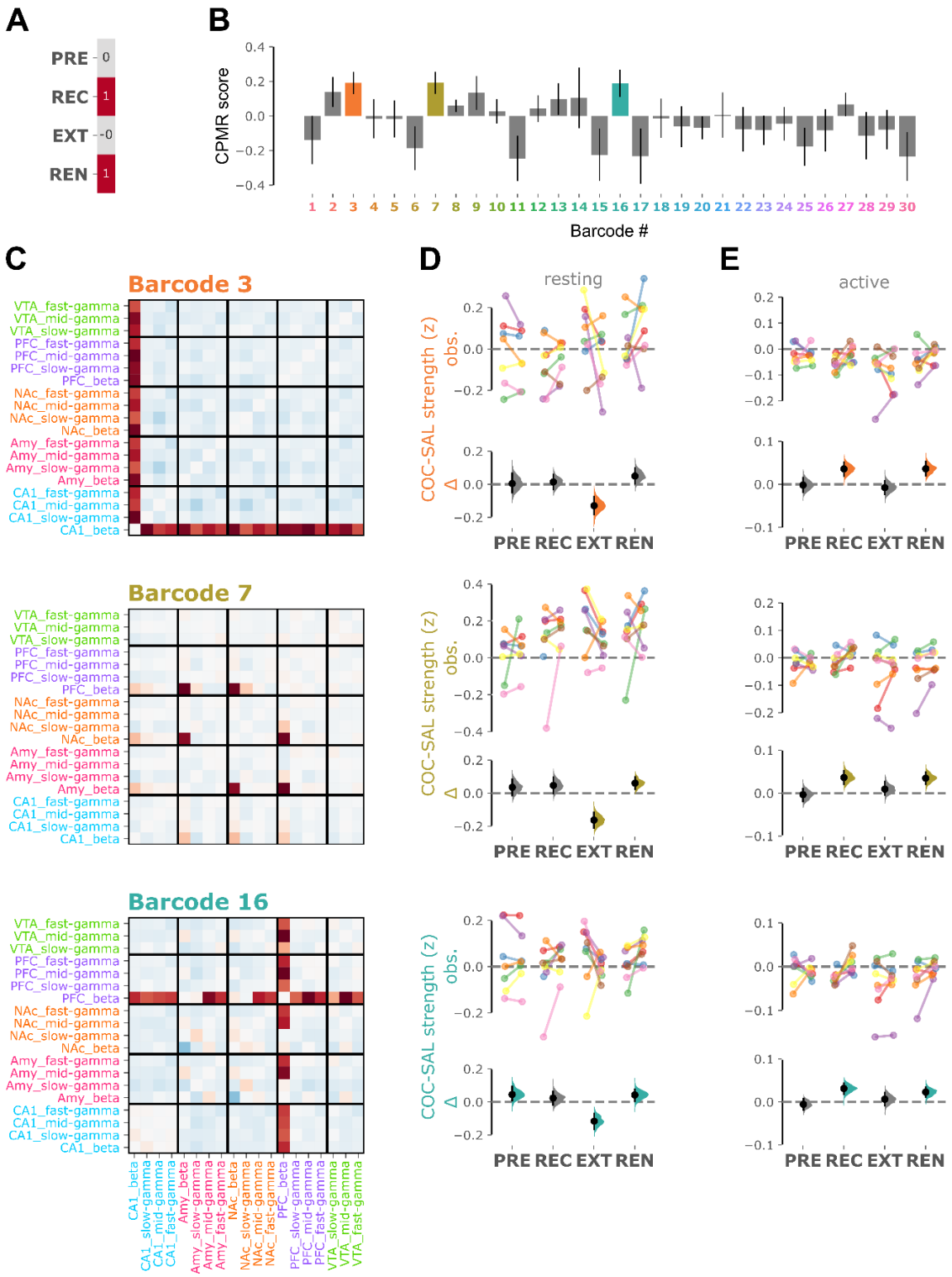


Figure 5.1: *Beta barcodes show the strongest neural correlate of cocaine-seeking behaviour.*

A: A "CPMR vector" was defined to score each barcode's relationship with cocaine-seeking behaviour. **B:** Barcode "CPMR scores". Error bars: mean ± SEM. **C:** Visualisation of the top-three CPMR-scored barcodes. **D-E:** Barcode zone strength modulation differences across stages for resting (**D**) and active (**E**) behavioural windows (see **2.9** for details). Top: SAL-COC animal observations; bottom: mean difference estimation plot. n = 100,000 bootstrapped 1 s windows per animal (n = 8).

Beta amplitudes

Positing that beta was the common underlying factor relating to CPMR, I next explored the individual contributions of beta for each region (where a beta IMF was extracted) were analysed in the same way. For all these regions, beta modulation strengths showed a similar "CPMR signature" (**Figure 5.2**), supporting the notion that CPMR-related beta enhancement is a global, not a region-specific phenomenon. Closer inspection of the region-isolated beta modulation data revealed some subtleties depending on the test stage, behavioural state (resting/active; see **2.9**) and, albeit to a lesser extent, brain region. Most apparently, zone-related beta enhancement during Recall and Renewal was more related to active (> 2 cm s^{-1}) behaviour, whereas the reversal effect of this beta modulation seen in Extinction was stronger during resting (< 2 cm s^{-1}) periods.

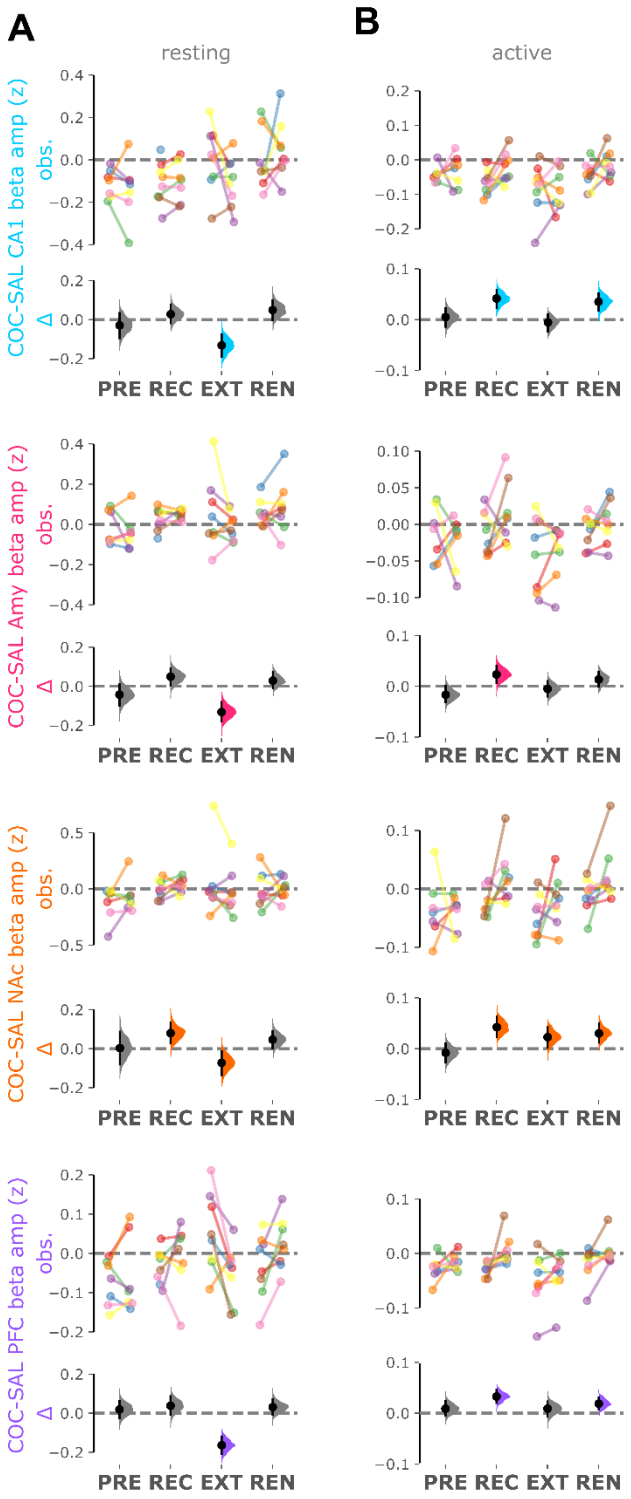


Figure 5.2: *Beta IMF amplitudes show a neural correlate of cocaine-seeking behaviour across regions.*

A-B: Region zone beta amplitude modulation differences across stages for resting (**A**) and active (**B**) behavioural windows (see **2.9** for details). Top: SAL-COC animal observations; bottom: mean difference estimation plot.

While no significant differences in zone speeds were observed at the group level for any of the test stages (**Figure 3.2**), it is still possible that beta modulation differences between zones could be explained by speed variability.[13] This was directly assessed using a mixed model analysis of covariance (ANCOVA), whereby beta amplitude variation explained by speed (and animal identity) is accounted for prior to the zone beta amplitude distributions being tested. This statistical analysis indicated that in Recall, beta amplitude modulation in all by zone in CA1 and Amy was significant at the $p < 10^{-3}$ level, and for NAc and PFC at the $p < 10^{-5}$ level. For Extinction, zone beta-modulation was significant for CA1 ($p < 10^{-3}$), Amy ($p < 10^{-3}$) and PFC ($p < 10^{-4}$). These speed-accounted effects were also weakly seen NAc during Renewal ($p < 10^{-2}$) and the reverse in the Pre-test for Amy ($p < 10^{-2}$).

The relationship between locomotion speed and beta amplitude was also visualised (**Figure 5.3**; see **2.X**). In the Pre-test, beta amplitude was significantly correlated to speed for all regions and zones ($r^{min, max, med} = [0.044, 0.231, 0.141]$, $p^{min, max, med} = [8.06 \times 10^{-39}, 1.43 \times 10^{-2}, 1.43 \times 10^{-11}]$, Pearson correlation coefficient). Strikingly, in the post-conditioning test stages, this speed–amplitude relationship was much weaker – sometimes to the point of insignificance, and in several cases, was reversed (i.e. a negative speed correlation). The extent of these correlation changes was also almost always stronger for the cocaine- vs saline-paired zones. A speculative interpretation is that a cocaine experience may affect motor-related influences of beta dynamics, however this specific hypothesis is untestable with this experimental data.

[13] Using 1-s behavioural windows; EXT and REN were significant at the $p < 0.001$ level; mixed ANOVA model, for the speed * zone interaction; regressing out variance explained by individual animals.

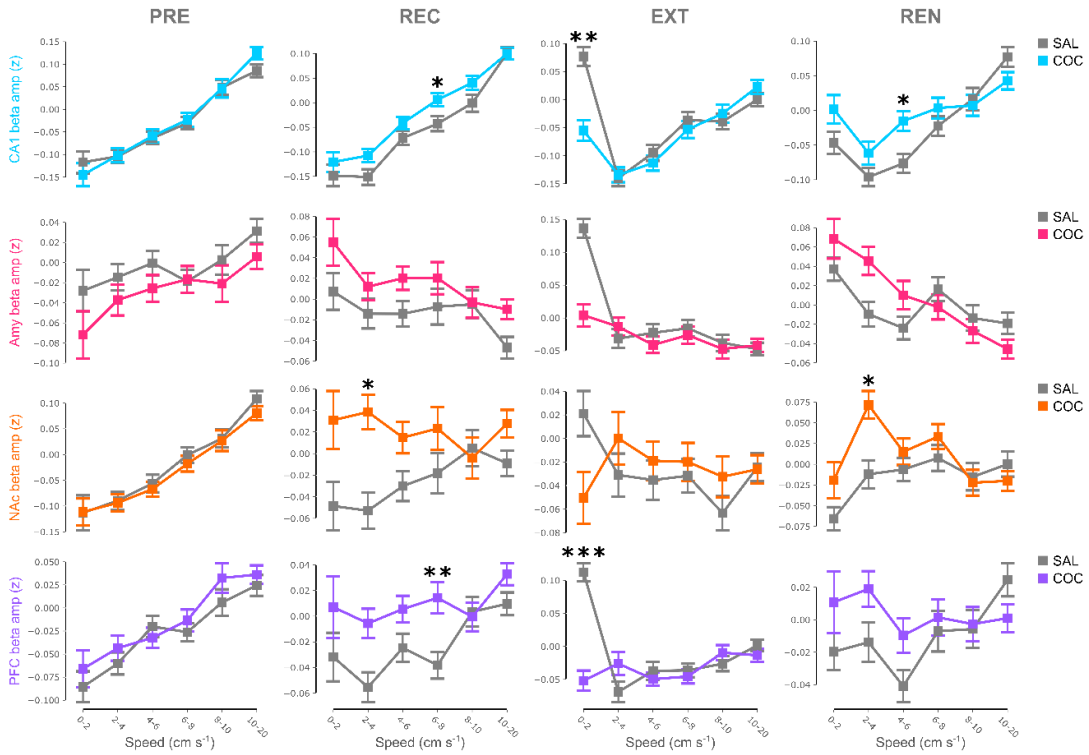


Figure 5.3: *Beta IMF amplitude modulation by speed across test stages.*

Error bars: mean ± SEM for 1 s speed bin windows over animals. ***p < 0.001; **p < 0.01; *p < 0.05; two-way mixed ANOVA linear model for zone*speed bin interaction, accounting for animal effects, with Bonferroni correction for multiple comparisons (n = 6 speed bins).

5.2 | Discussion

The fact that beta barcodes were stronger in the cocaine- vs saline-paired zone in the **REC** and **REN** stages of the task suggests that these higher-order patterns of global network co-ordination may represent a frequency-specific process by which cocaine-paired information is retrieved. Computational modelling has demonstrated that synchrony over longer conduction delays (i.e., between distally-connected brain regions) is much better tolerated by beta- than gamma oscillations (Kopell et al., 2000). This supplements the hypothesis that CPMR constitutes a global state of oscillatory co-ordination. This beta-enhancement effect was tied specifically to active behavioural periods, where LED trigger events (the most obvious readout of cocaine-seeking behaviour (**Figure 3.2**)) would have been more frequent. Intriguingly, a beta-enhancement *reversal* effect was seen in **EXT**, suggesting that beta amplitude modulation acts as a dual-mechanism for cocaine-paired memory retrieval and extinction. Behavioural evidence indicates that extinction is the process of the *new* learning, rather than un-learning a

CS-US association (see **1.1**). Perhaps, to supress the cocaine-retrieval process, a new brain-wide CS representation may be instated via a similar pattern of beta co-ordination, but by an orthogonal assembly of neurons. Distinguishing this beta modulation effect in **EXT** from that in **REC** and **REN** was that the **EXT** effect sizes were stronger during resting behaviour. Behaviourally, the largest difference in the proportion of time spent resting between zones was seen in **EXT** – where animals were less active in the saline-paired zone (**Figure 3.3A-B**). This beta enhancement could therefore be explained by a "rest duration -dependent beta enhancement" effect – where resting beta increases in amplitude, but only after a set period of inactivity. During **EXT**, these instances would be more frequent in the saline-paired zone. More specific analyses could address this issue, combining insights from the behavioural factor analysis (**Figure 3.4**) to potentially elucidate a more sophisticated relationship between beta and cocaine-seeking behaviour.

The complex relationship between the stages of the experiment, locomotion speed and beta barcode strength indeed made the interpretation of this data challenging. To dissect these variables, I considered the contributions of individual region betas, and their relationships with locomotion speed. To statistically account for speed-amplitude and animal-amplitude interaction effects, I applied a 2-way ANCOVA model to each region and test stage. While still preserving significant beta modulation by zone for all regions in the Recall stage, and all bar NAc during EXT, this covariation analysis indeed revealed that the interaction between zone and beta amplitude was in part explained by locomotive influences. Strikingly, correlational analysis suggested that cocaine experience may disrupt a prior-existing positive speed–amplitude relationship, positing a complex, cocaine experience-dependent relationship between beta co-ordination and ongoing behaviour.

To conclude this chapter, I will now briefly summarise a few *speculative* thoughts relating to this result, which perhaps apply in a more general sense to the field of behavioural neuroscience. The brain exists to serve a biological organism by processing and representing patterns of energy in the world, to ultimately translate them to an adaptive motor output. This translation process is immensely complex. Owing partly to this, a crude dichotomy between the cognitive- and motor functions of the brain is often implicitly assumed in behavioural neuroscience, prompting the notion that a neural process is only a true one if the effect exists after behavioural covariates are controlled for. This is indeed valid – especially when the mechanism in question specifically being explored is an internal one. However, in the case of

this analysis, the intended behaviour to be modelled was intrinsically related to locomotion speed (**Figure 3.4**). While analytical and statistical controls may help in disentangling the cognitive-versus-behavioural effects of beta modulation, both ultimately seem to relate to cocaine-seeking behaviour. The hypothesis that there exists a purely cognitive "CPMR state", which subsequently engages the motor system in cocaine-seeking behaviour is misguided. The cognitive–to–behavioural translation operation performed by the brain represents an incredibly complex information routing system. Anatomically, the NAc, and more broadly, the striatum, is situated to play a central role (Groenewegen et al., 1996; Everitt et al., 2001). The (in particular, dorsal-) striatum has been extensively linked to motor control – primarily via beta-band oscillations (Engel and Fries, 2010; Little and Brown, 2014; Khanna and Carmena, 2015). This may tenuously link to the results here as zone-dependent beta amplitude modulations in the NAc were more accounted for by speed with the ANCOVA. To elaborate, global beta co-ordination signatures correlate with a complex CPMR process, whereby "cognitively-centric" representations (more related to cortical and limbic areas) engage motor-influencing ones. Beta band oscillations present a good candidate for this process; as they are slow enough to facilitate cross-region coupling (Kopell et al., 2000), but fast enough to facilitate dopamine-dependent plasticity (Zhang et al., 2009).

6 | Orchestration of multiregional beta coordination

The analysis presented in **Chapter 5** suggests that CPMR is related to a brain-wide, rather than region-specific, phenomenon of oscillatory co-ordination in the beta range. This observation posits that these global beta co-engagement patterns are orchestrated by a shared mechanism. Conduction delays found in larger, cross-regional networks of neurons are longer and more variable (Ermentrout and Kopell, 1998). This principle underlies the fact that these large-scale networks of neurons preferentially synchronise over slower frequencies (Whittington et al., 2000; Engel et al., 2001; Fries, 2005). These slower oscillations report rhythmic fluctuations of network excitability, which transiently gate cross-regional synchrony of neuronal sub-populations over faster frequencies (i.e. beta and gamma). Such rapid timescales of neuronal co-activation are necessary to elicit convergent downstream responses (Lorente de Nó, 1939; Spruston and Johnston, 1992; Koch et al., 1996), and as such are thought to reflect a functionally-relevant syntax of neural information (Buzsáki, 2010).

My analysis suggested that the retrieval of cocaine-paired information manifested via the global co-ordination of neural activities in the beta range. This chapter presents two key sets of analyses focussed on revealing the potential mechanisms by which these transient events of frequency-specific co-ordination are mediated. In **6.1**, I explore phase-amplitude coupling relationships between beta activities and slower oscillations, revealing a particularly important role of the VTA 4 Hz IMF. In **6.2**, I present a method by which VTA cell-types were classified as putative glutamatergic or dopaminergic. Using this *preliminary* classification, I determined that putative dopaminergic cells in the VTA play an important role in multiregional beta co-ordination. In the future, this analysis will inform the design of a closed-loop optogenetic experiment that looks to provide a means of testing the causal role of multiregional beta co-ordination patterns in eliciting cocaine-seeking behaviour.

6.1 | Temporal orchestration of global beta co-ordination by theta and 4 Hz oscillations

I decided to explore the phase modulation of beta by slower oscillations to link this putative mechanism of CPMR to a universal coupling agent. Both theta and 4 Hz oscillations are evidenced to co-ordinate faster processes across brain regions with relevance to behavioural performance (Jones and Wilson, 2005; Siapas et al., 2005; Sjulson et al., 2018; Fujisawa and Buzsáki, 2011; Karalis et al., 2016). The tailored mEMD approach (**4.3**) extracted theta IMFs from all five regions, and 4 Hz IMFs from CA1 and VTA (**Figure 4.16**). Owing to this and the literature as cited, I focussed on investigating theta and 4 Hz oscillations each from CA1 and VTA (**Figure 6.1**).

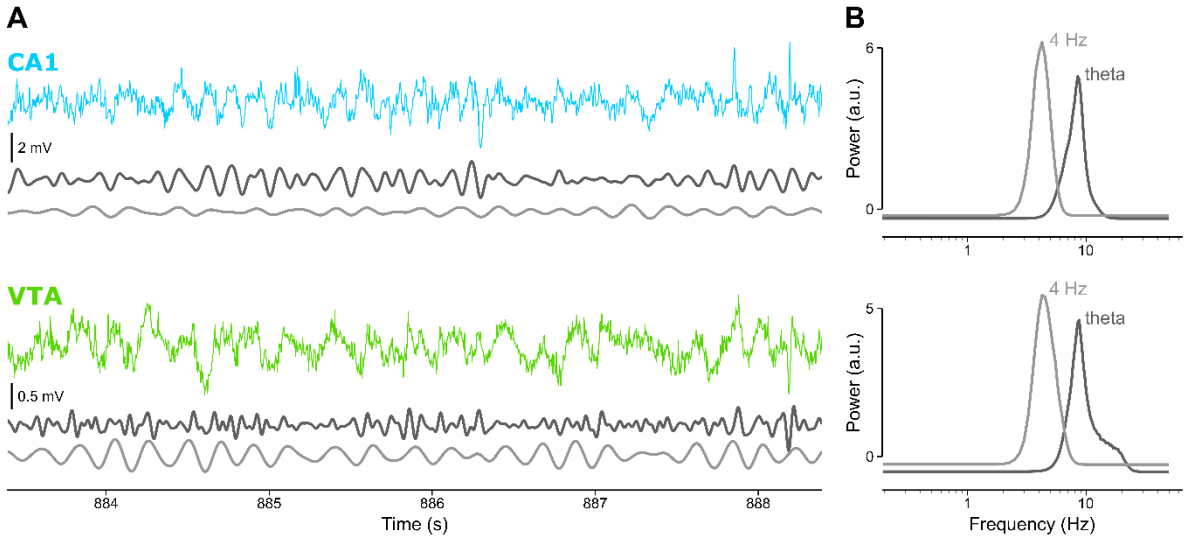


Figure 6.1: *Example extracted candidate coupling oscillations by tailored mEMD.*

A-B: Example theta and 4 Hz IMF traces (**A**) and power spectral density estimates (**B**) from CA1 (top) and VTA (bottom).

A role of VTA 4 Hz oscillations in modulating individual beta activities

I first assessed phase-amplitude coupling (PAC) of beta amplitudes by each of the candidate coupling oscillations, by calculating the average amplitude as a function of the coupling oscillation phase (**Figure 6.2A-D**). From this, PAC scores were derived (for details, see **2.10**), and used to quantitatively compare the influence each coupling oscillation had on the beta

amplitudes for each region (**Figure 6.2E-H**). As expected, CA1 beta was most modulated by local theta (**Figure 6.2E**), however CA1 beta amplitude was still considerably modulated by local 4 Hz, VTA theta and VTA 4 Hz (**Figure 6.2B-D**). For Amy and NAc betas, VTA 4 Hz yielded the strongest phase modulation (**Figure 6.2F,G**). This phase modulation was almost as strong for PFC beta (**Figure 6.2D**), which was most strongly modulated by CA1 theta (**Figure 6.2H**). Overall, VTA-, rather than CA1, coupling oscillations more strongly modulated beta amplitudes. Intriguingly, beta amplitude peaks over the four regions were most phase-aligned by VTA 4 Hz (**Figure 6.2D,I-L**), suggesting the temporal co-ordination of beta activities by VTA 4 Hz. This phase control of beta also implied a region-specific directionality; whereby CA1 beta would peak before that of Amy, NAc and PFC (**Figure 6.2L**).

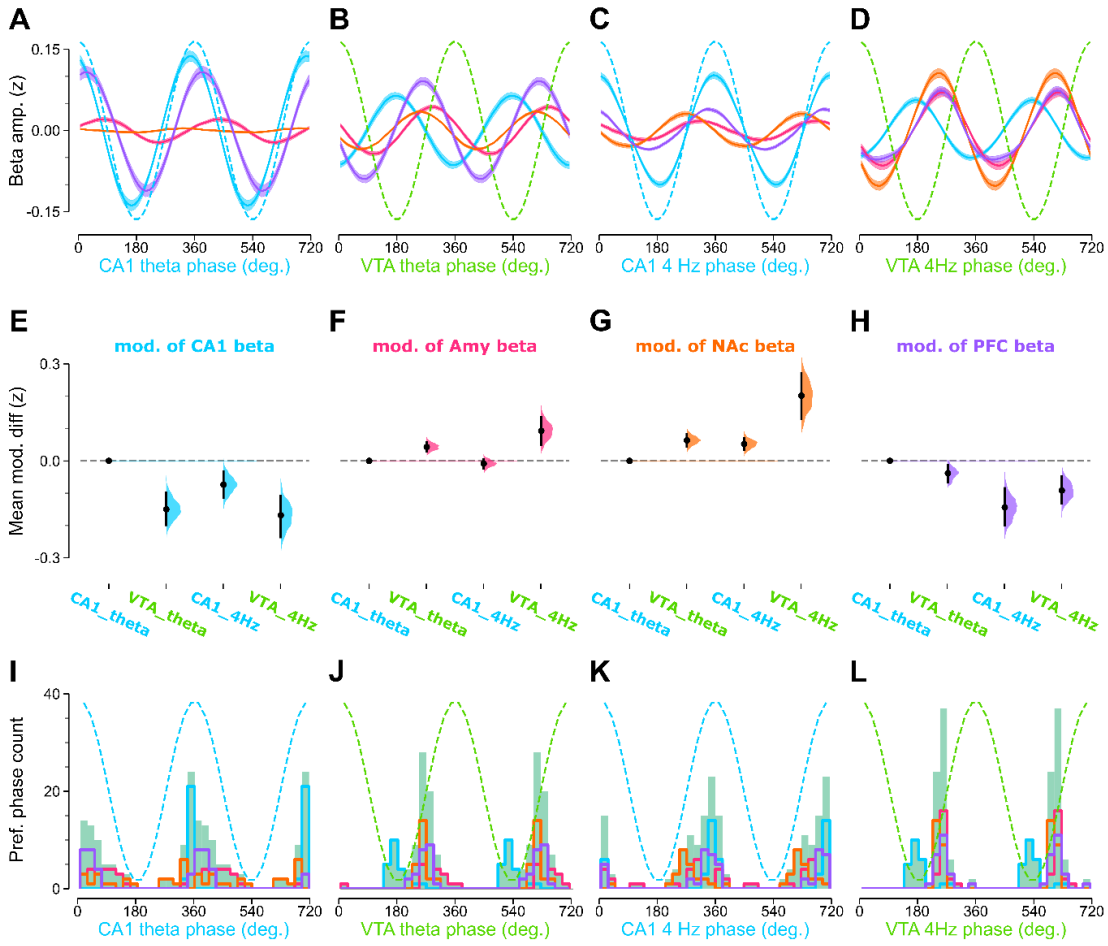


Figure 6.2: *VTA 4 Hz oscillations exert strong phase modulation and co-ordination of beta amplitudes.*

A-D: Phase-amplitude plots for beta amplitudes using the phase of each coupling oscillation [panel]. Graph shows mean (bold line) ± S.E.M (fill). **E-H:** Paired mean difference estimation plots of beta modulation scores (see **2.6**) of each region [panel]. **I-L:** Histograms showing the preferred phases of beta activities for each region (colour). N=23 recording days from 15 animals.

I next compared PAC scores between each of the supra-theta IMFs for each beta-region to explore the frequency-specificity of PAC by each of the candidate coupling oscillations (**Figure 6.3**). Theta oscillations in both CA1 and VTA tended to modulate slow-gamma more strongly (though not for PFC) (**Figure 6.3A-B**). While 4 Hz oscillations in CA1 did tend to modulate beta more strongly, these effect sizes were smaller (**Figure 6.3C**). More critically, CA1 4 Hz also yielded equal modulation of Amy and NAc fast-gamma. As fast-gamma barcode strengths tended to be anti-correlated with beta barcodes (**Figure 4.20-.22**) and also yielded negative CPMR scores (barcodes 11, 15, 17 in **Figure 5.1**), this made CA1 4 Hz a less-attractive candidate for the orchestration of CPMR-related beta co-ordination. In contrast, VTA 4 Hz oscillations overall exhibited the clearest beta-specific phase-modulation (**Figure 6.3D**). Amy-, NAc- and PFC beta amplitude modulation by VTA 4 Hz was stronger than any of the gamma amplitudes. This was not true of CA1, where slow- and mid-gamma amplitudes were more modulated, perhaps owing to a more complex PAC relationship.

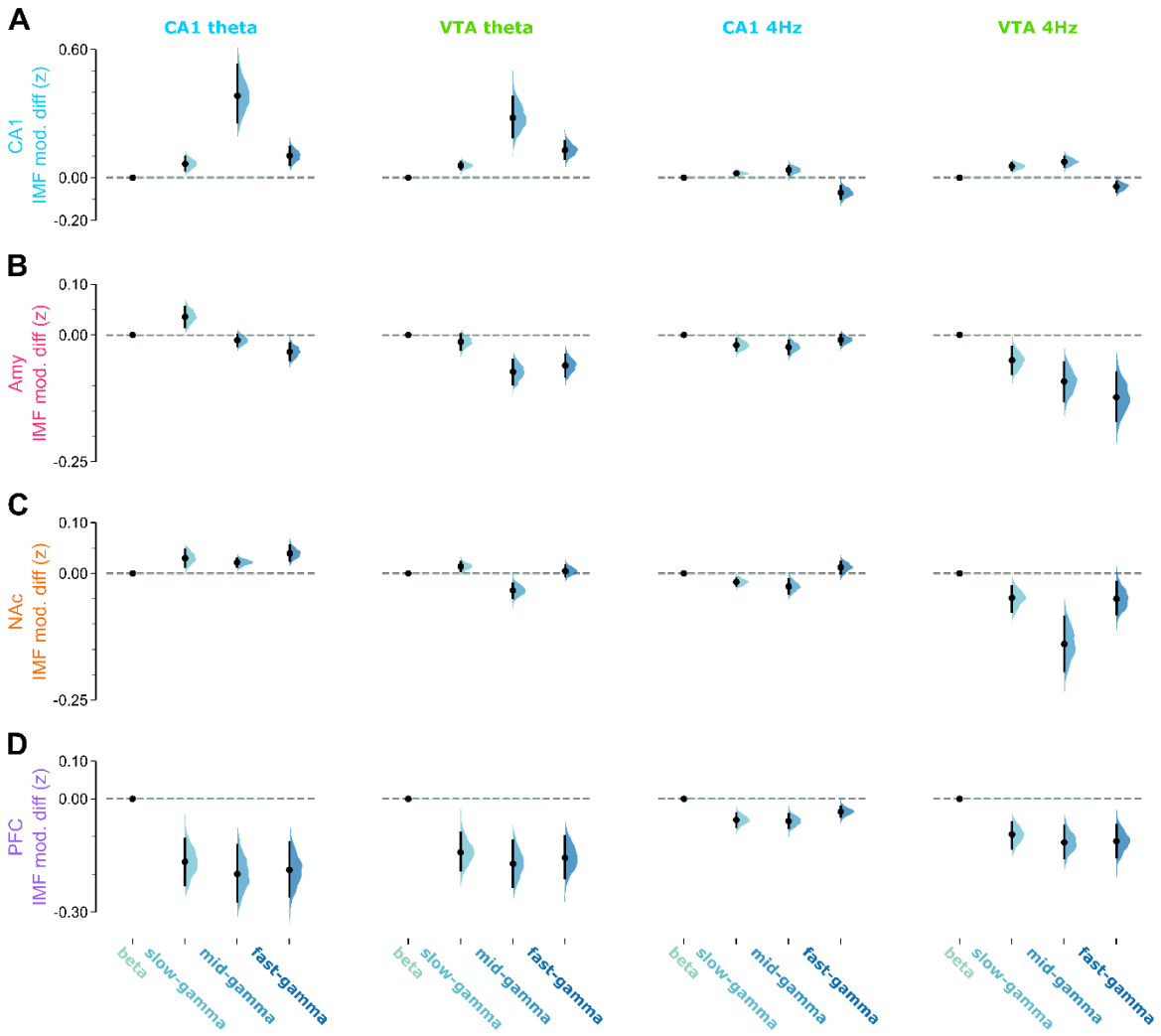


Figure 6.3: *VTA 4 Hz PAC of supra-theta IMFs is well-tuned to beta.*

A-D: Paired mean difference estimation plots comparing supra-theta IMF modulation of each region (row) for each candidate coupling oscillation (column). N=23 recording days from 15 animals.

A subset of VTA 4 Hz cycles exert strong phase modulation of beta barcodes

I hypothesised that VTA 4 Hz-mediated beta-peak phase alignment was a mechanism by which higher-order co-ordinations of beta activities – i.e., beta barcodes, were dynamically controlled. Counter-intuitively, a simple PAC analysis did not support this, as CA1 theta oscillations imposed the strongest modulation of beta barcodes on average (**Figure 6.4**). This unexpected result implied that while on average, beta amplitude peaks were well phase-aligned by VTA 4 Hz, these amplitudes did not tend to peak together in the same cycle.

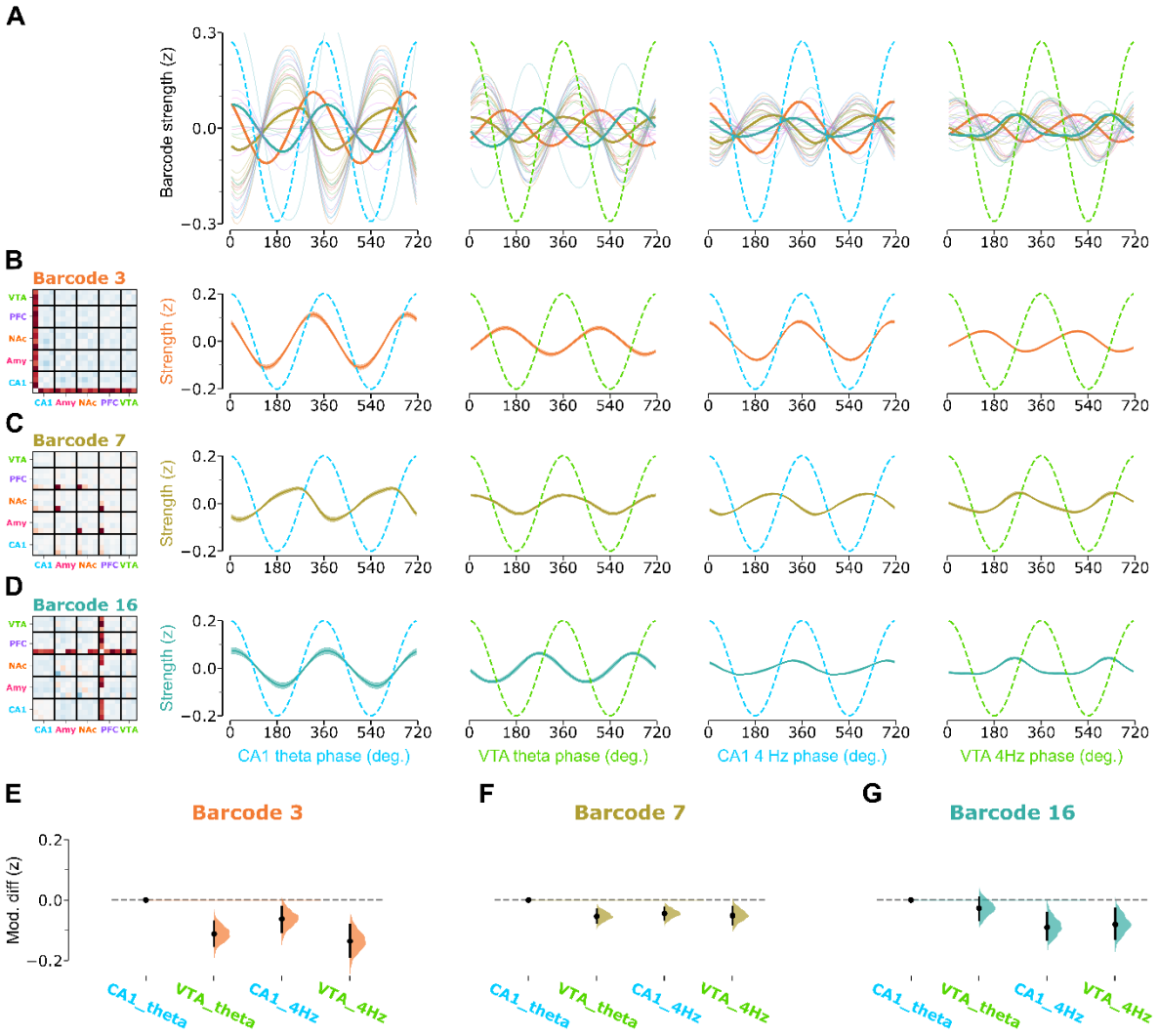


Figure 6.4: *Phase amplitude modulation of beta barcodes.*

A-D: Barcode strength as a function of the phase of each candidate coupling oscillation (columns). (**A**) shows all barcodes, example beta barcodes in bold. (**B-D**) show example beta barcodes with mean (bold line) ± S.E.M (fill). **E-G:** Paired mean difference estimation plots of beta barcode PAC scores for example beta barcode. N=23 recording days from 15 animals.

This raised the possibility that beta barcode modulation by VTA 4 Hz was highly variable between cycles. To assess this, I examined the distribution of beta barcode PAC scores calculated from *individual* cycles for each of the candidate coupling oscillations. I designed a simple non-parametric distribution analysis, which permitted the significance-testing of distribution differences at progressing intervals, starting with the highest values (for details, see **2.10**). This analysis revealed that while VTA 4 Hz cycles less-strongly modulated beta barcode amplitudes overall (**Figure 6.4**), the top proportion (~10%) of cycles tended to impose a stronger modulation than did CA1 theta/4 Hz or VTA theta (**Figure 6.5**). Likely owing to its

"purer" beta contributions and lower CA1 contributions, this result was strongest for barcode 7, where high-PAC VTA 4 Hz cycles significantly out-represented CA1 and VTA theta cycles, and did not significantly out-represent high-PAC CA1 4 Hz cycles (**Figure 6.5B**).

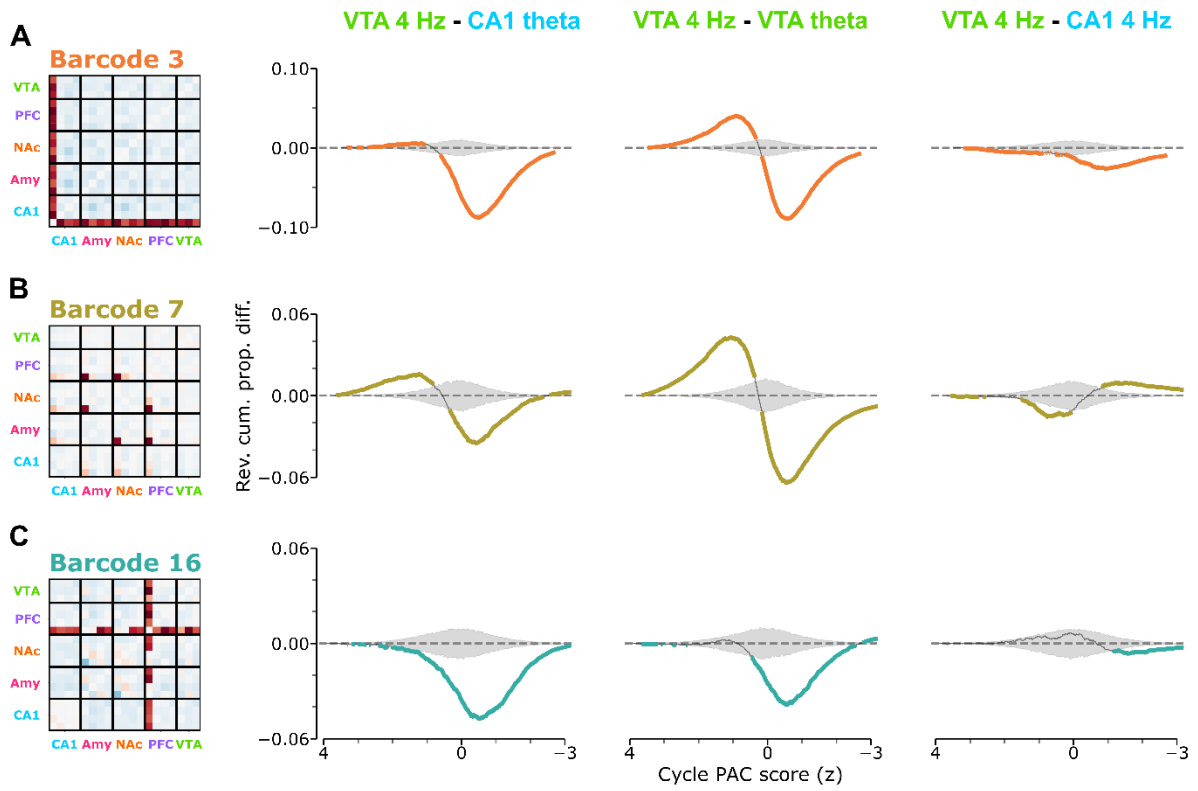


Figure 6.5: *High-PAC VTA 4 Hz cycles more strongly modulate beta barcodes.*

A-C: "Reverse cumulative frequency distribution comparison plots" (see **2.10**) comparing VTA 4 Hz individual cycle PAC scores to the other candidate coupling oscillations. Thick lines above y = 0 represent areas of the PAC distribution which are significantly dominated by VTA 4 Hz oscillations. Grey fill: 99% CI null distribution. N=115000 cycles; 5000 bootstrapped from 23 recording days of 15 animals.

I next split the cycles of each coupling oscillation into percentile bins according to their barcode 7 PAC score (**Figure 6.6**). This indeed confirmed that the top 10 % of VTA 4 Hz cycles more strongly coupled barcode 7 than did any of the other coupling oscillations (**Figure 6.6A-D**). Taking advantage of the fact that EMD preserves the non-stationary properties of oscillations (see **4.3**), I examined whether "high-PAC-β" cycles took a different waveform shape. For both theta oscillations, stronger PAC cycles were related to a slower cycle frequency (for VTA, this was phase-specific) (**Figure 6.6E-F**), and a faster locomotion speed (**Figure 6.6I-J**). This is

counter-intuitive, as slower CA1 theta cycle frequencies have been linked to *slower* locomotion speeds (Bender et al., 2015). This positive correlation between theta cycle frequency and speed was reproduced in my data for CA1, though a *negative* correlation (albeit weaker) was seen for VTA theta (data not shown). To briefly speculate, this PAC-dependent, speed-frequency relationship reversal for CA1 theta suggests that high-PAC-β theta cycles co-occur in CA1 and VTA, such that CA1 inherits the speed-cycle frequency relationship seen in VTA. This again supports VTA, rather than CA1 slow oscillations in being the key orchestrator of multiregional beta co-ordination. For CA1 4 Hz, neither cycle frequency (**Figure 6.6G**) or locomotion speed (**Figure 6.6K**) showed an obvious relationship with barcode 7 PAC. VTA 4 Hz oscillations, however, did show a barcode 7 PAC relationship to cycle frequency that was specific to the descending phase (**Figure 6.6H**) and unrelated to locomotion speed (**Figure 6.6L**).

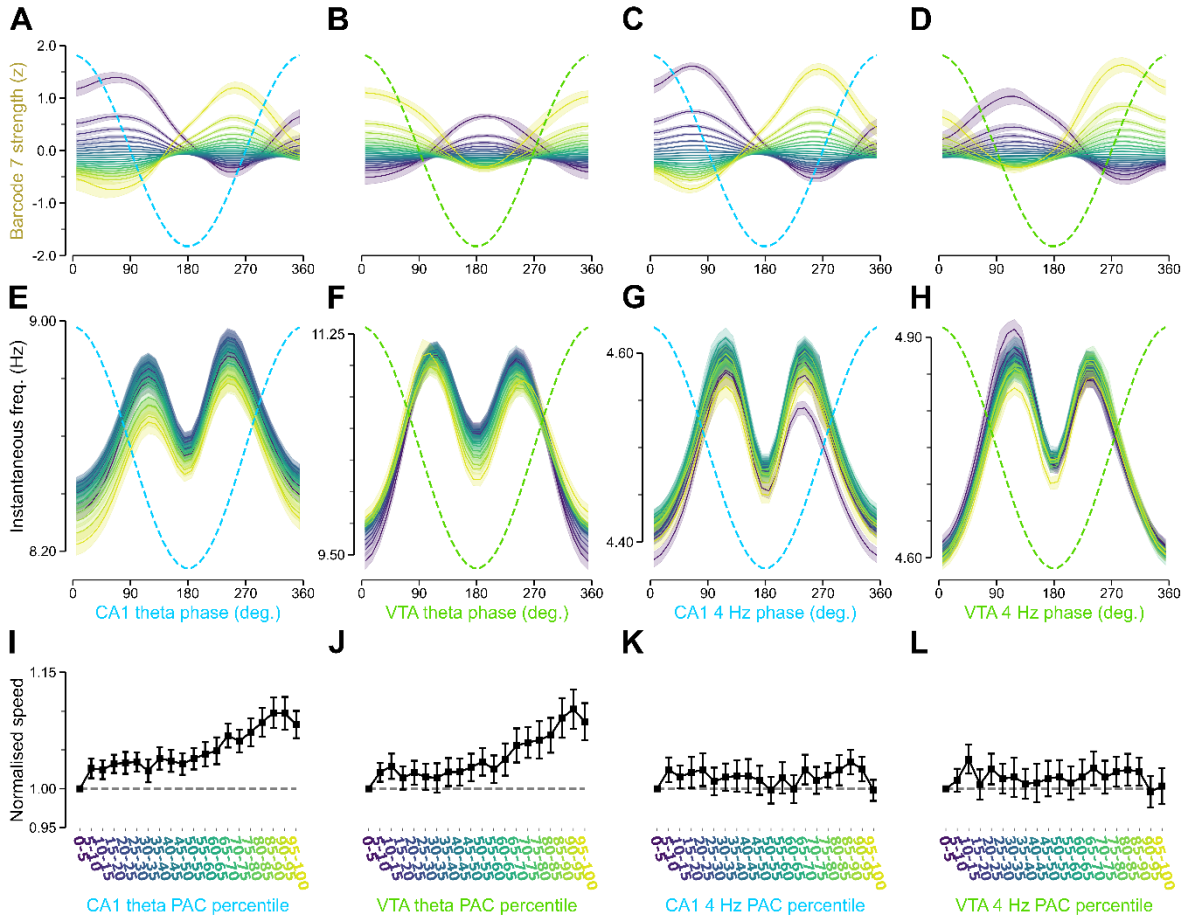


Figure 6.6: *VTA 4 Hz phase-specific cycle asymmetry predicts PAC of global beta co-ordination.*

For each candidate coupling oscillation, cycles were assigned a percentile bin according to their barcode-7 PAC score. **A-D:** Barcode #7 strength as a function of the phase, split by PAC percentile bin of each candidate coupling oscillation. **E-H:** Instantaneous frequencies of coupling oscillations, split by PAC percentile bin. **I-L:** normalised locomotion speed as a function of PAC percentile. N=23 recording days from 15 animals.

Finally, I assessed the modulation each candidate coupling oscillation had on the spiking activities of each region (**Figure 6.7**). These suggested that VTA, particularly 4 Hz, oscillations imposed the strongest modulation of cross-regional (i.e., Amy, NAc and PFC) spiking activity. The spiking activities were aligned to the descending phase of VTA 4 Hz, which corresponded to the beta PAC-dependent cycle slowing (**Figure 6.6H**). Combining this result with the knowledge that larger networks of neurons are synchronised over slower oscillations (Whittington et al., 2000; Engel et al., 2001; Fries, 2005), high-PAC-β VTA 4 Hz cycles may represent the recruitment of larger proportions of neurons throughout the brain.

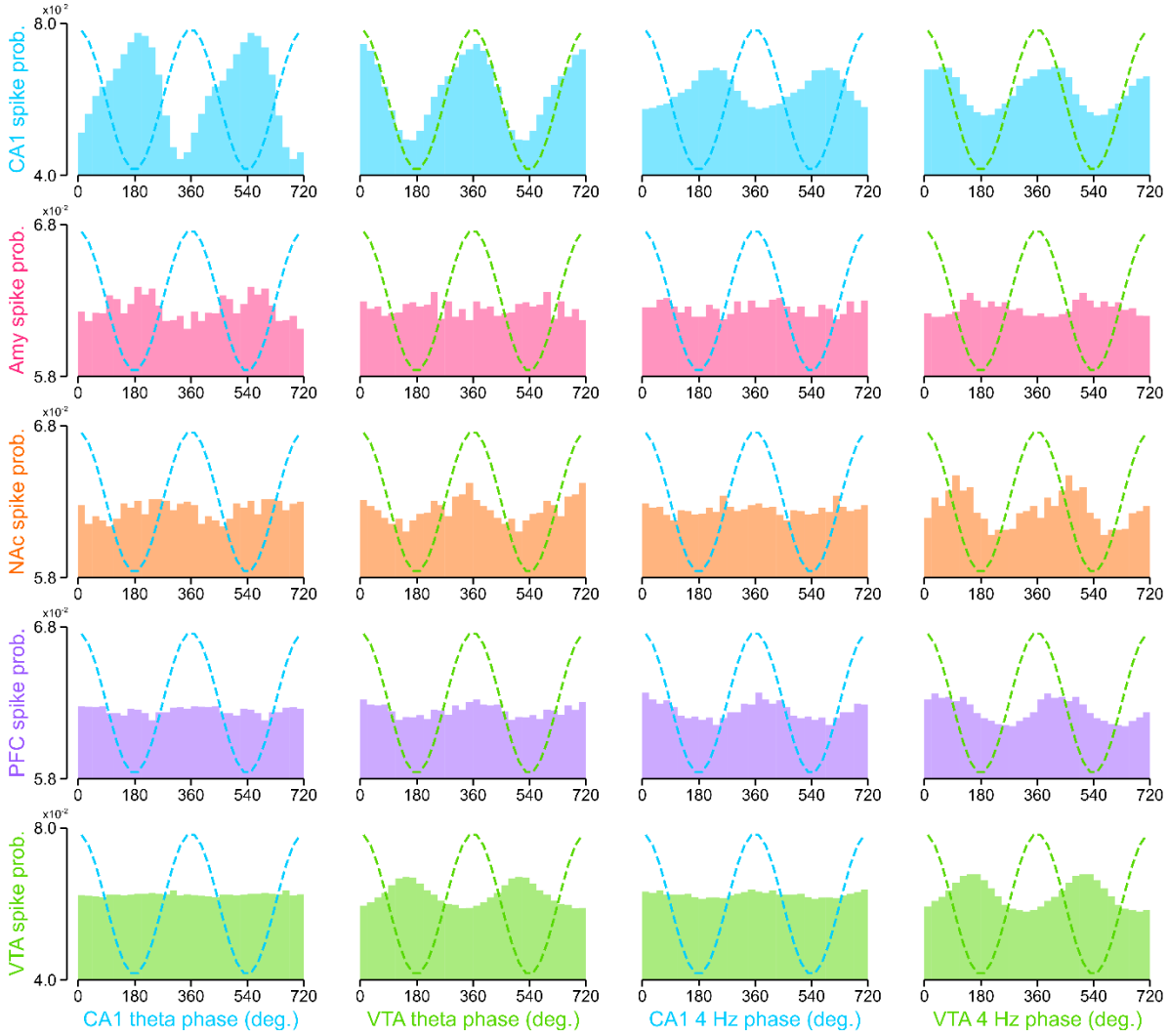


Figure 6.7: *VTA 4 Hz oscillations impose strong modulation of region spiking activities.*

n = 493, 272, 281, 393 and 189 cells, recorded from CA1, Amy, NAc, PFC and VTA, respectively over 23 recording days from 15 animals.

6.2 | VTA cell-type contributions to multiregional beta orchestration

The ultimate goal of this project is to test the causal relationship between global beta co-ordination and cocaine-seeking behaviour. In the future, I plan to use a closed-loop strategy to selectively disrupt these frequency-specific patterns of network activity during the behavioural protocol (**Chapter 3**), hypothesising that this perturbation should block the expression of cocaine-seeking behaviour. The analyses in **6.1** suggested that VTA 4 Hz oscillations exert cycle-specific temporal co-ordination of beta activities across regions. VTA 4 Hz cycles thus signal a putative timing mechanism by which CPMR-related processes are engaged, making them a promising *temporal* indicator for the closed-loop system. The second requirement for the closed loop system is to identify a *physical* target by which to disrupt global beta co-ordination. This will be achieved using an optogenetic strategy, whereby a genetically-defined population of neurons are made to express a light-sensitive opsin, such that they can be either activated or inhibited by light delivery (Fenno et al., 2011). As the results in **6.1** strongly suggested that VTA 4 Hz oscillations tended to yield a more global- and beta-specific control of region co-ordination, I decided to focus this analysis on cell populations in the VTA. In this final section, I discuss the analytical strategy I am working on to "decide" the specific VTA cell-type to be genetic targeted for the future closed-loop optogenetic experiment.

Optogenetic identification and characterisation of glutamatergic and dopaminergic VTA cells

I leveraged two existing datasets from my lab that both used an optogenetic strategy to optically activate VTA glutamatergic (Glu-ergic) (Roman Rothaermel's PhD thesis) or -dopaminergic (DAergic) (McNamara et al., 2014) cells by injecting a Cre-dependent Channelrhodopsin viral vector into the VTA of transgenic Vglut2-Cre or DAT-Cre mice, respectively (**Figure 6.8A-B**). Combining such a technique with extracellular tetrode recordings from the VTA provides an effective way to predict whether a recorded cell contained the Vglut2- or DAT-promotor – i.e. released glutamate or dopamine. This putative labelling of a cells molecular identity is known as "opto-tagging". I designed an opto-tagging assay for each dataset (for details, see **2.X**) to identify opto-tagged Glu-ergic and DAergic cells (**Figure 6.8C-D**).

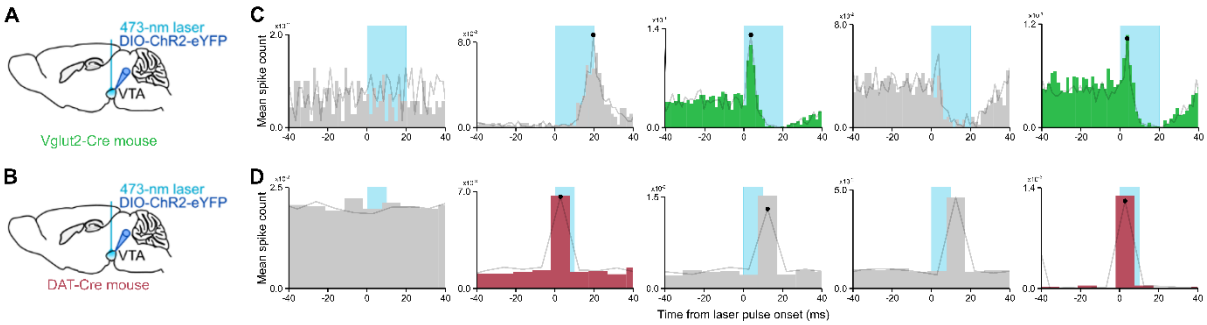


Figure 6.8: *Opto-tagging assay for VTA glutamatergic and dopaminergic cells.*

A-B: Molecular strategy to optogenetically activate glutamatergic (**A**) and dopaminergic (**B**) VTA cells. **C-D:** Opto-tagging assay performed on example cells for glutamatergic (**C**) and dopaminergic (**D**) optogenetic protocols. Non-grey responses indicate an opto-tagged cell (see **2.10** for details). Blue fill; laser-ON period.

Having now identified some "ground-truth" examples of Glu- and DA-ergic VTA cell-types, I next explored the firing properties of these opto-tagged cells. Using data from active behaviour that was clear of optical manipulation, I computed the mean firing-rate (FR), spike-waveform, inter-spike-interval (ISI) histogram and autocorrelogram (AC) for each cell (**Figure 6.9**). While much less is known about the Glu-ergic VTA cell population, the firing properties of the opto-tagged DAergic cells were consistent with previous reports of a triphasic waveform and variable ISI (Grace and Bunney, 1984; Dahan et al., 2007; Tsai et al., 2009; Juarez and Han, 2016). Cell ACs were especially variable between the opto-tagged DAergic population, though interestingly, the AC of one of these opto-tagged DA cells showed clear firing modulation in the beta range (**Figure 6.9G, bottom-left**). The group-averaged spike waveforms, ISI distributions and firing-rates all offered a promising degree of discriminability between cell-types. Showing the least within-group variability, though, were the ISI distributions (**Figure 6.9D-E**).

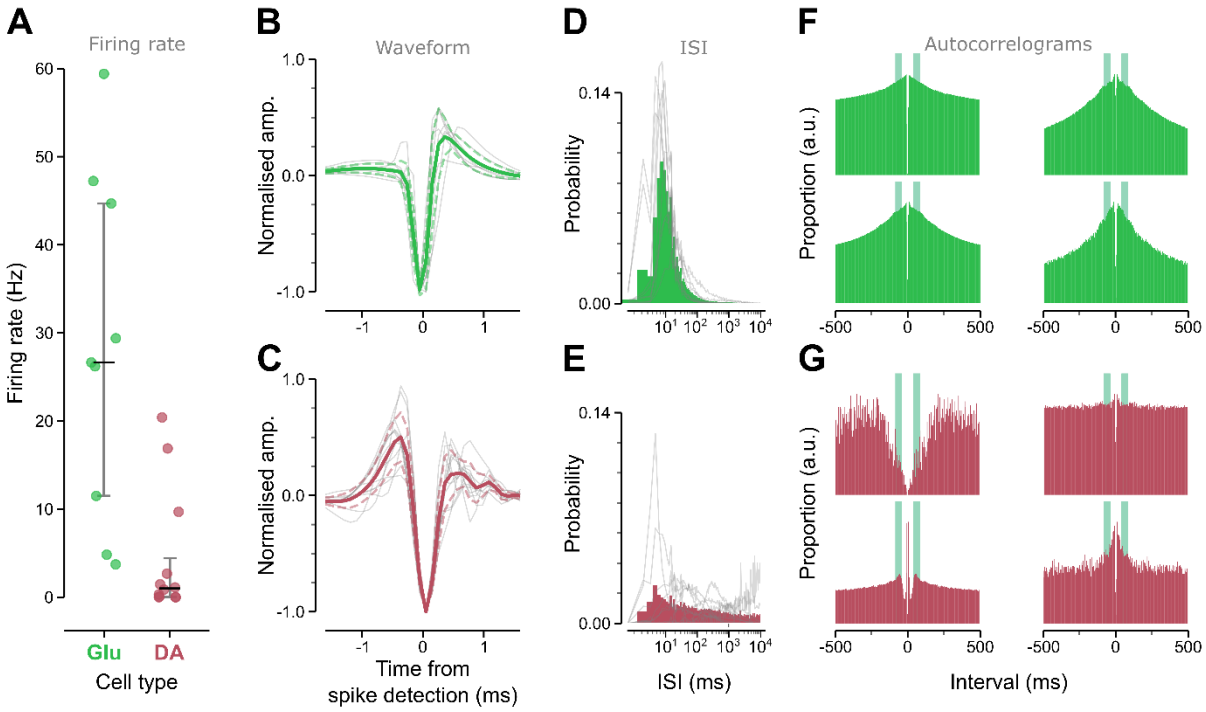


Figure 6.9: *Electrophysiological profiling of opto-tagged glutamatergic and dopaminergic VTA cells.*

A: Mean firing-rate observations (circles); horizontal lines: group medians; grey lines: IQR. **B-C:** Normalised spike waveforms of opto-tagged glutamatergic (**B**) and dopaminergic (**C**) cells. Thick coloured line: group mean; Dotted lines: group SD; thin grey lines: each cell. **D-E:** Average inter-spike-interval (ISI) histograms for opto-tagged glutamatergic (**D**) and dopaminergic (**E**) cells. Grey lines: each cell; coloured histogram: group mean. **F-G:** Example autocorrelograms from opto-tagged glutamatergic (**F**) and dopaminergic (**G**) cells. Highlighted interval indicates beta (15–25 Hz) range spike entrainment. N = 9 and 12 opto-tagged glutamatergic and dopaminergic cells, respectively.

ISI-based classification of VTA cell-types

Based on the observation[14] that the Glu- and DA-ergic opto-tagged ISI distributions could well-distinguish the two groups, I designed a classification strategy (**Figure 6.10**; see **2.10** for details) that used ISI histograms to predict the molecular identity (Glu vs DA) of all VTA cells that were recorded in five-site–implanted animals (**2.2**). In short, this classification applied linear discriminant analysis (LDA) to a cell-type–labelled feature matrix of ISI principal components (PCs) to define the optimal projection axis by which the opto-tagged cells were

[14] and the much-valued intuition of Roman, a fellow PhD student and lab member, who had been working on VTA cell-type classification for some time prior to my efforts

separated. This projection vector was then used to predict the molecular identity of all the other VTA cells from their ISI PCs. This operation classified 70.2% of the total recorded un-identifiable VTA cells (n = 181) as putative DAergic. While there are several issues with the validity of this classification (discussed in **6.3**), this proportion was roughly in-line with histological reports (Margolis et al., 2006; Lammel et al., 2015). I was thus sufficiently satisfied with this preliminary classification such to proceed in exploring the relationships that these two putative VTA cell populations had with global beta co-ordination. To reiterate, the findings reported in this next and final analysis should be taken lightly, but nevertheless yielded some promising insights.

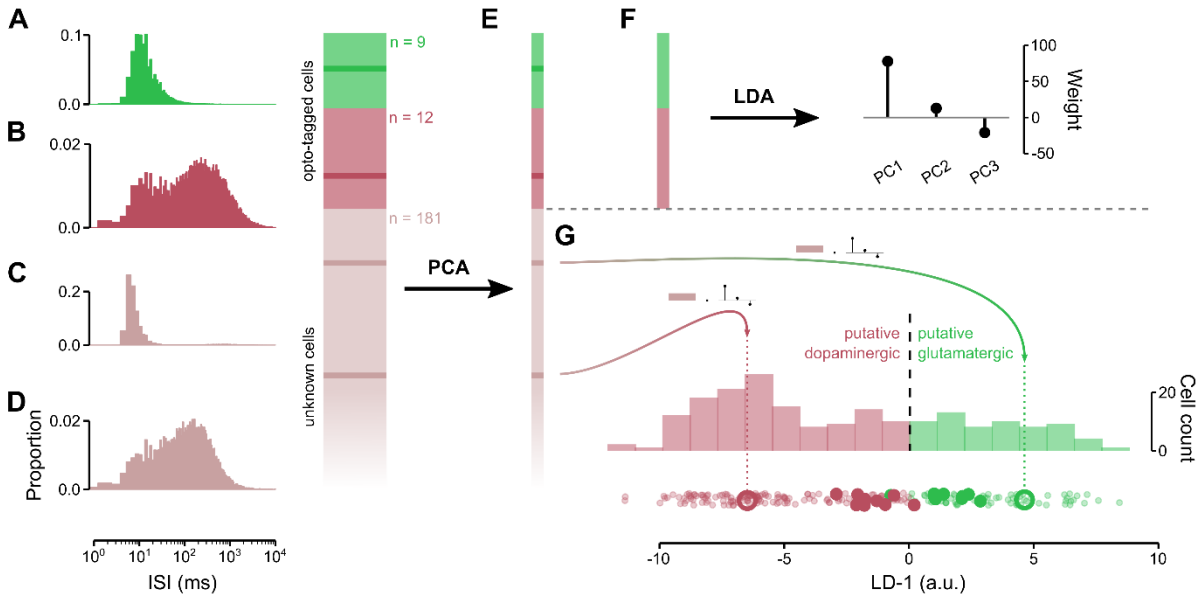


Figure 6.10: *ISI-based VTA cell-type classification.*

A-D: Example ISI histograms from an opto-tagged glutamatergic (**A**), opto-tagged dopaminergic (**B**) and two unidentifiable (**C-D**) VTA cells. **E:** Principal component analysis (PCA) was applied to the all ISI histograms. **F:** Linear discriminant analysis (LDA) was then applied to the first 3 principal components of the opto-labelled cell ISIs. **G:** This LD1 projection vector was then used to predict the cell-type identity (Glu/DA) of the unidentifiable cells.

The firing properties of VTA putative dopaminergic cells are more related to beta co-ordination

Having now putatively classified all the VTA cell-types recorded from CA1–Amy–NAc–PFC–VTA-implanted animals, I next explored how the firing patterns of these cells are tuned to neural oscillations (i.e., the IMFs extracted in **4.3**). First, I examined the spike-to-phase coupling of VTA cell-types to local IMFs. At the group level, putative Glu-ergic cells showed a significantly higher spike-phase coherence (as measured by Rayleigh test; see **2.10**) to local fast-gamma than DAergic cells. No other spike-phase coherence differences at the group level were noted for any of the other VTA IMFs (**Figure 6.11A**). A small proportion of putative Glu-ergic cells (~ 3 out of 63) tended to have the highest coherence-rank, though the majority of the putative DAergic population tended to out-rank their Glu-ergic counterparts (**Figure 6.11C**).

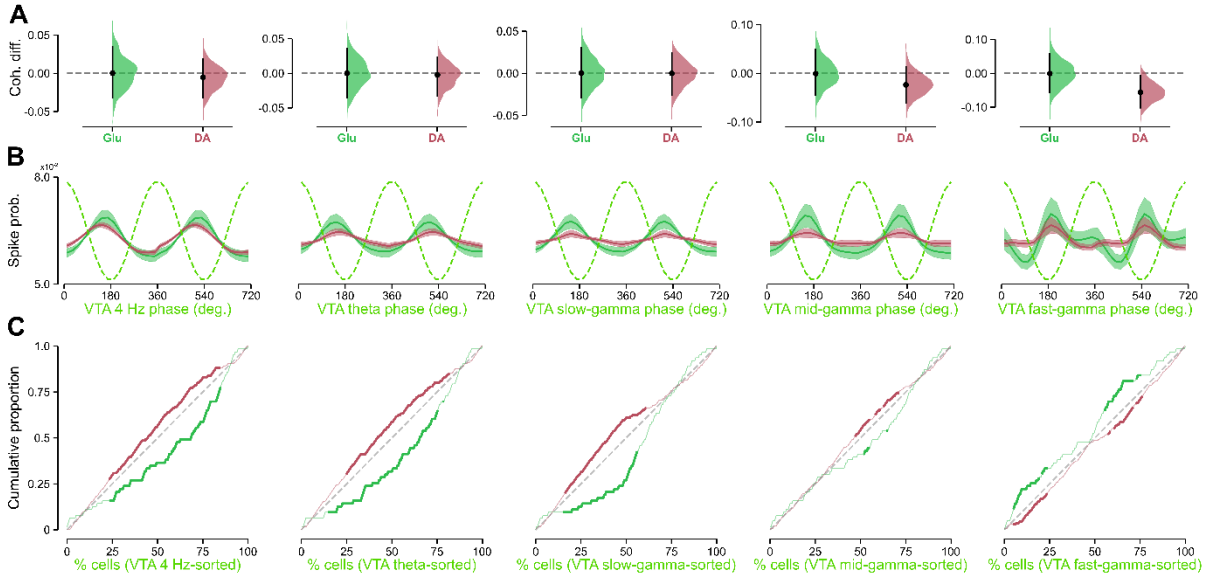


Figure 6.11: *The putative Glutamatergic cell population are more locked to VTA fast-gamma oscillations.*

A: VTA DA–Glu spike–beta-phase coherence mean difference estimation plot for each beta region. **B:** Putative VTA spike probability as a function of beta phase for each beta region. Solid line: mean; fill: ±SEM. **C:** Putative Glu-vs-DA beta coherence rank over-representation plot (see **2.10**) comparing putative cell-types. Thick lines: 95 % rank over-representation CI. n = 63 putative glutamatergic- and n = 136 putative dopaminergic cells, recorded from 12 individual animals over 28 recording sessions. 1 putative glutamatergic and 9 putative dopaminergic cells fired less than 200 spikes, so were excluded for the analysis in **A-C** (see footnote #14).

While the phase-coupling differences between the two putative cell-type populations were modest at best when considering coupling to local oscillations, much more dramatic effects were seen for cross-regional oscillation coupling. Putative DAergic cell firing patterns were significantly more phase-locked to beta IMFs of CA1, Amy, NAc and PFC (**Figure 6.12A-L**). This effect also was true of the other supra-theta IMFs – with the exception of fast-gamma; where only modest effect sizes were noted for Amy and NAc, and no significant difference was seen for PFC coherence (data not shown).[15] These results implicated that the putative DAergic VTA cell population in having a more intimate relationship with cross-regional oscillatory activities than the putative Glu-ergic population.

To resolve the frequency-specific profiles of these cross-regional relationships, I computed the spectrograms for each non-VTA region, and used the spike trains of each cell to trigger the average spectrogram response relative to a spiking event. Each cell-evoked spectrogram response was normalised by a speed-matched control, where each spike was assigned a new time, matching its speed bin (see **2.10** for details). This allowed me to compare the speed-controlled, spike-triggered spectral responses of each non-VTA region between VTA cell types (**Figure 6.12M-T**). Spiking events in the putative Glu-ergic population consistently preceded a reduction in ~ 4 Hz power (the onset commencing within 250 ms – i.e. a 4 Hz period). Increases in theta, beta and gamma power were also associated with these spiking events (**Figure 6.12M-P**), the most beta-specific of these seen for PFC (**Figure 6.12P**). For the putative DAergic population, strong power increases spanning the beta–fast-gamma range were seen for CA1 (**Figure 6.12M**), along with a moderate increase in ~ 4 Hz power – which was also seen in the other regions. For these other regions, and most strikingly, the strongest increases in spectral power associated by putative dopaminergic spiking were much more constrained to the beta and fast-gamma ranges (**Figure 6.12R-T**). These results posit a potential universal beta induction mechanism of putative DAergic cells, making them an attractive cellular target for the disruption of multiregional beta co-ordination.

[15] A potential caveat is that the Rayleigh z-statistic (see **2.9**) tends to over-estimate phase-coherence when there are fewer (< 200) phase samples [spikes], potentially biasing the putative DAergic population to have higher coherence values. Accordingly, I only considered cells which fired at least 200 spikes. Also, the results were the same when spike phases of each cell were bootstrapped at various sample sizes.

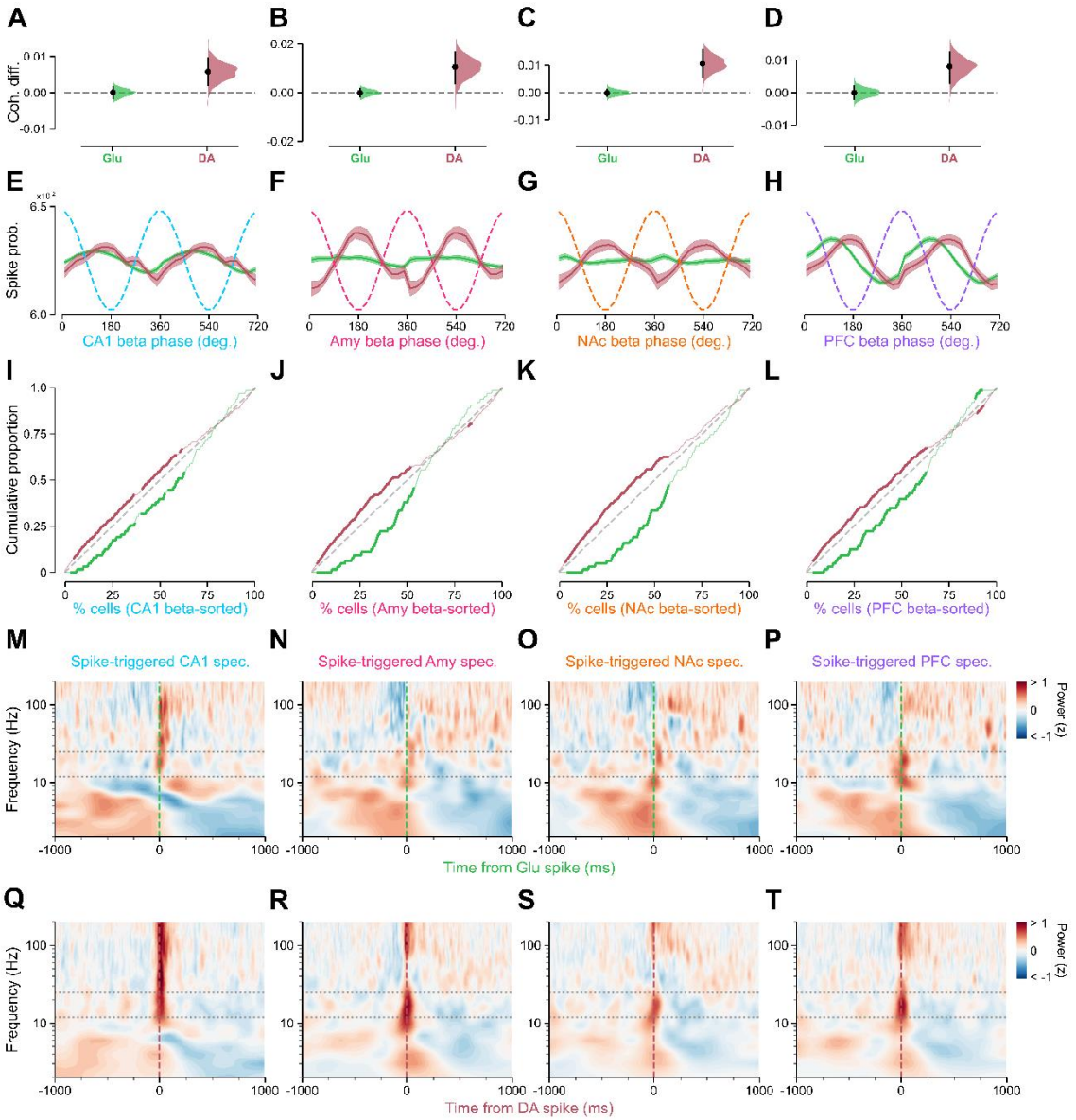


Figure 6.12: *Putative VTA dopaminergic cells are preferentially tuned to multiregional beta.*

A-L: Putative VTA dopaminergic cell firing more is more strongly tuned to beta IMFs of CA1, Amy, NAc and PFC. **A-D:** VTA DA–Glu spike–beta-phase coherence mean difference estimation plot for each beta region. **E-H:** Putative VTA spike probability as a function of beta phase for each beta region. Solid line: mean; fill: ±SEM. **I-L:** Putative Glu-vs-DA beta coherence rank over-representation plot (see **2.6**) comparing putative cell-types. Thick lines: 95 % rank over-representation CI. **M-T:** Putative VTA dopaminergic cells more strongly trigger beta power the regions – (before and) after controlling for speed and total number spikes (see **2.10** for full details). n = 63 putative glutamatergic- and n=136 putative dopaminergic cells, recorded from 12 individual animals over 28 cluster-cut sessions. 1 putative glutamatergic and 9 putative dopaminergic cells fired less than 200 spikes, so were excluded for the analysis in **A-D** (see footnote #11).

6.3 | Discussion

The results of **Chapter 5** showed that CPMR is most likely related to multiregional patterns of co-ordination tied to the beta (15–25 Hz) range. As discussed in **5.2**, beta may represent the optimal frequency range for cross-structural, multimodal integration: slow enough to permit long-range synchronisation (Kopell et al., 2000), but fast enough to represent a functional informational syntax across these global neural networks (Buzsáki, 2010). This chapter explored some of the potential mechanisms by which these large-scale patterns of frequency-specific co-ordination may be orchestrated.

Beta-specific phase modulation by VTA 4 Hz

I am aware of only two rodent studies that examined multiregional co-ordination by PAC mechanisms. Both indeed implicated 4 Hz oscillations in providing a platform for synchronisation over faster frequencies (Fujisawa and Buzsáki, 2011; Karalis and Sirota, 2018). Fujisawa and Buzsáki (2011) showed that 4 Hz oscillations adaptively synchronise CA1, PFC and VTA activities, while phase-modulating working memory-related gamma activities across the regions. This study used a bandpass filtering approach to isolate 4 Hz, theta and gamma signals; and did not claim that a specific region was responsible for dynamic synchronisation mechanism. The advantage I had in using the region-tailored mEMD approach (**4.3**) was that oscillations were extracted in a semi-unsupervised manner, according to a mode mixing minimisation criterion. This data-driven frequency extraction approach is hence a less artificial one, meaning that PAC comparisons between the candidate coupling oscillations was a more valid pursuit. VTA 4 Hz oscillations emerged as the "clear favourite" in mediating the temporal orchestration of cross-regional spiking and beta-specific co-ordination patterns. As well as strongly modulating beta amplitudes (particularly for Amy, NAc and PFC), VTA 4 Hz oscillations also imposed a robust phase-alignment between region beta activities. Interestingly, the preferred phase for CA1 beta was immediately before that for the other beta regions, suggesting a complex interaction between VTA 4 Hz and CA1 beta is involved in the engagement of multiregional beta co-ordination.

Cycle-specific modulation of multiregional beta co-ordination by VTA 4 Hz

Surprisingly, the cross-regional co-ordination patterns represented by the beta barcodes were shown to undergo less PAC on average, compared to the other candidate oscillations. However, in almost all cases, PAC scores in the top proportion of VTA 4 Hz cycles would be higher than those of other cycles, meaning that a subset VTA 4 Hz cycles might represent key windows by which CPMR-related beta co-ordination is mediated brain-wide. This phenomenon of cycle-to-cycle PAC variability has been recently elucidated for within-region PAC by hippocampal theta cycles. These "theta-nested spectral components" (tSCs) were linked to specific input sources as well as mnemonic operations (Lopes-dos-Santos et al., 2018). Extending this principle, high-PAC-β VTA 4 Hz cycles likely represent a similar computational phenomenon. To test the *behavioural* relevance of these cycles, I plan to selectively disrupt beta co-ordination specifically in high-PAC- β cycles (i.e., closed-loop intervention) during my behavioural model of cocaine-seeking behaviour (**Chapter 3**). For this to be achieved, high-PAC-β VTA 4 Hz cycles must be predicted in real time.

Initial analysis revealed that stronger barcode 7 PAC scores correlated with a slower descending phase of VTA 4 Hz cycles. As beta amplitudes tended to be strongest closer to the peaks than the troughs of (theta and) 4 Hz oscillations, I computed cycle PAC scores from cycles detected between troughs – i.e. the first half of the cycle is ascending, and the latter, descending. This means that high-PAC-β–related slower descending phase of VTA 4 Hz is a phenomenon which happens *after* the beta peak of that VTA 4 Hz cycle. This does not rule out the possibility that phase-specific VTA cycle slowing may not be able to predict future beta increases. Very simply, this analysis can be run again, where the "cycle start" phase should be defined just before the phase relating to PAC-dependent slowing (i.e., on or just after the peak). Additionally, VTA 4 Hz cycles to be used for the predictive analysis should be limited to those occurring in a sequential chain of a specified minimum length. This may also reveal whether high-PAC-β cycles tend to occur in a sequence, more independently and/or are predicted by characteristics in immediately preceding cycles. Additionally, the relationship between high-PAC-β cycles and cocaine-seeking behaviour could be directly interrogated and combined with cycle waveform dynamics to more elaborately describe and inform putative windows for closed-loop intervention. While this work was beyond the time constraints for this thesis, the initial observation (**Figure 6.6**) indeed was able to relate cycle waveform shape to a neural phenomenon that was linked to cocaine-seeking behaviour, and adds to literature which

highlight the functional importance of waveform cycle asymmetry (Buzsáki et al., 1985; Dijk et al., 2010; Belluscio et al., 2012; Schaworonkow and Nikulin, 2019). As well as testing the fidelity by which multiregional beta co-ordination is predicted by VTA 4 Hz cycle waveform shape, the importance of this cycle-specific non-stationarity in relation to cocaine-seeking behaviour should be directly assessed. Marrying the interpretations of **6.1**, I speculate that *slower* VTA 4 Hz descending phases may represent synchrony between a *larger* proportion of brain-wide neural networks, manifesting as CPMR-related multiregional beta co-ordination.

Validity of VTA cell-type classification method

The obvious caveat with the ISI-based cell-type classification (**6.2**) is that no data was available to assess opto-tagged VTA GABAergic cells. This method thus forced "true" GABAergic cells to be labelled as glutamatergic or dopaminergic. The glutamate carboxylase (GAD) enzyme converts glutamate into GABA (Capitani et al., 2003) and as such is the key molecular and genetic marker for GABAergic neurons. GAD+ cells in the rodent VTA range roughly 30–70 %, depending on VTA subregion (Margolis et al., 2006; Nair-Roberts et al., 2008; Lammel et al., 2015). In future experiments, I plan to opto-tag GABAergic VTA cells in the same way such that all three cell types can be predicted, and their relationships with multiregional beta dynamics assessed. This three-way cell-type classification will likely additionally incorporate spike waveform properties – as they have been demonstrated to well-distinguish GABAergic from DAergic VTA cells in mice (Chieng et al., 2011; Fujisawa and Buzsáki, 2011).

In my data, 70.2 % of the total recorded un-identifiable VTA cells (n=181) were classified as putative dopaminergic. While this is slightly higher than 50–60 % claimed by histological reports (Margolis et al., 2006; Lammel et al., 2015) and in addition to the GABAergic problem, it should be noted that several of these mice had VTA implants which were deliberately implanted along the medial axis of the VTA, where the dopaminergic make-up has been reported to be as low as 12–25 %, and glutamatergic ~ 37.5 % (Lammel et al., 2015). Further complicating the story, a large proportion (as much as 60 %) of VTA neurons test positive for a two – and in some cases all three, neurotransmitter markers (Margolis et al., 2006; Björklund and Dunnett, 2007; Yamaguchi et al., 2011; Lammel et al., 2015; Morales and Margolis, 2017; Beier et al., 2019). Though this does not mean that these neurotransmitters are co-released at VTA terminals (Beier et al., 2015; Morales and Margolis, 2017; Root et al., 2020), DA/Glu-

(Stuber et al., 2010), DA/GABA- (Tritsch et al., 2012) and Glu/GABA (Root et al., 2014) co-release at non-VTA targets in rodents has indeed been demonstrated. It has been argued, owing in part to this molecular heterogeneity of VTA cell-types, that classification of VTA cell-types by electrophysiological metrics will be accurate (Margolis et al., 2006). While this challenges my analysis, the ISI characteristics of Glu-ergic and DAergic cells which I observed and used are consistent with electrophysiological recording experiments that validated the molecular identities of the recorded cells (Grace and Bunney, 1984; Dahan et al., 2007; Tsai et al., 2009; Juarez and Han, 2016). Perhaps owing to the stringent opto-tagging criteria I defined (**2.10**), the "ground truth" opto-tagged cells showed well-distinguishable ISI properties. While I do not claim that these (and indeed the predicted) cells release only a single neurotransmitter, my "cell-type classification method" should more pragmatically be thought of as a strategy to predict for each recorded cell, which transgenic mouse line (vGluT2-Cre or DAT-Cre) would most likely lead to that cell being photo-manipulatable following a Cre-dependent viral injection.

Multiregional beta co-ordination, dopamine and cocaine-seeking behaviour

Caveats aside, the results in **6.2** posit the VTA dopaminergic population in playing an important role in the facilitation of multiregional beta co-ordination. The fact that this putative CPMR mechanism is seemingly related to DA is perhaps not surprising. Increases in VTA DAergic firing rates are indeed observed following the presentation of a reward-paired CS (Schultz, 1986; Ljungberg et al., 1992; Horvitz, 2000; Cohen et al., 2012; Totah et al., 2013). Single cocaine experiences have been demonstrated to enhance the excitability of DAergic VTA cells via the depression of inhibitory (Nugent et al., 2007) and potentiation of excitatory (Ungless et al., 2001) input synapses, offering a molecular explanation to these results. Combining this knowledge with my results, VTA DA-facilitated multiregional beta co-ordination enhancement may reflect an incentive salience-type mechanism by which neural representations of cocaine-paired stimuli are able to elicit attractive behavioural responses.

The most established link between DA and beta oscillations is noted in Parkinson's disease (PD), which constitutes a loss of dopaminergic neurons, primarily in the substantia nigra pars compacta (SNc) (Mosharov et al., 2009). Both human observations (Hammond et al., 2007) and rodent models (West et al., 2018) have linked this motor pathology to enhanced beta power.

Replenishment of DA levels by the DA precursor, leva-dopa, yields improvement in the akinetic motor impairments and is correlated with reduced duration of beta amplitude "bursts" (Tinkhauser et al., 2017). While these observations seem to contradict my results, which indicate a positive relationship between dopamine and beta, there are a few key distinctions to be made. Firstly, owing to DAergic neural pathology that is selective to the SNc over VTA, beta power enhancement in PD is tied to the basal ganglia (containing the dorsal, not ventral striatum); which is less related to cognitive memory processing and more the direct control of motor operations. Also, these Parkinsonian observations only speak to the actions of *tonic* (sustained) dopamine levels and relate to long-term adaptive changes to the basal ganglia circuitry (Blandini et al., 2000). Contrastingly, my analysis explored how VTA dopaminergic cell spiking activity (a proxy for *phasic* DA release) in a *non-diseased* model related to the *transient* dynamics of beta co-ordination over limbic and cortical targets that are more involved in memory and cognition, rather than motor control.

My results suggest that multiregional beta co-ordination events may be facilitated by phasic dopamine delivery from VTA neurons. The direct interrogation of the actions of such transient DA signals can be measured in rodents *in vivo* using fast-scan cyclic voltammetry (FSCV), which estimates transient concentrations of specific monoamine neurotransmitters from a voltage-specific oxidation response (Wipf et al., 1988). However, very few studies have combined multisite electrophysiological recordings with parallel FSCV-assisted DA measurement. One study combined FSCV and electrophysiological recording techniques in both the shell and core regions of the NAc during a cocaine self-administration protocol, and showed correlated firing rate increases between the shell and core specifically where phasic DA responses were measured (Owesson-White et al., 2009). Phasic DA transients are also been are well-synchronised between hemispheres of the striatum (Fox et al., 2016). These observations hint at a phasic dopamine-driven mechanism by which the synchrony between activities of distant regions is enhanced. I speculate that larger-scale coupling of network activities is reflected by high-PAC-β VTA 4 Hz descending phase slowing and facilitated by synchronous, global DA delivery that is paced by VTA 4 Hz oscillations.

7 | Summary

The key findings of this thesis are graphically summarised in **Figure 7.1**. Establishing a successful experimental model of cocaine-seeking behaviour (**Chapter 3**), along with a set of physiologically-validated descriptions of frequency-resolved multiregional patterns of neural co-ordination [barcodes] (**Chapter 4**) elucidated the finding that such barcodes comprising specifically of beta interactions showed the strongest neural correlate of cocaine-paired memory retrieval (CPMR) (**Chapter 5**). To explore how this putative mechanism of CPMR may emerge, I explored the modulation of multiregional beta activities in both the temporal and physical domains (**Chapter 6**). These findings revealed a cycle-specific role of VTA 4 Hz oscillations in dominating the control of beta barcodes, and preliminarily posit VTA DAergic cells as an important facilitator of multiregional beta. These results will inform a future closed-loop experiment, which will assess the causal validity to the "**beta ~ CPMR hypothesis**".

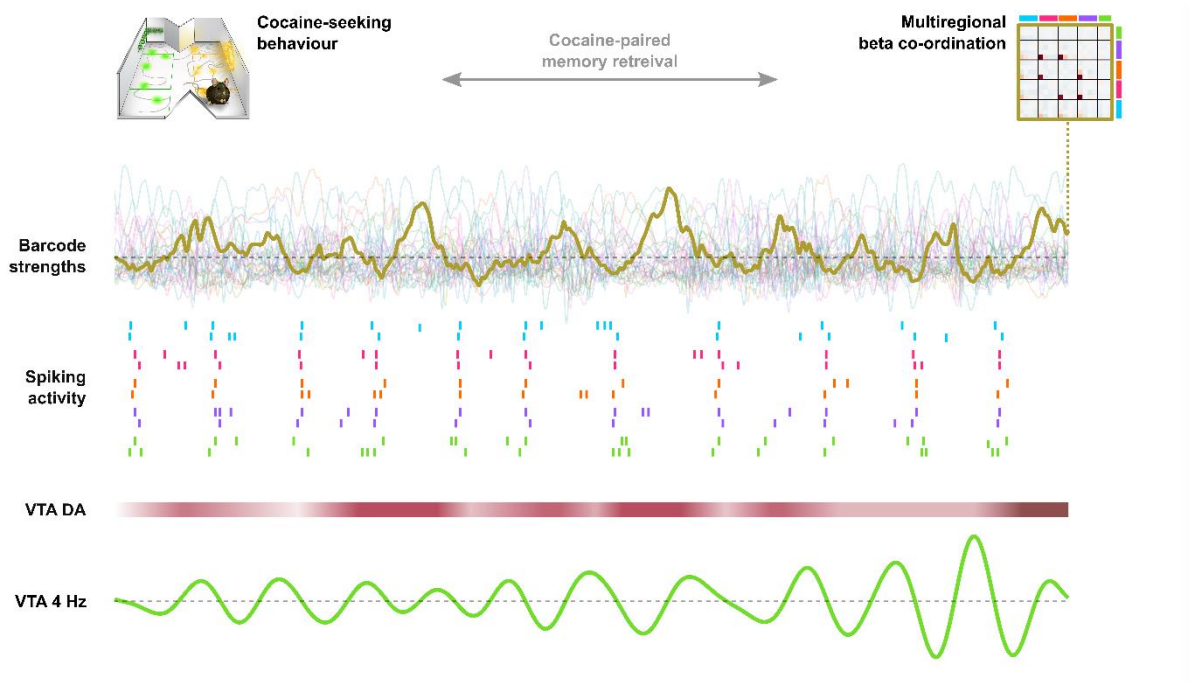


Figure 7.1: *Graphical summary of key findings.*

References

Akam, T., Kullmann, D.M., 2014. Oscillatory multiplexing of population codes for selective communication in the mammalian brain. Nat. Rev. Neurosci. 15, 111–122. https://doi.org/10.1038/nrn3668

Arroyo, M., Markou, A., Robbins, T.W., Everitt, B.J., 1998. Acquisition, maintenance and reinstatement of intravenous cocaine self-administration under a second-order schedule of reinforcement in rats: effects of conditioned cues and continuous access to cocaine. Psychopharmacology (Berl.) 140, 331–344. https://doi.org/10.1007/s002130050774

Aussel, A., Buhry, L., Tyvaert, L., Ranta, R., 2018. A detailed anatomical and mathematical model of the hippocampal formation for the generation of sharp-wave ripples and theta-nested gamma oscillations. J. Comput. Neurosci. 45, 207–221. https://doi.org/10.1007/s10827-018-0704-x

Baimbridge, K.G., Miller, J.J., 1981. Calcium uptake and retention during long-term potentiation of neuronal activity in the rat hippocampal slice preparation. Brain Res. 221, 299–305. https://doi.org/10.1016/0006-8993(81)90779-4

Bannerman, D.M., Sprengel, R., Sanderson, D.J., McHugh, S.B., Rawlins, J.N.P., Monyer, H., Seeburg, P.H., 2014. Hippocampal synaptic plasticity, spatial memory and anxiety. Nat. Rev. Neurosci. 15, 181–192. https://doi.org/10.1038/nrn3677

Bechara, A., 2004. The role of emotion in decision-making: evidence from neurological patients with orbitofrontal damage. Brain Cogn. 55, 30–40. https://doi.org/10.1016/j.bandc.2003.04.001

Beier, K.T., Gao, X.J., Xie, S., DeLoach, K.E., Malenka, R.C., Luo, L., 2019. Topological Organization of Ventral Tegmental Area Connectivity Revealed by Viral-Genetic Dissection of Input-Output Relations. Cell Rep. 26, 159-167.e6. https://doi.org/10.1016/j.celrep.2018.12.040

Beier, K.T., Steinberg, E.E., DeLoach, K.E., Xie, S., Miyamichi, K., Schwarz, L., Gao, X.J., Kremer, E.J., Malenka, R.C., Luo, L., 2015. Circuit Architecture of VTA Dopamine Neurons Revealed by Systematic Input-Output Mapping. Cell 162, 622–634. https://doi.org/10.1016/j.cell.2015.07.015

Bellone, C., Lüscher, C., 2006. Cocaine triggered AMPA receptor redistribution is reversed in vivo by mGluR-dependent long-term depression. Nat. Neurosci. 9, 636–641. https://doi.org/10.1038/nn1682

Belluscio, M.A., Mizuseki, K., Schmidt, R., Kempter, R., Buzsáki, G., 2012. Cross-Frequency Phase–Phase Coupling between Theta and Gamma Oscillations in the Hippocampus. J. Neurosci. 32, 423–435. https://doi.org/10.1523/JNEUROSCI.4122-11.2012

Bender, F., Gorbati, M., Cadavieco, M.C., Denisova, N., Gao, X., Holman, C., Korotkova, T., Ponomarenko, A., 2015. Theta oscillations regulate the speed of locomotion via a hippocampus to lateral septum pathway. Nat. Commun. 6. https://doi.org/10.1038/ncomms9521

Benuck, M., Lajtha, A., Reith, M.E.A., 1987. Pharmacokinetics of systemically administered cocaine and locomotor stimulation in mice. J. Pharmacol. Exp. Ther. 243, 144–149.

Berger, H., 1929. Ueber das Elektroenkephalogram des Menschen. Über Elektrenkephalogramm Menschen 87, 527–570.

Bi, G., Poo, M., 1998. Synaptic Modifications in Cultured Hippocampal Neurons: Dependence on Spike Timing, Synaptic Strength, and Postsynaptic Cell Type. J. Neurosci. 18, 10464–10472. https://doi.org/10.1523/JNEUROSCI.18-24-10464.1998

Bindra, D., 1974. A motivational view of learning, performance, and behavior modification. Psychol. Rev. 81, 199–213. https://doi.org/10.1037/h0036330

Bird, C.M., Burgess, N., 2008. The hippocampus and memory: insights from spatial processing. Nat. Rev. Neurosci. 9, 182–194. https://doi.org/10.1038/nrn2335

Bissière, S., Humeau, Y., Lüthi, A., 2003. Dopamine gates LTP induction in lateral amygdala by suppressing feedforward inhibition. Nat. Neurosci. 6, 587–592. https://doi.org/10.1038/nn1058

Björklund, A., Dunnett, S.B., 2007. Dopamine neuron systems in the brain: an update. Trends Neurosci., Fifty years of dopamine research 30, 194–202. https://doi.org/10.1016/j.tins.2007.03.006

Blandini, F., Nappi, G., Tassorelli, C., Martignoni, E., 2000. Functional changes of the basal ganglia circuitry in Parkinson's disease. Prog. Neurobiol. 62, 63–88. https://doi.org/10.1016/S0301-0082(99)00067-2

Bliss, T.V., Collingridge, G.L., 1993. A synaptic model of memory: long-term potentiation in the hippocampus. Nature 361, 31–39. https://doi.org/10.1038/361031a0

Bliss, T.V., Lomo, T., 1973. Long-lasting potentiation of synaptic transmission in the dentate area of the anaesthetized rabbit following stimulation of the perforant path. J. Physiol. 232, 331–356. https://doi.org/10.1113/jphysiol.1973.sp010273

Bolles, R.C., 1972. Reinforcement, expectancy, and learning. Psychol. Rev. 79, 394–409. https://doi.org/10.1037/h0033120

Bonnet, L., Comte, A., Tatu, L., Millot, J.-L., Moulin, T., Medeiros de Bustos, E., 2015. The role of the amygdala in the perception of positive emotions: an "intensity detector." Front. Behav. Neurosci. 9. https://doi.org/10.3389/fnbeh.2015.00178

Bouton, M.E., 2004. Context and behavioral processes in extinction. Learn. Mem. Cold Spring Harb. N 11, 485–94. https://doi.org/10.1101/lm.78804

Bouton, M.E., 2002. Context, ambiguity, and unlearning: sources of relapse after behavioral extinction. Biol. Psychiatry 52, 976–986. https://doi.org/10.1016/s0006-3223(02)01546-9

Bouton, M.E., 1993. Context, time, and memory retrieval in the interference paradigms of Pavlovian learning. Psychol. Bull. 114, 80–99. https://doi.org/10.1037/0033-2909.114.1.80

Bouton, M.E., Peck, C.A., 1989. Context effects on conditioning, extinction, and reinstatement in an appetitive conditioning preparation. Anim. Learn. Behav. 17, 188–198. https://doi.org/10.3758/BF03207634

Bragin, A., Jandó, G., Nádasdy, Z., Hetke, J., Wise, K., Buzsáki, G., 1995. Gamma (40-100 Hz) oscillation in the hippocampus of the behaving rat. J. Neurosci. 15, 47–60. https://doi.org/10.1523/jneurosci.15-01-00047.1995

Breathing coordinates limbic network dynamics underlying memory consolidation | bioRxiv [WWW Document], n.d. URL https://www.biorxiv.org/content/10.1101/392530v1 (accessed 2.4.21).

Breiter, H.C., Gollub, R.L., Weisskoff, R.M., Kennedy, D.N., Makris, N., Berke, J.D., Goodman, J.M., Kantor, H.L., Gastfriend, D.R., Riorden, J.P., Mathew, R.T., Rosen, B.R., Hyman, S.E., 1997. Acute Effects of Cocaine on Human Brain Activity and Emotion. Neuron 19, 591–611. https://doi.org/10.1016/S0896-6273(00)80374-8

Brenhouse, H.C., Andersen, S.L., 2008. Delayed Extinction and Stronger Reinstatement of Cocaine Conditioned Place Preference in Adolescent Rats, Compared to Adults. Behav. Neurosci. 122, 460–465. https://doi.org/10.1037/0735-7044.122.2.460

Brookes, M.J., Woolrich, M., Luckhoo, H., Price, D., Hale, J.R., Stephenson, M.C., Barnes, G.R., Smith, S.M., Morris, P.G., 2011. Investigating the electrophysiological basis of resting state networks using magnetoencephalography. Proc. Natl. Acad. Sci. 108, 16783–16788. https://doi.org/10.1073/pnas.1112685108

Brunet, N., Vinck, M., Bosman, C.A., Singer, W., Fries, P., 2014. Gamma or no gamma, that is the question. Trends Cogn. Sci. 18, 507–509. https://doi.org/10.1016/j.tics.2014.08.006

Buzsáki, G., 2010. Neural syntax: cell assemblies, synapsembles, and readers. Neuron 68, 362–85. https://doi.org/10.1016/j.neuron.2010.09.023

Buzsáki, G., 2004. Large-scale recording of neuronal ensembles. Nat. Neurosci. 7, 446–451. https://doi.org/10.1038/nn1233

Buzsáki, G., 2002. Theta Oscillations in the Hippocampus. Neuron 33, 325–340. https://doi.org/10.1016/S0896-6273(02)00586-X

Buzsáki, G., Rappelsberger, P., Kellényi, L., 1985. Depth profiles of hippocampal rhythmic slow activity ('theta rhythm') depend on behaviour. Electroencephalogr. Clin. Neurophysiol. 61, 77–88. https://doi.org/10.1016/0013-4694(85)91075-2

Buzsáki, G., Schomburg, E.W., 2015. What does gamma coherence tell us about inter-regional neural communication? Nat. Neurosci. 18, 484–489. https://doi.org/10.1038/nn.3952

Buzsáki, G., Wang, X.-J., 2012. Mechanisms of Gamma Oscillations. Annu. Rev. Neurosci. 35, 203–225. https://doi.org/10.1146/annurev-neuro-062111-150444

Cahill, L., McGaugh, J.L., 1996. Modulation of memory storage. Curr. Opin. Neurobiol. 6, 237–242. https://doi.org/10.1016/s0959-4388(96)80078-x

Cameron, D., Williams, J., 1994. Cocaine inhibits GABA release in the VTA through endogenous 5-HT. J. Neurosci. 14, 6763–6767. https://doi.org/10.1523/JNEUROSCI.14-11-06763.1994

Capitani, G., De Biase, D., Aurizi, C., Gut, H., Bossa, F., Grütter, M.G., 2003. Crystal structure and functional analysis of Escherichia coli glutamate decarboxylase. EMBO J. 22, 4027–4037. https://doi.org/10.1093/emboj/cdg403

Caporale, N., Dan, Y., 2008. Spike timing-dependent plasticity: a Hebbian learning rule. Annu. Rev. Neurosci. 31, 25–46. https://doi.org/10.1146/annurev.neuro.31.060407.125639

Cardinal, R.N., Robbins, T.W., Everitt, B.J., 2000. The effects of d-amphetamine, chlordiazepoxide, alpha-flupenthixol and behavioural manipulations on choice of signalled and unsignalled delayed reinforcement in rats. Psychopharmacology (Berl.) 152, 362–375. https://doi.org/10.1007/s002130000536

Carey, R.J., Damianopoulos, E.N., 1992. Opponent-process theory and drug conditioning: an assessment for conditioned stimulant-induced movement. Behav. Brain Res. 51, 139–147. https://doi.org/10.1016/S0166-4328(05)80207-4

Carey, R.J., DePalma, G., Damianopoulos, E., 2005. Evidence for Pavlovian conditioning of cocaine-induced responses linked to emotional behavioral effects. Pharmacol. Biochem. Behav. 80, 123–134. https://doi.org/10.1016/j.pbb.2004.10.012

Catanese, J., Carmichael, J.E., Matthijs, X., Van Der Meer, A.A., 2016. Low-and high-gamma oscillations deviate in opposite directions from zero-phase synchrony in the limbic corticostriatal loop. J Neurophysiol 116, 5–17. https://doi.org/10.1152/jn.00914.2015.-The

Chaudhury, D., Walsh, J.J., Friedman, A.K., Juarez, B., Ku, S.M., Koo, J.W., Ferguson, D., Tsai, H.-C., Pomeranz, L., Christoffel, D.J., Nectow, A.R., Ekstrand, M., Domingos, A., Mazei-Robison, M.S., Mouzon, E., Lobo, M.K., Neve, R.L., Friedman, J.M., Russo, S.J., Deisseroth, K., Nestler, E.J., Han, M.-H., 2013. Rapid regulation of depression-related behaviours by control of midbrain dopamine neurons. Nature 493, 532–536. https://doi.org/10.1038/nature11713

Chieng, B., Azriel, Y., Mohammadi, S., Christie, M.J., 2011. Distinct cellular properties of identified dopaminergic and GABAergic neurons in the mouse ventral tegmental area. J. Physiol. 589, 3775–3787. https://doi.org/10.1113/jphysiol.2011.210807

Childress, A.R., McLellan, A.T., Ehrman, R., O'Brien, C.P., 1988. Classically conditioned responses in opioid and cocaine dependence: a role in relapse? NIDA Res. Monogr. 84, 25–43.

Childress, A.R., Mozley, P.D., McElgin, W., Fitzgerald, J., Reivich, M., O'Brien, C.P., 1999. Limbic Activation During Cue-Induced Cocaine Craving. Am. J. Psychiatry 156, 11–18. https://doi.org/10.1176/ajp.156.1.11

Church, W.H., Justice, J.B., Byrd, L.D., 1987. Extracellular dopamine in rat striatum following uptake inhibition by cocaine, nomifensine and benztropine. Eur. J. Pharmacol. 139, 345–348. https://doi.org/10.1016/0014-2999(87)90592-9

Claridge-Chang, A., Assam, P.N., 2016. Estimation statistics should replace significance testing. Nat. Methods 13, 108–109. https://doi.org/10.1038/nmeth.3729

Cohen, J., 2013. Statistical Power Analysis for the Behavioral Sciences. Academic Press.

Cohen, J.Y., Haesler, S., Vong, L., Lowell, B.B., Uchida, N., 2012. Neuron-type-specific signals for reward and punishment in the ventral tegmental area. Nature 482, 85–88. https://doi.org/10.1038/nature10754

Cole, S., Voytek, B., 2019. Cycle-by-cycle analysis of neural oscillations. J. Neurophysiol. 122, 849–861. https://doi.org/10.1152/jn.00273.2019

Cole, S.R., Voytek, B., 2017. Brain Oscillations and the Importance of Waveform Shape. Trends Cogn. Sci. 21, 137–149. https://doi.org/10.1016/j.tics.2016.12.008

Colgin, L.L., Denninger, T., Fyhn, M., Hafting, T., Bonnevie, T., Jensen, O., Moser, M.-B., Moser, E.I., 2009. LETTERS Frequency of gamma oscillations routes flow of information in the hippocampus. Nature 462. https://doi.org/10.1038/nature08573

Collingridge, G.L., Herron, C.E., Lester, R.A., 1988. Synaptic activation of N-methyl-D-aspartate receptors in the Schaffer collateral-commissural pathway of rat hippocampus. J. Physiol. 399, 283–300. https://doi.org/10.1113/jphysiol.1988.sp017080

Collingridge, G.L., Kehl, S.J., McLennan, H., 1983. Excitatory amino acids in synaptic transmission in the Schaffer collateral-commissural pathway of the rat hippocampus. J. Physiol. 334, 33–46.

Colominas, M., Schlotthauer, G., Torres, M.E., Flandrin, P., 2012. Noise-Assisted EMD Methods in Action. Adv Adapt Data Anal. https://doi.org/10.1142/S1793536912500252

Coricelli, G., Dolan, R.J., Sirigu, A., 2007. Brain, emotion and decision making: the paradigmatic example of regret. Trends Cogn. Sci. 11, 258–265. https://doi.org/10.1016/j.tics.2007.04.003

Csicsvari, J., Hirase, H., Czurko, A., Buzsáki, G., 1998. Reliability and State Dependence of Pyramidal Cell–Interneuron Synapses in the Hippocampus: an Ensemble Approach in the Behaving Rat. Neuron 21, 179–189. https://doi.org/10.1016/S0896-6273(00)80525-5

Cunningham, C.L., Gremel, C.M., Groblewski, P.A., 2006. Drug-induced conditioned place preference and aversion in mice. Nat. Protoc. 1, 1662–1670. https://doi.org/10.1038/nprot.2006.279

Dahan, L., Astier, B., Vautrelle, N., Urbain, N., Kocsis, B., Chouvet, G., 2007. Prominent Burst Firing of Dopaminergic Neurons in the Ventral Tegmental Area during Paradoxical Sleep. Neuropsychopharmacology 32, 1232–1241. https://doi.org/10.1038/sj.npp.1301251

Dalley, J.W., Lääne, K., Theobald, D.E.H., Armstrong, H.C., Corlett, P.R., Chudasama, Y., Robbins, T.W., 2005. Time-limited modulation of appetitive Pavlovian memory by D1 and NMDA receptors in the nucleus accumbens. Proc. Natl. Acad. Sci. 102, 6189–6194. https://doi.org/10.1073/pnas.0502080102

de N, R.L., 1939. Transmission of impulses through cranial motor nuclei. J. Neurophysiol. 2, 402–464. https://doi.org/10.1152/jn.1939.2.5.402

Deering, R., Kaiser, J.F., 2005. The use of a masking signal to improve empirical mode decomposition. Presented at the Acoustics, Speech, and Signal Processing, 1988. ICASSP-88., 1988 International Conference on, p. iv/485-iv/488 Vol. 4. https://doi.org/10.1109/ICASSP.2005.1416051

dela Peña, I., Gevorkiana, R., Shi, W.-X., 2015. Psychostimulants affect dopamine transmission through both dopamine transporter-dependent and independent mechanisms. Eur. J. Pharmacol. 764, 562–570. https://doi.org/10.1016/j.ejphar.2015.07.044

Di Chiara, G., Imperato, A., 1988. Drugs abused by humans preferentially increase synaptic dopamine concentrations in the mesolimbic system of freely moving rats. Proc. Natl. Acad. Sci. U. S. A. 85, 5274–5278. https://doi.org/10.1073/pnas.85.14.5274

Dijk, H. van, Werf, J. van der, Mazaheri, A., Medendorp, W.P., Jensen, O., 2010. Modulations in oscillatory activity with amplitude asymmetry can produce cognitively relevant event-related responses. Proc. Natl. Acad. Sci. 107, 900–905. https://doi.org/10.1073/pnas.0908821107

Domenech, P., Koechlin, E., 2015. Executive control and decision-making in the prefrontal cortex. Curr. Opin. Behav. Sci., Cognitive control 1, 101–106. https://doi.org/10.1016/j.cobeha.2014.10.007

Dong, Y., Saal, D., Thomas, M., Faust, R., Bonci, A., Robinson, T., Malenka, R.C., 2004. Cocaine-induced potentiation of synaptic strength in dopamine neurons: Behavioral correlates in GluRA(–/–) mice. Proc. Natl. Acad. Sci. 101, 14282–14287. https://doi.org/10.1073/pnas.0401553101

Donnelly, N.A., Holtzman, T., Rich, P.D., Nevado-Holgado, A.J., Fernando, A.B.P., Van Dijck, G., Holzhammer, T., Paul, O., Ruther, P., Paulsen, O., Robbins, T.W., Dalley, J.W., 2014. Oscillatory Activity in the Medial Prefrontal Cortex and Nucleus Accumbens Correlates with Impulsivity and Reward Outcome. PLoS ONE 9, e111300–e111300. https://doi.org/10.1371/journal.pone.0111300

Douglass, A.M., Kucukdereli, H., Ponserre, M., Markovic, M., Gründemann, J., Strobel, C., Alcala Morales, P.L., Conzelmann, K.-K., Lüthi, A., Klein, R., 2017. Central amygdala circuits modulate food consumption through a positive-valence mechanism. Nat. Neurosci. 20, 1384–1394. https://doi.org/10.1038/nn.4623

Dudek, S.M., Bear, M.F., 1992. Homosynaptic long-term depression in area CA1 of hippocampus and effects of N-methyl-D-aspartate receptor blockade. Proc. Natl. Acad. Sci. U. S. A. 89, 4363–4367. https://doi.org/10.1073/pnas.89.10.4363

Durst, M., Könczöl, K., Balázsa, T., Eyre, M.D., Tóth, Z.E., 2019. Reward-representing D1-type neurons in the medial shell of the accumbens nucleus regulate palatable food intake. Int. J. Obes. 43, 917–927. https://doi.org/10.1038/s41366-018-0133-y

Düzel, E., Bunzeck, N., Guitart-Masip, M., Wittmann, B., Schott, B.H., Tobler, P.N., 2009. Functional imaging of the human dopaminergic midbrain. Trends Neurosci. 32, 321–328. https://doi.org/10.1016/j.tins.2009.02.005

Engel, A.K., Fries, P., 2010. Beta-band oscillations-signalling the status quo? Curr. Opin. Neurobiol. 20, 156–165. https://doi.org/10.1016/j.conb.2010.02.015

Engel, A.K., Fries, P., Singer, W., 2001. Dynamic predictions: Oscillations and synchrony in top–down processing. Nat. Rev. Neurosci. 2, 704–716. https://doi.org/10.1038/35094565

Ermentrout, G.B., Kopell, N., 1998. Fine structure of neural spiking and synchronization in the presence of conduction delays. Proc. Natl. Acad. Sci. 95, 1259–1264. https://doi.org/10.1073/pnas.95.3.1259

Everitt, B.J., Dickinson, A., Robbins, T.W., 2001. The neuropsychological basis of addictive behaviour. Brain Res. Rev., The Brain in Health and Disease - from Molecules to Man. Swiss National Foundation Symposium NRP 38 36, 129–138. https://doi.org/10.1016/S0165-0173(01)00088-1

Everitt, B.J., Robbins, T.W., 2005. Neural systems of reinforcement for drug addiction: from actions to habits to compulsion. Nat. Neurosci. 8, 1481–1489. https://doi.org/10.1038/nn1579

Fadok, J.P., Markovic, M., Tovote, P., Lüthi, A., 2018. New perspectives on central amygdala function. Curr. Opin. Neurobiol., Neurobiology of Behavior 49, 141–147. https://doi.org/10.1016/j.conb.2018.02.009

Fenno, L., Yizhar, O., Deisseroth, K., 2011. The Development and Application of Optogenetics. Annu. Rev. Neurosci. 34, 389–412. https://doi.org/10.1146/annurev-neuro-061010-113817

Fernández-Ruiz, A., Oliva, A., Nagy, G.A., Maurer, A.P., Berényi, A., Buzsáki, G., 2017. Entorhinal-CA3 Dual-Input Control of Spike Timing in the Hippocampus by Theta-Gamma Coupling. Neuron 93, 1213-1226.e5. https://doi.org/10.1016/j.neuron.2017.02.017

Filip, M., Frankowska, M., Jastrzębska, J., Wydra, K., Przegaliński, E., 2013. Preclinical studies on comorbidity between depression and psychostimulant addiction. Pharmacol. Rep. 65, 1529–1534. https://doi.org/10.1016/S1734-1140(13)71514-7

Fischbach-Weiss, S., Reese, R.M., Janak, P.H., 2018. Inhibiting Mesolimbic Dopamine Neurons Reduces the Initiation and Maintenance of Instrumental Responding. Neuroscience 372, 306–315. https://doi.org/10.1016/j.neuroscience.2017.12.003

Fosso, O., Molinas, M., 2017. Method for Mode Mixing Separation in Empirical Mode Decomposition.

Fowler, J.S., Volkow, N.D., Wolf, A.P., Dewey, S.L., Schlyer, D.J., Macgregor, R.R., Hitzemann, R., Logan, J., Bendriem, B., Gatley, S.J., 1989. Mapping cocaine binding sites in human and baboon brain in vivo. Synap. N. Y. N 4, 371–377. https://doi.org/10.1002/syn.890040412

Fox, M.E., Mikhailova, M.A., Bass, C.E., Takmakov, P., Gainetdinov, R.R., Budygin, E.A., Wightman, R.M., 2016. Cross-hemispheric dopamine projections have functional significance. Proc. Natl. Acad. Sci. 113, 6985–6990. https://doi.org/10.1073/pnas.1603629113

Fries, P., 2005. A mechanism for cognitive dynamics: neuronal communication through neuronal coherence. Trends Cogn. Sci. 9, 474–480. https://doi.org/10.1016/j.tics.2005.08.011

Fujisawa, S., Buzsáki, G., 2011. A 4 Hz Oscillation Adaptively Synchronizes Prefrontal, VTA, and Hippocampal Activities. Neuron 72, 153–165. https://doi.org/10.1016/j.neuron.2011.08.018

Girardeau, P., Navailles, S., Durand, A., Vouillac-Mendoza, C., Guillem, K., Ahmed, S.H., 2019. Relapse to cocaine use persists following extinction of drug-primed craving. Neuropharmacology 155, 185–193. https://doi.org/10.1016/j.neuropharm.2019.05.036

Grace, A., Bunney, B., 1984. The control of firing pattern in nigral dopamine neurons: single spike firing. J. Neurosci. 4, 2866–2876. https://doi.org/10.1523/JNEUROSCI.04-11-02866.1984

Grant, S., London, E.D., Newlin, D.B., Villemagne, V.L., Liu, X., Contoreggi, C., Phillips, R.L., Kimes, A.S., Margolin, A., 1996. Activation of memory circuits during cue-elicited cocaine craving. Proc. Natl. Acad. Sci. U. S. A. 93, 12040–12045.

Gray, T.S., Bingaman, E.W., 1996. The amygdala: corticotropin-releasing factor, steroids, and stress. Crit. Rev. Neurobiol. 10, 155–168. https://doi.org/10.1615/critrevneurobiol.v10.i2.10

Groblewski, P.A., Cunningham, C.L., 2012. Repeated microinjections into the medial prefrontal cortex (mPFC) impair extinction of conditioned place preference in mice. Behav. Brain Res. 230, 299–303. https://doi.org/10.1016/j.bbr.2012.01.059

Groblewski, P.A., Ryabinin, A.E., Cunningham, C.L., 2012. Activation and role of the medial prefrontal cortex (mPFC) in extinction of ethanol-induced associative learning in mice. Neurobiol. Learn. Mem. 97, 37–46. https://doi.org/10.1016/j.nlm.2011.09.001

Groenewegen, H.J., Wright, C.I., Beijer, A.V., 1996. The nucleus accumbens: gateway for limbic structures to reach the motor system? Prog. Brain Res. 107, 485–511. https://doi.org/10.1016/s0079-6123(08)61883-x

Halsey, L.G., Curran-Everett, D., Vowler, S.L., Drummond, G.B., 2015. The fickle P value generates irreproducible results. Nat. Methods 12, 179–185. https://doi.org/10.1038/nmeth.3288

Hammond, C., Bergman, H., Brown, P., 2007. Pathological synchronization in Parkinson's disease: networks, models and treatments. Trends Neurosci. 30, 357–364. https://doi.org/10.1016/j.tins.2007.05.004

Han, X., Jing, M.-Y., Zhao, T.-Y., Wu, N., Song, R., Li, J., 2017. Role of dopamine projections from ventral tegmental area to nucleus accumbens and medial prefrontal cortex in reinforcement behaviors assessed using optogenetic manipulation. Metab. Brain Dis. 32, 1491–1502. https://doi.org/10.1007/s11011-017-0023-3

Hanlon, C.A., Dowdle, L.T., Moss, H., Canterberry, M., George, M.S., 2016. Mobilization of Medial and Lateral Frontal-Striatal Circuits in Cocaine Users and Controls: An Interleaved

TMS/BOLD Functional Connectivity Study. Neuropsychopharmacology 41, 3032–3041. https://doi.org/10.1038/npp.2016.114

Hardung, S., Epple, R., Jäckel, Z., Eriksson, D., Uran, C., Senn, V., Gibor, L., Yizhar, O., Diester, I., 2017. A Functional Gradient in the Rodent Prefrontal Cortex Supports Behavioral Inhibition. Curr. Biol. 27, 549–555. https://doi.org/10.1016/j.cub.2016.12.052

Harmer, C.J., Mackay, C.E., Reid, C.B., Cowen, P.J., Goodwin, G.M., 2006. Antidepressant Drug Treatment Modifies the Neural Processing of Nonconscious Threat Cues. Biol. Psychiatry 59, 816–820. https://doi.org/10.1016/j.biopsych.2005.10.015

Harris, A.Z., Gordon, J.A., 2015. Long-Range Neural Synchrony in Behavior. Annu. Rev. Neurosci. 38, 171–194. https://doi.org/10.1146/annurev-neuro-071714-034111

Harris, K.D., Henze, D.A., Csicsvari, J., Hirase, H., Buzsáki, G., 2000. Accuracy of tetrode spike separation as determined by simultaneous intracellular and extracellular measurements. J. Neurophysiol. 84, 401–414. https://doi.org/10.1152/jn.2000.84.1.401

Hebb, D.O., 1949. The organization of behavior; a neuropsychological theory, The organization of behavior; a neuropsychological theory. Wiley, Oxford, England.

Hernández Ruiz de Eguilaz, M., Martínez de Morentin Aldabe, B., Almiron-Roig, E., Pérez-Diez, S., San Cristóbal Blanco, R., Navas-Carretero, S., Martínez, J.A., 2018. Multisensory influence on eating behavior: Hedonic consumption. Endocrinol. Diabetes Nutr. 65, 114–125. https://doi.org/10.1016/j.endinu.2017.09.008

Herwig, U., Lutz, J., Scherpiet, S., Scheerer, H., Kohlberg, J., Opialla, S., Preuss, A., Steiger, V.R., Sulzer, J., Weidt, S., Stämpfli, P., Rufer, M., Seifritz, E., Jäncke, L., Brühl, A.B., 2019. Training emotion regulation through real-time fMRI neurofeedback of amygdala activity. NeuroImage 184, 687–696. https://doi.org/10.1016/j.neuroimage.2018.09.068

Hestrin, S., 1993. Different glutamate receptor channels mediate fast excitatory synaptic currents in inhibitory and excitatory cortical neurons. Neuron 11, 1083–1091. https://doi.org/10.1016/0896-6273(93)90221-c

Heymann, G., Jo, Y.S., Reichard, K.L., McFarland, N., Chavkin, C., Palmiter, R.D., Soden, M.E., Zweifel, L.S., 2020. Synergy of Distinct Dopamine Projection Populations in Behavioral Reinforcement. Neuron 105, 909-920.e5. https://doi.org/10.1016/j.neuron.2019.11.024

Ho, J., Tumkaya, T., Aryal, S., Choi, H., Claridge-Chang, A., 2019. Moving beyond P values: data analysis with estimation graphics. Nat. Methods 16, 565–566. https://doi.org/10.1038/s41592-019-0470-3

Hoerbelt, P., Lindsley, T.A., Fleck, M.W., 2015. Dopamine Directly Modulates GABAA Receptors. J. Neurosci. 35, 3525–3536. https://doi.org/10.1523/JNEUROSCI.4390-14.2015

Horvitz, J.C., 2000. Mesolimbocortical and nigrostriatal dopamine responses to salient non-reward events. Neuroscience 96, 651–656. https://doi.org/10.1016/S0306-4522(00)00019-1

Huang, C.C., Liang, Y.C., Hsu, K.S., 2001. Characterization of the mechanism underlying the reversal of long term potentiation by low frequency stimulation at hippocampal CA1 synapses. J. Biol. Chem. 276, 48108–48117. https://doi.org/10.1074/jbc.M106388200

Huang, N.E., Shen, Z., Long, S.R., Wu, M.C., Shih, H.H., Zheng, Q., Yen, N.-C., Tung, C.C., Liu, H.H., 1998. The empirical mode decomposition and the Hilbert spectrum for nonlinear and non-stationary time series analysis. Proc. R. Soc. Lond. Ser. Math. Phys. Eng. Sci. 454, 903–995. https://doi.org/10.1098/rspa.1998.0193

Hull, C.L., 1943. Principles of behavior: an introduction to behavior theory, Principles of behavior: an introduction to behavior theory. Appleton-Century, Oxford, England.

Hummos, A., Nair, S.S., 2017. An integrative model of the intrinsic hippocampal theta rhythm. PLOS ONE 12, e0182648. https://doi.org/10.1371/journal.pone.0182648

Huston, J.P., Silva, M.A. de S., Topic, B., Müller, C.P., 2013. What's conditioned in conditioned place preference? Trends Pharmacol. Sci. 34, 162–166. https://doi.org/10.1016/j.tips.2013.01.004

Iversen, L., 2006. Neurotransmitter transporters and their impact on the development of psychopharmacology. Br. J. Pharmacol. 147, S82–S88. https://doi.org/10.1038/sj.bjp.0706428

Jarrahi, B., Mantini, D., Balsters, J.H., Michels, L., Kessler, T.M., Mehnert, U., Kollias, S.S., 2015. Differential functional brain network connectivity during visceral interoception as revealed by independent component analysis of fMRI time-series. Hum. Brain Mapp. 36, 4438–4468. https://doi.org/10.1002/hbm.22929

Javitch, J.A., Blaustein, R.O., Snyder, S.H., 1984. [3H]mazindol binding associated with neuronal dopamine and norepinephrine uptake sites. Mol. Pharmacol. 26, 35–44.

Ji, X., Saha, S., Kolpakova, J., Guildford, M., Tapper, A.R., Martin, G.E., 2017. Dopamine Receptors Differentially Control Binge Alcohol Drinking-Mediated Synaptic Plasticity of the Core Nucleus Accumbens Direct and Indirect Pathways. J. Neurosci. Off. J. Soc. Neurosci. 37, 5463–5474. https://doi.org/10.1523/JNEUROSCI.3845-16.2017

Jinno, S., Klausberger, T., Marton, L.F., Dalezios, Y., Roberts, J.D.B., Fuentealba, P., Bushong, E.A., Henze, D., Buzsáki, G., Somogyi, P., 2007. Neuronal Diversity in GABAergic Long-Range Projections from the Hippocampus. J. Neurosci. 27, 8790–8804. https://doi.org/10.1523/JNEUROSCI.1847-07.2007

Johnston, D., Wu, S.M., 1995. Foundations of Cellular Neurophysiology. MIT Press.

Jones, M.W., Wilson, M.A., 2005. Theta Rhythms Coordinate Hippocampal–Prefrontal Interactions in a Spatial Memory Task. PLoS Biol. 3, e402–e402. https://doi.org/10.1371/journal.pbio.0030402

Jones, S.R., 2016. When brain rhythms aren't 'rhythmic': implication for their mechanisms and meaning. Curr. Opin. Neurobiol., Systems neuroscience 40, 72–80. https://doi.org/10.1016/j.conb.2016.06.010

Juarez, B., Han, M.-H., 2016. Diversity of Dopaminergic Neural Circuits in Response to Drug Exposure. Neuropsychopharmacology 41, 2424–2446. https://doi.org/10.1038/npp.2016.32

Jutten, C., Herault, J., 1991. Blind separation of sources, part I: An adaptive algorithm based on neuromimetic architecture. Signal Process. 24, 1–10. https://doi.org/10.1016/0165-1684(91)90079-X

Kadir, S.N., Goodman, D.F.M., Harris, K.D., 2014. High-dimensional cluster analysis with the Masked EM Algorithm. Neural Comput. 26, 2379–2394. https://doi.org/10.1162/NECO_a_00661

Kai, N., Nishizawa, K., Tsutsui, Y., Ueda, S., Kobayashi, K., 2015. Differential roles of dopamine D1 and D2 receptor-containing neurons of the nucleus accumbens shell in behavioral sensitization. J. Neurochem. 135, 1232–1241. https://doi.org/10.1111/jnc.13380

Kandel, E.R., 2012. The molecular biology of memory: cAMP, PKA, CRE, CREB-1, CREB-2, and CPEB. Mol. Brain 5, 14. https://doi.org/10.1186/1756-6606-5-14

Kang-Park, M.-H., Sarda, M.A., Jones, K.H., Moore, S.D., Shenolikar, S., Clark, S., Wilson, W.A., 2003. Protein Phosphatases Mediate Depotentiation Induced by High-Intensity Theta-Burst Stimulation. J. Neurophysiol. 89, 684–690. https://doi.org/10.1152/jn.01041.2001

Kanoski, S.E., Walls, E.K., Davidson, T.L., 2007. Interoceptive “satiety” signals produced by leptin and CCK. Peptides 28, 988–1002. https://doi.org/10.1016/j.peptides.2007.02.015

Karalis, N., Dejean, C., Chaudun, F., Khoder, S., Rozeske, R.R., Wurtz, H., Bagur, S., Benchenane, K., Sirota, A., Courtin, J., Herry, C., 2016. 4-Hz oscillations synchronize prefrontal–amygdala circuits during fear behavior. Nat. Neurosci. 19, 605–612. https://doi.org/10.1038/nn.4251

Kennerley, S.W., Walton, M.E., 2011. Decision Making and Reward in Frontal Cortex. Behav. Neurosci. 125, 297–317. https://doi.org/10.1037/a0023575

Khanna, P., Carmena, J.M., 2015. Neural oscillations: beta band activity across motor networks. Curr. Opin. Neurobiol. 32, 60–67. https://doi.org/10.1016/j.conb.2014.11.010

Khoo, S.Y.-S., Sciascia, J.M., Brown, A., Chaudhri, N., 2020. Comparing ABA, AAB, and ABC Renewal of Appetitive Pavlovian Conditioned Responding in Alcohol- and Sucrose-Trained Male Rats. Front. Behav. Neurosci. 14. https://doi.org/10.3389/fnbeh.2020.00005

Kim, J., Park, B.-H., Lee, J.H., Park, S.K., Kim, J.-H., 2011. Cell type-specific alterations in the nucleus accumbens by repeated exposures to cocaine. Biol. Psychiatry 69, 1026–1034. https://doi.org/10.1016/j.biopsych.2011.01.013

Kiss, T., Orbán, G., Érdi, P., 2006. Modeling hippocampal theta oscillation: Applications in neuropharmacology and robot navigation. Int. J. Intell. Syst. 21, 903–917. https://doi.org/10.1002/int.20168

Klausberger, T., Somogyi, P., 2008. Neuronal Diversity and Temporal Dynamics: The Unity of Hippocampal Circuit Operations. Science 321, 53–57. https://doi.org/10.1126/science.1149381

Koch, C., Rapp, M., Segev, I., 1996. A Brief History of Time (Constants). Cereb. Cortex 6, 93–101. https://doi.org/10.1093/cercor/6.2.93

Koob, G.F., 2009. Brain stress systems in the amygdala and addiction. Brain Res. 1293, 61–75. https://doi.org/10.1016/j.brainres.2009.03.038

Kopell, N., Ermentrout, G.B., Whittington, M.A., Traub, R.D., 2000. Gamma rhythms and beta rhythms have different synchronization properties. Proc. Natl. Acad. Sci. 97, 1867–1872. https://doi.org/10.1073/pnas.97.4.1867

Korovaichuk, A., Makarova, J., Makarov, V.A., Benito, N., Herreras, O., 2010. Minor Contribution of Principal Excitatory Pathways to Hippocampal LFPs in the Anesthetized Rat: A Combined Independent Component and Current Source Density Study. J. Neurophysiol. 104, 484–497. https://doi.org/10.1152/jn.00297.2010

Krebs, R.M., Heipertz, D., Schuetze, H., Duzel, E., 2011. Novelty increases the mesolimbic functional connectivity of the substantia nigra/ventral tegmental area (SN/VTA) during reward

anticipation: Evidence from high-resolution fMRI. NeuroImage 58, 647–655. https://doi.org/10.1016/j.neuroimage.2011.06.038

Kuhar, M.J., Ritz, M.C., Boja, J.W., 1991. The dopamine hypothesis of the reinforcing properties of cocaine. Trends Neurosci. 14, 299–302. https://doi.org/10.1016/0166-2236(91)90141-G

Kupchik, Y.M., Brown, R.M., Heinsbroek, J.A., Lobo, M.K., Schwartz, D.J., Kalivas, P.W., 2015. Coding the direct/indirect pathways by D1 and D2 receptors is not valid for accumbens projections. Nat. Neurosci. 18, 1230–1232. https://doi.org/10.1038/nn.4068

Lacey, M.G., Mercuri, N.B., North, R.A., 1990. Actions of cocaine on rat dopaminergic neurones in vitro. Br. J. Pharmacol. 99, 731–735. https://doi.org/10.1111/j.1476-5381.1990.tb12998.x

Lak, A., Okun, M., Moss, M.M., Gurnani, H., Farrell, K., Wells, M.J., Reddy, C.B., Kepecs, A., Harris, K.D., Carandini, M., 2020. Dopaminergic and Prefrontal Basis of Learning from Sensory Confidence and Reward Value. Neuron 105, 700-711.e6. https://doi.org/10.1016/j.neuron.2019.11.018

Lammel, S., Steinberg, E.E., Földy, C., Wall, N.R., Beier, K., Luo, L., Malenka, R.C., 2015. Diversity of Transgenic Mouse Models for Selective Targeting of Midbrain Dopamine Neurons. Neuron 85, 429–438. https://doi.org/10.1016/j.neuron.2014.12.036

Lasztóczi, B., Klausberger, T., 2017. Distinct gamma oscillations in the distal dendritic fields of the dentate gyrus and the CA1 area of mouse hippocampus. Brain Struct. Funct. 222, 3355–3365. https://doi.org/10.1007/s00429-017-1421-3

Lesting, J., Daldrup, T., Narayanan, V., Himpe, C., Seidenbecher, T., Pape, H.-C., 2013. Directional Theta Coherence in Prefrontal Cortical to Amygdalo-Hippocampal Pathways Signals Fear Extinction. PLoS ONE 8, e77707–e77707. https://doi.org/10.1371/journal.pone.0077707

Li, Z., Chen, Z., Fan, G., Li, A., Yuan, J., Xu, T., 2018. Cell-Type-Specific Afferent Innervation of the Nucleus Accumbens Core and Shell. Front. Neuroanat. 12. https://doi.org/10.3389/fnana.2018.00084

Lisman, J., Schulman, H., Cline, H., 2002. The molecular basis of CaMKII function in synaptic and behavioural memory. Nat. Rev. Neurosci. 3, 175–190. https://doi.org/10.1038/nrn753

Lisman, J.E., Jensen, O., 2013. The θ-γ neural code. Neuron 77, 1002–1016. https://doi.org/10.1016/j.neuron.2013.03.007

Little, S., Brown, P., 2014. The functional role of beta oscillations in Parkinson's disease. Parkinsonism Relat. Disord. 20 Suppl 1, S44-48. https://doi.org/10.1016/S1353-8020(13)70013-0

Liu, Q., Pu, L., Poo, M., 2005. Repeated cocaine exposure in vivo facilitates LTP induction in midbrain dopamine neurons. Nature 437, 1027–1031. https://doi.org/10.1038/nature04050

Ljungberg, T., Apicella, P., Schultz, W., 1992. Responses of monkey dopamine neurons during learning of behavioral reactions. J. Neurophysiol. 67, 145–163. https://doi.org/10.1152/jn.1992.67.1.145

Lopes-dos-Santos, V., van de Ven, G.M., Morley, A., Trouche, S., Campo-Urriza, N., Dupret, D., 2018. Parsing Hippocampal Theta Oscillations by Nested Spectral Components during Spatial Exploration and Memory-Guided Behavior. Neuron 100, 940-952.e7. https://doi.org/10.1016/j.neuron.2018.09.031

Lüthi, A., Lüscher, C., 2014. Pathological circuit function underlying addiction and anxiety disorders. Nat. Neurosci. 17, 1635–1643. https://doi.org/10.1038/nn.3849

Lynch, G., Muller, D., Seubert, P., Larson, J., 1988. Long-term potentiation: Persisting problems and recent results. Brain Res. Bull. 21, 363–372. https://doi.org/10.1016/0361-9230(88)90148-7

Lytton, W.W., Sejnowski, T.J., 1991. Simulations of cortical pyramidal neurons synchronized by inhibitory interneurons. J. Neurophysiol. 66, 1059–1079. https://doi.org/10.1152/jn.1991.66.3.1059

MacKillop, J., Amlung, M.T., Few, L.R., Ray, L.A., Sweet, L.H., Munafò, M.R., 2011. Delayed reward discounting and addictive behavior: a meta-analysis. Psychopharmacology (Berl.) 216, 305–321. https://doi.org/10.1007/s00213-011-2229-0

Magee, J.C., Johnston, D., 1997. A synaptically controlled, associative signal for Hebbian plasticity in hippocampal neurons. Science 275, 209–213. https://doi.org/10.1126/science.275.5297.209

Magland, J., Jun, J., Lovero, E., Morley, A., Hurwitz, C., Buccino, A., Garcia, S., Barnett, A., 2020. SpikeForest: reproducible web-facing ground-truth validation of automated neural spike sorters. https://doi.org/10.1101/2020.01.14.900688

Margolis, E.B., Lock, H., Hjelmstad, G.O., Fields, H.L., 2006. The ventral tegmental area revisited: is there an electrophysiological marker for dopaminergic neurons? J. Physiol. 577, 907–924. https://doi.org/10.1113/jphysiol.2006.117069

Markram, H., Lübke, J., Frotscher, M., Sakmann, B., 1997. Regulation of synaptic efficacy by coincidence of postsynaptic APs and EPSPs. Science 275, 213–215. https://doi.org/10.1126/science.275.5297.213

McCloskey, M., Cohen, N.J., 1989. Catastrophic Interference in Connectionist Networks: The Sequential Learning Problem, in: Bower, G.H. (Ed.), Psychology of Learning and Motivation. Academic Press, pp. 109–165. https://doi.org/10.1016/S0079-7421(08)60536-8

McGarry, L.M., Carter, A.G., 2017. Prefrontal Cortex Drives Distinct Projection Neurons in the Basolateral Amygdala. Cell Rep. 21, 1426–1433. https://doi.org/10.1016/j.celrep.2017.10.046

McKendrick, G., Graziane, N.M., 2020. Drug-Induced Conditioned Place Preference and Its Practical Use in Substance Use Disorder Research. Front. Behav. Neurosci. 14. https://doi.org/10.3389/fnbeh.2020.582147

McNamara, C.G., Tejero-Cantero, Á., Trouche, S., Campo-Urriza, N., Dupret, D., 2014. Dopaminergic neurons promote hippocampal reactivation and spatial memory persistence. Nat. Neurosci. 17, 1658–1660. https://doi.org/10.1038/nn.3843

Meador, K.J., Ray, P.G., Echauz, J.R., Loring, D.W., Vachtsevanos, G.J., 2002. Gamma coherence and conscious perception. Neurology 59, 847–854. https://doi.org/10.1212/wnl.59.6.847

Meer, M.A.A. van der, Redish, A.D., 2011. Theta Phase Precession in Rat Ventral Striatum Links Place and Reward Information. J. Neurosci. 31, 2843–2854. https://doi.org/10.1523/JNEUROSCI.4869-10.2011

Merlo Pich, E., Lorang, M., Yeganeh, M., Rodriguez de Fonseca, F., Raber, J., Koob, G.F., Weiss, F., 1995. Increase of extracellular corticotropin-releasing factor-like immunoreactivity levels in the amygdala of awake rats during restraint stress and ethanol withdrawal as measured by microdialysis. J. Neurosci. Off. J. Soc. Neurosci. 15, 5439–5447.

Middleton, S.J., McHugh, T.J., 2016. Silencing CA3 disrupts temporal coding in the CA1 ensemble. Nat. Neurosci. 19, 945–951. https://doi.org/10.1038/nn.4311

Miles, F.J., Everitt, B.J., Dickinson, A., 2003. Oral cocaine seeking by rats: action or habit? Behav. Neurosci. 117, 927–938. https://doi.org/10.1037/0735-7044.117.5.927

Mizuseki, K., Sirota, A., Pastalkova, E., Buzsáki, G., 2009. Theta Oscillations Provide Temporal Windows for Local Circuit Computation in the Entorhinal-Hippocampal Loop. Neuron 64, 267–280. https://doi.org/10.1016/J.NEURON.2009.08.037

Morales, M., Margolis, E.B., 2017. Ventral tegmental area: cellular heterogeneity, connectivity and behaviour. Nat. Rev. Neurosci. 18, 73–85. https://doi.org/10.1038/nrn.2016.165

Morey, R.D., Hoekstra, R., Rouder, J.N., Lee, M.D., Wagenmakers, E.-J., 2016. The fallacy of placing confidence in confidence intervals. Psychon. Bull. Rev. 23, 103–123. https://doi.org/10.3758/s13423-015-0947-8

Morris, R.G.M., Garrud, P., Rawlins, J.N.P., O'Keefe, J., 1982. Place navigation impaired in rats with hippocampal lesions. Nature 297, 681–683. https://doi.org/10.1038/297681a0

Mosharov, E.V., Larsen, K.E., Kanter, E., Phillips, K.A., Wilson, K., Schmitz, Y., Krantz, D.E., Kobayashi, K., Edwards, R.H., Sulzer, D., 2009. Interplay between Cytosolic Dopamine, Calcium, and α-Synuclein Causes Selective Death of Substantia Nigra Neurons. Neuron 62, 218–229. https://doi.org/10.1016/j.neuron.2009.01.033

Mueller, D., Stewart, J., 2000. Cocaine-induced conditioned place preference: reinstatement by priming injections of cocaine after extinction. Behav. Brain Res. 115, 39–47. https://doi.org/10.1016/s0166-4328(00)00239-4

Myers, K.M., Davis, M., 2002. Behavioral and neural analysis of extinction. Neuron 36, 567–584. https://doi.org/10.1016/s0896-6273(02)01064-4

Nair-Roberts, R.G., Chatelain-Badie, S.D., Benson, E., White-Cooper, H., Bolam, J.P., Ungless, M.A., 2008. Stereological estimates of dopaminergic, GABAergic and glutamatergic neurons in the ventral tegmental area, substantia nigra and retrorubral field in the rat. Neuroscience 152, 1024–1031. https://doi.org/10.1016/j.neuroscience.2008.01.046

Neve, K.A., Seamans, J.K., Trantham-Davidson, H., 2004. Dopamine receptor signaling. J. Recept. Signal Transduct. Res. 24, 165–205. https://doi.org/10.1081/rrs-200029981

Nguyen, P.V., Woo, N.H., 2003. Regulation of hippocampal synaptic plasticity by cyclic AMP-dependent protein kinases. Prog. Neurobiol. 71, 401–437. https://doi.org/10.1016/j.pneurobio.2003.12.003

Nicola, W., Clopath, C., 2019. A diversity of interneurons and Hebbian plasticity facilitate rapid compressible learning in the hippocampus. Nat. Neurosci. 22, 1168–1181. https://doi.org/10.1038/s41593-019-0415-2

Nicolaysen, L.C., Pan, H.-T., Justice, J.B., 1988. Extracellular cocaine and dopamine concentrations are linearly related in rat striatum. Brain Res. 456, 317–323. https://doi.org/10.1016/0006-8993(88)90234-X

Nikolaou, F., Orphanidou, C., Murphy, K., Wise, R.G., Mitsis, G.D., 2018. Investigation Of Interaction Between Physiological Signals And fMRI Dynamic Functional Connectivity Using Independent Component Analysis. Annu. Int. Conf. IEEE Eng. Med. Biol. Soc. IEEE Eng. Med. Biol. Soc. Annu. Int. Conf. 2018, 1019–1023. https://doi.org/10.1109/EMBC.2018.8512465

Nugent, F.S., Penick, E.C., Kauer, J.A., 2007. Opioids block long-term potentiation of inhibitory synapses. Nature 446, 1086–1090. https://doi.org/10.1038/nature05726

O'Keefe, J., Dostrovsky, J., 1971. The hippocampus as a spatial map. Preliminary evidence from unit activity in the freely-moving rat. Brain Res. 34, 171–5.

O'Keefe, J., Nadel, L., 1978. The Hippocampus as a Cognitive Map. Oxford: Clarendon Press.

O'Keefe, J., Recce, M.L., 1993. Phase relationship between hippocampal place units and the EEG theta rhythm. Hippocampus 3, 317–330. https://doi.org/10.1002/hipo.450030307

operant conditioning chamber – APA Dictionary of Psychology [WWW Document], n.d. URL https://dictionary.apa.org/operant-conditioning-chamber (accessed 12.30.20).

Otis, J.M., Mueller, D., 2011. Inhibition of β -Adrenergic Receptors Induces a Persistent Deficit in Retrieval of a Cocaine-Associated Memory Providing Protection against Reinstatement. Neuropsychopharmacology 36, 1912–1920. https://doi.org/10.1038/npp.2011.77

Owesson-White, C.A., Ariansen, J., Stuber, G.D., Cleaveland, N.A., Cheer, J.F., Wightman, R.M., Carelli, R.M., 2009. Neural Encoding of Cocaine Seeking Behavior is Coincident with Phasic Dopamine Release in the Accumbens Core and Shell. Eur. J. Neurosci. 30, 1117–1127. https://doi.org/10.1111/j.1460-9568.2009.06916.x

Pachitariu, M., Steinmetz, N., Kadir, S., Carandini, M., Kenneth D., H., 2016. Kilosort: realtime spike-sorting for extracellular electrophysiology with hundreds of channels (preprint). Neuroscience. https://doi.org/10.1101/061481

Park, A.J., Havekes, R., Choi, J.H., Luczak, V., Nie, T., Huang, T., Abel, T., 2014. A presynaptic role for PKA in synaptic tagging and memory. Neurobiol. Learn. Mem. 114, 101–112. https://doi.org/10.1016/j.nlm.2014.05.005

Parkinson, J.A., Olmstead, M.C., Burns, L.H., Robbins, T.W., Everitt, B.J., 1999. Dissociation in effects of lesions of the nucleus accumbens core and shell on appetitive pavlovian approach behavior and the potentiation of conditioned reinforcement and locomotor activity by D-amphetamine. J. Neurosci. Off. J. Soc. Neurosci. 19, 2401–2411.

Pavlov (1927), P.I., 2010. Conditioned reflexes: An investigation of the physiological activity of the cerebral cortex. Ann. Neurosci. 17, 136–141. https://doi.org/10.5214/ans.0972-7531.1017309

Pawlak, V., Kerr, J.N.D., 2008. Dopamine Receptor Activation Is Required for Corticostriatal Spike-Timing-Dependent Plasticity. J. Neurosci. 28, 2435–2446. https://doi.org/10.1523/JNEUROSCI.4402-07.2008

Pignatelli, M., Bonci, A., 2015. Role of Dopamine Neurons in Reward and Aversion: A Synaptic Plasticity Perspective. Neuron 86, 1145–1157. https://doi.org/10.1016/j.neuron.2015.04.015

Pollandt, S., Liu, J., Orozco-Cabal, L., Grigoriadis, D.E., Vale, W.W., Gallagher, J.P., Shinnick-Gallagher, P., 2006. Cocaine withdrawal enhances long-term potentiation induced by corticotropin-releasing factor at central amygdala glutamatergic synapses via CRF, NMDA receptors and PKA. Eur. J. Neurosci. 24, 1733–1743. https://doi.org/10.1111/j.1460-9568.2006.05049.x

Pompanin, S., Jelcic, N., Cecchin, D., Cagnin, A., 2014. Impulse control disorders in frontotemporal dementia: spectrum of symptoms and response to treatment. Gen. Hosp. Psychiatry 36, 760.e5-760.e7. https://doi.org/10.1016/j.genhosppsych.2014.06.005

Prus, A.J., James, J.R., Rosecrans, J.A., 2009. Conditioned Place Preference, in: Buccafusco, J.J. (Ed.), Methods of Behavior Analysis in Neuroscience, Frontiers in Neuroscience. CRC Press/Taylor & Francis, Boca Raton (FL).

Quinn, A.J., Green, G.G., Hymers, M., 2020. Delineating single subject oscillatory brain networks with Spatio-Spectral Eigenmodes. bioRxiv 2020.06.21.157412. https://doi.org/10.1101/2020.06.21.157412

Quinn, A.J., Lopes-dos-Santos, V., Dupret, D., Nobre, A.C., Woolrich, M.W., 2021. EMD: Empirical Mode Decomposition and Hilbert-Huang Spectral Analyses in Python. J. Open Source Softw. 6, 2977. https://doi.org/10.21105/joss.02977

Quirk, G.J., Armony, J.L., LeDoux, J.E., 1997. Fear conditioning enhances different temporal components of tone-evoked spike trains in auditory cortex and lateral amygdala. Neuron 19, 613–624. https://doi.org/10.1016/s0896-6273(00)80375-x

Rainnie, D.G., Bergeron, R., Sajdyk, T.J., Patil, M., Gehlert, D.R., Shekhar, A., 2004. Corticotrophin releasing factor-induced synaptic plasticity in the amygdala translates stress into emotional disorders. J. Neurosci. Off. J. Soc. Neurosci. 24, 3471–3479. https://doi.org/10.1523/JNEUROSCI.5740-03.2004

Reakkamnuan, C., Cheaha, D., Kumarnsit, E., 2017. Nucleus accumbens local field potential power spectrums, phase-amplitude couplings and coherences following morphine treatment. Acta Neurobiol. Exp. (Warsz.) 77, 214–224.

Rebec, G.V., Sun, W., 2005. Neuronal Substrates of Relapse to Cocaine-Seeking Behavior: Role of Prefrontal Cortex. J. Exp. Anal. Behav. 84, 653–666. https://doi.org/10.1901/jeab.2005.105-04

Rennó-Costa, C., Teixeira, D.G., Soltesz, I., 2019. Regulation of gamma-frequency oscillation by feedforward inhibition: A computational modeling study. Hippocampus 29, 957–970. https://doi.org/10.1002/hipo.23093

Rescorla, R., Wagner, A., 1972. A theory of Pavlovian conditioning: Variations in the effectiveness of reinforcement and nonreinforcement, in: Classical Conditioning II: Current Research and Theory.

Rescorla, R.A., 2001. Retraining of extinguished Pavlovian stimuli. J. Exp. Psychol. Anim. Behav. Process. 27, 115–124. https://doi.org/10.1037/0097-7403.27.2.115

Rescorla, R.A., 1988. Behavioral studies of Pavlovian conditioning. Annu. Rev. Neurosci. 11, 329–352. https://doi.org/10.1146/annurev.ne.11.030188.001553

Ritz, M.C., Lamb, R.J., Goldberg, S.R., Kuhar, M.J., 1987. Cocaine receptors on dopamine transporters are related to self-administration of cocaine. Science 237, 1219–1223. https://doi.org/10.1126/science.2820058

Robbins, T.W., Roberts, A.C., 2007. Differential regulation of fronto-executive function by the monoamines and acetylcholine. Cereb. Cortex N. Y. N 1991 17 Suppl 1, i151-160. https://doi.org/10.1093/cercor/bhm066

Roberto, M., Cruz, M.T., Gilpin, N.W., Sabino, V., Schweitzer, P., Bajo, M., Cottone, P., Madamba, S.G., Stouffer, D.G., Zorrilla, E.P., Koob, G.F., Siggins, G.R., Parsons, L.H., 2010. Corticotropin Releasing Factor–Induced Amygdala Gamma-Aminobutyric Acid Release Plays a Key Role in Alcohol Dependence. Biol. Psychiatry, Metabotropic Glutamate Receptor Agonist Modulation of Alcohol Consumption 67, 831–839. https://doi.org/10.1016/j.biopsych.2009.11.007

Robinson, T.E., Kolb, B., 1999. Alterations in the morphology of dendrites and dendritic spines in the nucleus accumbens and prefrontal cortex following repeated treatment with amphetamine or cocaine. Eur. J. Neurosci. 11, 1598–1604. https://doi.org/10.1046/j.1460-9568.1999.00576.x

Rogan, M.T., Stäubli, U.V., LeDoux, J.E., 1997. Fear conditioning induces associative long-term potentiation in the amygdala. Nature 390, 604–607. https://doi.org/10.1038/37601

Rolls, E.T., 1996. A theory of hippocampal function in memory. Hippocampus 6, 601–620. https://doi.org/10.1002/(SICI)1098-1063(1996)6:6<601::AID-HIPO5>3.0.CO;2-J

Roman Rothaermel, Alexander J. Morley, Laura Lefèvre, Vítor Lopes-dos-Santos, Charlie J. ClarkeWilliams, Pavel V. Perestenko, David Dupret, n.d. Organizing brain-wide cell assemblies to handle environmental contingencies. Prep.

Root, D.H., Barker, D.J., Estrin, D.J., Miranda-Barrientos, J.A., Liu, B., Zhang, S., Wang, H.L., Vautier, F., Ramakrishnan, C., Kim, Y.S., Fenno, L., Deisseroth, K., Morales, M., 2020. Distinct Signaling by Ventral Tegmental Area Glutamate, GABA, and Combinatorial Glutamate-GABA Neurons in Motivated Behavior. Cell Rep. 32, 108094–108094. https://doi.org/10.1016/j.celrep.2020.108094

Root, D.H., Mejias-Aponte, C., Zhang, S., Wang, H., Hoffman, A.F., Lupica, C.R., Morales, M., 2014. Single rodent mesohabenular axons release glutamate and GABA. Nat. Neurosci. 17, 1543–1551. https://doi.org/10.1038/nn.3823

Roseman, L., Demetriou, L., Wall, M.B., Nutt, D.J., Carhart-Harris, R.L., 2018. Increased amygdala responses to emotional faces after psilocybin for treatment-resistant depression. Neuropharmacology 142, 263–269. https://doi.org/10.1016/j.neuropharm.2017.12.041

Rosenkranz, J.A., Grace, A.A., 2002. Dopamine-mediated modulation of odour-evoked amygdala potentials during pavlovian conditioning. Nature 417, 282–287. https://doi.org/10.1038/417282a

Rossi, N.A., Reid, L.D., 1976. Affective states associated with morphine injections. Physiol. Psychol. 4, 269–274. https://doi.org/10.3758/BF03332869

Rouault, M., Drugowitsch, J., Koechlin, E., 2019. Prefrontal mechanisms combining rewards and beliefs in human decision-making. Nat. Commun. 10, 301. https://doi.org/10.1038/s41467-018-08121-w

Salinas, E., Sejnowski, T.J., 2001. Correlated neuronal activity and the flow of neural information. Nat. Rev. Neurosci. 2, 539–550. https://doi.org/10.1038/35086012

Schaworonkow, N., Nikulin, V.V., 2019. Spatial neuronal synchronization and the waveform of oscillations: Implications for EEG and MEG. PLOS Comput. Biol. 15, e1007055. https://doi.org/10.1371/journal.pcbi.1007055

Scheffer-Teixeira, R., Belchior, H., Leão, R.N., Ribeiro, S., Tort, A.B.L., 2013. On High-Frequency Field Oscillations (>100 Hz) and the Spectral Leakage of Spiking Activity. J. Neurosci. 33, 1535–1539. https://doi.org/10.1523/JNEUROSCI.4217-12.2013

Schomburg, E.W., Fernández-Ruiz, A., Mizuseki, K., Berényi, A., Anastassiou, C.A., Koch, C., Buzsáki, G., 2014. Theta Phase Segregation of Input-Specific Gamma Patterns in Entorhinal-Hippocampal Networks. Neuron 84, 470–485. https://doi.org/10.1016/j.neuron.2014.08.051

Schultz, W., 1986. Responses of midbrain dopamine neurons to behavioral trigger stimuli in the monkey. J. Neurophysiol. 56, 1439–1461. https://doi.org/10.1152/jn.1986.56.5.1439

Schultz, W., Dayan, P., Montague, P.R., 1997. A Neural Substrate of Prediction and Reward. Science 275, 1593–1599. https://doi.org/10.1126/SCIENCE.275.5306.1593

Schultz, W., Romo, R., 1990. Dopamine neurons of the monkey midbrain: contingencies of responses to stimuli eliciting immediate behavioral reactions. J. Neurophysiol. 63, 607–624. https://doi.org/10.1152/jn.1990.63.3.607

Scoville, W.B., Milner, B., 1957. Loss of recent memory after bilateral hippocampal lesions. J. Neurol. Neurosurg. Psychiatry 20, 11–21. https://doi.org/10.1136/jnnp.20.1.11

See, R.E., Fuchs, R.A., Ledford, C.C., McLAUGHLIN, J., 2003. Drug Addiction, Relapse, and the Amygdala. Ann. N. Y. Acad. Sci. 985, 294–307. https://doi.org/10.1111/j.1749-6632.2003.tb07089.x

Senior, T.J., Huxter, J.R., Allen, K., O'Neill, J., Csicsvari, J., 2008. Gamma Oscillatory Firing Reveals Distinct Populations of Pyramidal Cells in the CA1 Region of the Hippocampus. J. Neurosci. 28, 2274–2286. https://doi.org/10.1523/JNEUROSCI.4669-07.2008

Shekhar, A., Truitt, W., Rainnie, D., Sajdyk, T., 2005. Role of stress, corticotrophin releasing factor (CRF) and amygdala plasticity in chronic anxiety. Stress Amst. Neth. 8, 209–219. https://doi.org/10.1080/10253890500504557

Shen, W., Flajolet, M., Greengard, P., Surmeier, D.J., 2008. Dichotomous dopaminergic control of striatal synaptic plasticity. Science 321, 848–851. https://doi.org/10.1126/science.1160575

Shirvalkar, P.R., Rapp, P.R., Shapiro, M.L., 2010. Bidirectional changes to hippocampal theta–gamma comodulation predict memory for recent spatial episodes. Proc. Natl. Acad. Sci. 107, 7054–7059. https://doi.org/10.1073/pnas.0911184107

Siapas, A.G., Lubenov, E.V., Wilson, M.A., 2005. Prefrontal Phase Locking to Hippocampal Theta Oscillations. Neuron 46, 141–151. https://doi.org/10.1016/J.NEURON.2005.02.028

Sirota, A., Montgomery, S., Fujisawa, S., Isomura, Y., Zugaro, M., Buzsáki, G., 2008. Entrainment of Neocortical Neurons and Gamma Oscillations by the Hippocampal Theta Rhythm. Neuron 60, 683–697. https://doi.org/10.1016/j.neuron.2008.09.014

Sjulson, L., Peyrache, A., Cumpelik, A., Cassataro, D., Buzsáki, G., 2018. Cocaine Place Conditioning Strengthens Location-Specific Hippocampal Coupling to the Nucleus Accumbens. Neuron 98, 926-934.e5. https://doi.org/10.1016/j.neuron.2018.04.015

Skaggs, W.E., McNaughton, B.L., Wilson, M.A., Barnes, C.A., 1996. Theta phase precession in hippocampal neuronal populations and the compression of temporal sequences. Hippocampus 6, 149–172. https://doi.org/10.1002/(SICI)1098-1063(1996)6:2<149::AID-HIPO6>3.0.CO;2-K

Skinner, B.F., 1930. ON THE CONDITIONS OF ELICITATION OF CERTAIN EATING REFLEXES. Proc. Natl. Acad. Sci. U. S. A. 16, 433–438.

Soares-Cunha, C., de Vasconcelos, N.A.P., Coimbra, B., Domingues, A.V., Silva, J.M., Loureiro-Campos, E., Gaspar, R., Sotiropoulos, I., Sousa, N., Rodrigues, A.J., 2020. Nucleus

accumbens medium spiny neurons subtypes signal both reward and aversion. Mol. Psychiatry 25, 3241–3255. https://doi.org/10.1038/s41380-019-0484-3

Sokolenko, E., Hudson, M.R., Nithianantharajah, J., Jones, N.C., 2019. The mGluR2/3 agonist LY379268 reverses NMDA receptor antagonist effects on cortical gamma oscillations and phase coherence, but not working memory impairments, in mice. J. Psychopharmacol. Oxf. Engl. 33, 1588–1599. https://doi.org/10.1177/0269881119875976

Spealman, R.D., Bergman, J., Madras, B.K., 1991. Self-administration of the high-affinity cocaine analog 2 beta-carbomethoxy-3 beta-(4-fluorophenyl)tropane. Pharmacol. Biochem. Behav. 39, 1011–1013. https://doi.org/10.1016/0091-3057(91)90067-c

Spiteri, T., Le Pape, G., Ågmo, A., 2000. What is learned during place preference conditioning? A comparison of food- and morphine-induced reward. Psychobiology 28, 367–382. https://doi.org/10.3758/BF03331994

Spruston, N., Johnston, D., 1992. Perforated patch-clamp analysis of the passive membrane properties of three classes of hippocampal neurons. J. Neurophysiol. 67, 508–529. https://doi.org/10.1152/jn.1992.67.3.508

Stathis, M., Scheffel, U., Lever, S.Z., Boja, J.W., Kuhar, M.J., Carroll, F.I., 1995. Rate of binding of various inhibitors at the dopamine transporter in vivo. Psychopharmacology (Berl.) 119, 376–384. https://doi.org/10.1007/BF02245852

Stefanik, M.T., Kalivas, P.W., 2013. Optogenetic dissection of basolateral amygdala projections during cue-induced reinstatement of cocaine seeking. Front. Behav. Neurosci. 7, 213. https://doi.org/10.3389/fnbeh.2013.00213

Steinmetz, N.A., Zatka-Haas, P., Carandini, M., Harris, K.D., 2019. Distributed coding of choice, action and engagement across the mouse brain. Nature 576, 266–273. https://doi.org/10.1038/s41586-019-1787-x

Stewart, J., de Wit, H., Eikelboom, R., 1984. Role of unconditioned and conditioned drug effects in the self-administration of opiates and stimulants. Psychol. Rev. 91, 251–268.

Stringer, C., Pachitariu, M., Steinmetz, N., Reddy, C.B., Carandini, M., Harris, K.D., 2019. Spontaneous behaviors drive multidimensional, brainwide activity. Science 364. https://doi.org/10.1126/science.aav7893

Stuber, G.D., Hnasko, T.S., Britt, J.P., Edwards, R.H., Bonci, A., 2010. Dopaminergic terminals in the nucleus accumbens but not the dorsal striatum corelease glutamate. J. Neurosci. Off. J. Soc. Neurosci. 30, 8229–8233. https://doi.org/10.1523/JNEUROSCI.1754-10.2010

Stujenske, J.M., Likhtik, E., Topiwala, M.A., Gordon, J.A., 2014. Fear and Safety Engage Competing Patterns of Theta-Gamma Coupling in the Basolateral Amygdala. Neuron 83, 919–933. https://doi.org/10.1016/j.neuron.2014.07.026

Sun, Q., Li, X., Ren, M., Zhao, M., Zhong, Q., Ren, Y., Luo, P., Ni, H., Zhang, X., Zhang, C., Yuan, J., Li, A., Luo, M., Gong, H., Luo, Q., 2019. A whole-brain map of long-range inputs to GABAergic interneurons in the mouse medial prefrontal cortex. Nat. Neurosci. 22, 1357–1370. https://doi.org/10.1038/s41593-019-0429-9

Sutton, R.S., 1988. Learning to predict by the methods of temporal differences. Mach. Learn. 3, 9–44. https://doi.org/10.1007/BF00115009

Taylor, S.B., Anglin, J.M., Paode, P.R., Riggert, A.G., Olive, M.F., Conrad, C.D., 2014. Chronic stress may facilitate the recruitment of habit- and addiction-related neurocircuitries through neuronal restructuring of the striatum. Neuroscience 280, 231–242. https://doi.org/10.1016/j.neuroscience.2014.09.029

Terrier, J., Lüscher, C., Pascoli, V., 2016. Cell-Type Specific Insertion of GluA2-Lacking AMPARs with Cocaine Exposure Leading to Sensitization, Cue-Induced Seeking, and Incubation of Craving. Neuropsychopharmacology 41, 1779–1789. https://doi.org/10.1038/npp.2015.345

Tinkhauser, G., Pogosyan, A., Tan, H., Herz, D.M., Kühn, A.A., Brown, P., 2017. Beta burst dynamics in Parkinson's disease OFF and ON dopaminergic medication. Brain J. Neurol. 140, 2968–2981. https://doi.org/10.1093/brain/awx252

Totah, N.K.B., Kim, Y., Moghaddam, B., 2013. Distinct prestimulus and poststimulus activation of VTA neurons correlates with stimulus detection. J. Neurophysiol. 110, 75–85. https://doi.org/10.1152/jn.00784.2012

Tritsch, N.X., Ding, J.B., Sabatini, B.L., 2012. Dopaminergic neurons inhibit striatal output through non-canonical release of GABA. Nature 490, 262–266. https://doi.org/10.1038/nature11466

Trouche, S., Koren, V., Doig, N.M., Ellender, T.J., El-Gaby, M., Lopes-dos-Santos, V., Reeve, H.M., Perestenko, P.V., Garas, F.N., Magill, P.J., Sharott, A., Dupret, D., 2019. A Hippocampus-Accumbens Tripartite Neuronal Motif Guides Appetitive Memory in Space. Cell 0. https://doi.org/10.1016/j.cell.2018.12.037

Trouche, S., Perestenko, P.V., van de Ven, G.M., Bratley, C.T., McNamara, C.G., Campo-Urriza, N., Black, S.L., Reijmers, L.G., Dupret, D., 2016. Recoding a cocaine-place memory engram to a neutral engram in the hippocampus. Nat. Neurosci. 19, 564–567. https://doi.org/10.1038/nn.4250

Tsai, H.-C., Zhang, F., Adamantidis, A., Stuber, G.D., Bonci, A., de Lecea, L., Deisseroth, K., 2009. Phasic firing in dopaminergic neurons is sufficient for behavioral conditioning. Science 324, 1080–1084. https://doi.org/10.1126/science.1168878

Tye, K.M., Mirzabekov, J.J., Warden, M.R., Ferenczi, E.A., Tsai, H.-C., Finkelstein, J., Kim, S.-Y., Adhikari, A., Thompson, K.R., Andalman, A.S., Gunaydin, L.A., Witten, I.B., Deisseroth, K., 2013. Dopamine neurons modulate neural encoding and expression of depression-related behaviour. Nature 493, 537–541. https://doi.org/10.1038/nature11740

Ungless, M.A., Whistler, J.L., Malenka, R.C., Bonci, A., 2001. Single cocaine exposure in vivo induces long-term potentiation in dopamine neurons. Nature 411, 583–587. https://doi.org/10.1038/35079077

United Kingdom drug situation 2019: summary [WWW Document], n.d. . GOV.UK. URL https://www.gov.uk/government/publications/united-kingdom-drug-situation-focal-point-annual-report/uk-drug-situation-2019-summary (accessed 1.1.21).

Van den Oever, M.C., Rotaru, D.C., Heinsbroek, J.A., Gouwenberg, Y., Deisseroth, K., Stuber, G.D., Mansvelder, H.D., Smit, A.B., 2013. Ventromedial prefrontal cortex pyramidal cells have a temporal dynamic role in recall and extinction of cocaine-associated memory. J. Neurosci. Off. J. Soc. Neurosci. 33, 18225–18233. https://doi.org/10.1523/JNEUROSCI.2412-13.2013

van der Maaten, L., Hinton, G., 2008. Visualizing data using t-SNE. J. Mach. Learn. Res.

Waltereit, R., Weller, M., 2003. Signaling from cAMP/PKA to MAPK and synaptic plasticity. Mol. Neurobiol. 27, 99–106. https://doi.org/10.1385/MN:27:1:99

Weinshenker, D., Schroeder, J.P., 2007. There and Back Again: A Tale of Norepinephrine and Drug Addiction. Neuropsychopharmacology 32, 1433–1451. https://doi.org/10.1038/sj.npp.1301263

West, T.O., Berthouze, L., Halliday, D.M., Litvak, V., Sharott, A., Magill, P.J., Farmer, S.F., 2018. Propagation of beta/gamma rhythms in the cortico-basal ganglia circuits of the parkinsonian rat. J. Neurophysiol. 119, 1608–1628. https://doi.org/10.1152/jn.00629.2017

Whitaker, L.R., Degoulet, M., Morikawa, H., 2013. Social Deprivation Enhances VTA Synaptic Plasticity and Drug-Induced Contextual Learning. Neuron 77, 335–345. https://doi.org/10.1016/j.neuron.2012.11.022

Whitelaw, R.B., Markou, A., Robbins, T.W., Everitt, B.J., 1996. Excitotoxic lesions of the basolateral amygdala impair the acquisition of cocaine-seeking behaviour under a second-order schedule of reinforcement. Psychopharmacology (Berl.) 127, 213–224.

Whittington, M.A., Traub, R.D., Kopell, N., Ermentrout, B., Buhl, E.H., 2000. Inhibition-based rhythms: experimental and mathematical observations on network dynamics. Int. J. Psychophysiol. Off. J. Int. Organ. Psychophysiol. 38, 315–336. https://doi.org/10.1016/s0167-8760(00)00173-2

Williams, B.A., 1975. The Blocking of Reinforcement Control1. J. Exp. Anal. Behav. 24, 215–225. https://doi.org/10.1901/jeab.1975.24-215

Wipf, D.O., Kristensen, E.W., Deakin, M.R., Wightman, R.Mark., 1988. Fast-scan cyclic voltammetry as a method to measure rapid heterogeneous electron-transfer kinetics. Anal. Chem. 60, 306–310. https://doi.org/10.1021/ac00155a006

Wu, Z., Huang, N., 2009. Ensemble Empirical Mode Decomposition: a Noise-Assisted Data Analysis Method. Adv. Adapt. Data Anal. 1, 1–41. https://doi.org/10.1142/S1793536909000047

Xia, Y., Driscoll, J.R., Wilbrecht, L., Margolis, E.B., Fields, H.L., Hjelmstad, G.O., 2011. Nucleus Accumbens Medium Spiny Neurons Target Non-Dopaminergic Neurons in the Ventral Tegmental Area. J. Neurosci. 31, 7811–7816. https://doi.org/10.1523/JNEUROSCI.1504-11.2011

Yamaguchi, T., Wang, H.-L., Li, X., Ng, T.H., Morales, M., 2011. Mesocorticolimbic glutamatergic pathway. J. Neurosci. Off. J. Soc. Neurosci. 31, 8476–8490. https://doi.org/10.1523/JNEUROSCI.1598-11.2011

Yang, H., de Jong, J.W., Tak, Y., Peck, J., Bateup, H.S., Lammel, S., 2018. Nucleus Accumbens Subnuclei Regulate Motivated Behavior via Direct Inhibition and Disinhibition of VTA Dopamine Subpopulations. Neuron 97, 434-449.e4. https://doi.org/10.1016/j.neuron.2017.12.022

Ye, J.-H., Ren, J., 2006. Cocaine inhibition of GABA(A) current: role of dephosphorylation. Crit. Rev. Neurobiol. 18, 85–94. https://doi.org/10.1615/critrevneurobiol.v18.i1-2.90

Yin, H.H., Knowlton, B.J., Balleine, B.W., 2004. Lesions of dorsolateral striatum preserve outcome expectancy but disrupt habit formation in instrumental learning. Eur. J. Neurosci. 19, 181–189. https://doi.org/10.1111/j.1460-9568.2004.03095.x

Yuan, H., Ding, L., Zhu, M., Zotev, V., Phillips, R., Bodurka, J., 2015. Reconstructing Large-Scale Brain Resting-State Networks from High-Resolution EEG: Spatial and Temporal Comparisons with fMRI. Brain Connect. 6, 122–135. https://doi.org/10.1089/brain.2014.0336

Zarnadze, S., Bäuerle, P., Santos-Torres, J., Böhm, C., Schmitz, D., Geiger, J.R., Dugladze, T., Gloveli, T., n.d. Cell-specific synaptic plasticity induced by network oscillations. eLife 5. https://doi.org/10.7554/eLife.14912

Zhang, J.-C., Lau, P.-M., Bi, G.-Q., 2009. Gain in sensitivity and loss in temporal contrast of STDP by dopaminergic modulation at hippocampal synapses. Proc. Natl. Acad. Sci. U. S. A. 106, 13028–13033. https://doi.org/10.1073/pnas.0900546106

Zheng, J., Anderson, K.L., Leal, S.L., Shestyuk, A., Gulsen, G., Mnatsakanyan, L., Vadera, S., Hsu, F.P.K., Yassa, M.A., Knight, R.T., Lin, J.J., 2017. Amygdala-hippocampal dynamics during salient information processing. Nat. Commun. 8. https://doi.org/10.1038/ncomms14413

Zheng, J., Stevenson, R.F., Mander, B.A., Mnatsakanyan, L., Hsu, F.P.K., Vadera, S., Knight, R.T., Yassa, M.A., Lin, J.J., 2019. Multiplexing of Theta and Alpha Rhythms in the Amygdala-Hippocampal Circuit Supports Pattern Separation of Emotional Information. Neuron. https://doi.org/10.1016/J.NEURON.2019.03.025

Zimmerman, J.L., 2012. Cocaine intoxication. Crit. Care Clin. 28, 517–526. https://doi.org/10.1016/j.ccc.2012.07.003